

Master thesis : Conception of a high-power, high-frequency optical laser source emitting over a wide area

Auteur : Bruyère, Thomas

Promoteur(s) : Redouté, Jean-Michel

Faculté : Faculté des Sciences appliquées

Diplôme : Master : ingénieur civil électricien, à finalité spécialisée en "electronic systems and devices"

Année académique : 2021-2022

URI/URL : <http://hdl.handle.net/2268.2/14577>

Avertissement à l'attention des usagers :

Tous les documents placés en accès ouvert sur le site le site MatheO sont protégés par le droit d'auteur. Conformément aux principes énoncés par la "Budapest Open Access Initiative"(BOAI, 2002), l'utilisateur du site peut lire, télécharger, copier, transmettre, imprimer, chercher ou faire un lien vers le texte intégral de ces documents, les disséquer pour les indexer, s'en servir de données pour un logiciel, ou s'en servir à toute autre fin légale (ou prévue par la réglementation relative au droit d'auteur). Toute utilisation du document à des fins commerciales est strictement interdite.

Par ailleurs, l'utilisateur s'engage à respecter les droits moraux de l'auteur, principalement le droit à l'intégrité de l'oeuvre et le droit de paternité et ce dans toute utilisation que l'utilisateur entreprend. Ainsi, à titre d'exemple, lorsqu'il reproduira un document par extrait ou dans son intégralité, l'utilisateur citera de manière complète les sources telles que mentionnées ci-dessus. Toute utilisation non explicitement autorisée ci-avant (telle que par exemple, la modification du document ou son résumé) nécessite l'autorisation préalable et expresse des auteurs ou de leurs ayants droit.



Conception of a high-power, high-frequency optical laser source emitting over a wide area

*Master thesis conducted for obtaining the Master's degree of Science in
Electrical Engineering major in Electronic Systems and Devices*

Thomas Bruyère - 20172399

SUPERVISOR: REDOUTÉ Jean-Michel

PHD SUPERVISOR: PIERRE Hervé

JURY MEMBERS: VANDERBEMDEN Philippe

DRION Guillaume

UNIVERSITY OF LIÈGE
FACULTY OF APPLIED SCIENCES
ACADEMIC YEAR 2021 - 2022

Conception of a high-power, high-frequency optical laser source emitting over a wide area

Thomas Bruyère

Faculty: Applied Sciences at the University of Liège

Section: Electrical Engineering

Supervisor: Jean-Michel Redouté

Academic year 2021-2022

Abstract

This Master's Thesis aims at conceiving a high-power, high-frequency optical laser source able to emit light over a wide area and also to be configurable. In the long run, this laser source will be used to fulfil two specific functions which are, on the one hand, the accurate measurement of the distance between a sensor and a target according to the Time-of-Flight (ToF) principle and, on the other hand, the realization of a three-dimensional camera capable of observing a whole area of this same target.

The first part of this thesis presents the different aspects of the ToF principle which consists in measuring the time needed for light to travel between a sensor and a target as well as the Single Photon Avalanche Diode (SPAD) concept which is an excellent photodetector for 3D imaging. The theories of operation of a Light-Emitting Diode (LED) and a laser diode are then explained in order to compare the advantages and drawbacks of each in order to conceive the optical laser source. This part concludes that laser diodes are more suitable for this type of application.

The second part focuses on the complete realization of the electrical system of the optical laser source. Firstly, the different electronic devices and components needed and their connections are presented. Then, the design of the Printed Circuit Board (PCB) is described, with details of the assembly of the different devices and components. The next step develops the method used to dissipate the heat from the PCB and more specifically from the laser diodes. Finally, the implementation of the software architecture is explained in order to establish the I²C communication protocol between the devices forming the laser source.

The last part focuses on the experimentation of the conceived optical laser source. The results demonstrate that the laser source, composed of nine diodes, achieves the different objectives set.

The next step, which is outside the scope of this thesis, will be to integrate the optical laser source onto an interface board containing an integrated sensor, peripheral circuits and a Field-Programmable Gate Array (FPGA) module in order to test the two specific functions mentioned above. This board is under development in the Microsys laboratory.

Conception d'une source laser optique de haute puissance et haute fréquence émettant sur une large surface

Thomas Bruyère

Faculté: Sciences Appliquées à l'Université de Liège

Section: Ingénieur Electricien

Promoteur: Jean-Michel Redouté

Année Académique 2021-2022

Résumé

Cette thèse de fin d'étude a pour objectif de concevoir une source laser optique de haute puissance et haute fréquence capable à la fois d'émettre de la lumière sur une surface étendue et aussi d'être configurable. A terme, cette source laser sera utilisée dans le but de répondre à deux fonctions spécifiques qui sont, d'une part, la mesure précise de la distance entre un capteur et une cible selon le principe du temps de vol et, d'autre part, la réalisation d'une caméra tri-dimensionnelle capable d'observer une zone entière de cette même cible.

La première partie de cette thèse présente les différents aspects du principe du temps de vol qui consiste à mesurer le temps nécessaire à la lumière pour se déplacer entre un capteur et une cible ainsi que le concept de diode à avalanche à photon unique qui est un excellent photodétecteur pour l'imagerie 3D. Les théories de fonctionnement d'une diode électroluminescente et d'une diode laser sont ensuite expliquées afin de comparer les avantages et les inconvénients de chacune d'entre elles dans le but de concevoir la source laser optique. Cette partie conclut que les diodes laser sont plus adaptées pour ce type d'application.

La seconde partie se concentre sur la réalisation complète du système électrique de la source laser optique. Dans un premier temps, les différents dispositifs et composants électroniques nécessaires ainsi que leurs connexions sont présentés. Ensuite, la conception du circuit imprimé est décrite, avec les détails d'assemblage des différents dispositifs et composants. L'étape suivante développe la méthode utilisée pour dissiper la chaleur du circuit imprimé et plus particulièrement celle des diodes laser. Enfin, l'implémentation de l'architecture software est expliquée dans le but d'établir le protocole de communication I²C entre les dispositifs formant la source laser.

La dernière partie se concentre sur l'expérimentation de la source laser optique ainsi conçue. Les résultats démontrent que cette source laser, composée de neuf diodes, atteint les différents objectifs fixés.

La prochaine étape, qui n'entre pas dans le cadre de cette thèse, consistera à intégrer la source laser optique dans une carte d'interface contenant un capteur intégré, des circuits périphériques ainsi qu'un module FPGA dans le but de tester les deux fonctions spécifiques dont il est question ci-dessus. Cette carte est en phase de développement au sein du laboratoire Microsys.

Acknowledgements

First of all, I would like to thank Prof. J.-M. Redouté, my thesis supervisor, who gave me the opportunity to do this thesis. I am very grateful for his guidance, his advice, his sincerity and his words of encouragement, which were very valuable, especially at the beginning of this project. I also thank him for allowing me to use all the equipment of the Microsys laboratory.

Then, I am very grateful to Hervé Pierre for his support and advice throughout this thesis. I am grateful to him for his invaluable guidance, his availability at all hours of the day and night and his enthusiasm throughout this semester.

Of course, I do not forget the other people of the Microsys laboratory, François Piron, Morgan Diepart and Gabriel Di Gregorio, for their comments and advice on my project and for the coffee breaks.

Finally, I would like to thank my family, my girlfriend Juliette and my friends for the support they have given me, not only for this thesis but also during the five years of study punctuated by this work.

Liège, June 9th, 2022

Thomas Bruyère

Contents

1	Introduction	1
1.1	Context of the Project	1
1.1.1	Theory of operation of a LED	4
1.1.2	Theory of operation of a Laser Diode	6
1.1.3	Differences between a LED and a Laser Diode	10
1.1.4	Laser safety classes	12
1.2	The Project	13
1.2.1	State of the project before this thesis	13
1.2.2	Objectives and constraints of this thesis	14
1.2.3	Structure of this thesis	15
2	Tools	16
2.1	Altium Designer	16
2.2	Python with PyQt	17
2.3	Arduino	17
2.4	I ² C Communication Protocol	18
2.4.1	I ² C Bus Interface	18
2.4.2	I ² C Bus Communication	20
3	Electrical System	22
3.1	Block Diagram	22
3.2	Devices and Components of the Electrical System	24
3.2.1	LM1084 Low Dropout Positive Regulator	26
3.2.2	LM3478 Step-Up Converter	29
3.2.3	TPS82085 Step-Down Converter	37
3.2.4	PLT5 450B Laser Diodes	39
3.2.5	iC-HSB Ultrafast Laser Drivers	42
3.2.6	Si5340 Clock Generator	45
3.2.7	Ultra Miniature Coaxial Connectors	49
3.2.8	LMK00301 Differential Clock Buffer	51
3.2.9	Arduino Nano 33 IoT	55
3.3	PCB Design	57
3.3.1	Components footprint	57
3.3.2	Components placement	57
3.3.3	PCB layout	59
3.3.4	Usefulness of differential pairs	60
3.3.5	Impedance matching	62

3.4	Thermal Dissipation	63
3.5	Software Architecture	65
3.5.1	General scan function	66
3.5.2	Functions related to iC-HSB Laser Drivers	66
3.5.2.1	Function to write a single bit to a register	68
3.5.2.2	Function to write two bits to a register	68
3.5.2.3	Function to write one byte to a register	68
3.5.2.4	Function to read one byte from a register	68
3.5.2.5	Function to reset registers	68
3.5.3	Functions related to MCP4562 Single Digital Rheostat	69
3.5.3.1	Function that configures the rheostat	69
3.5.4	Main build file	69
3.5.4.1	First part: initialization and definition	69
3.5.4.2	Second part: <i>setup</i> function	70
3.5.4.3	Third part: <i>loop</i> function	71
3.5.4.4	Fourth part: finalization	72
3.6	Main Problems Encountered and Solutions	72
3.7	Conclusion	73
4	Laser Source Experimental Phase	74
4.1	Optical Test Setup	74
4.2	Performing Tests	76
4.2.1	Preliminary verification tests	76
4.2.1.1	Laser source composed of a single laser diode	77
4.2.1.2	Laser source composed of nine laser diodes	77
4.2.1.3	Test of Si5340 Clock Generator	79
4.2.2	Performance tests	80
4.2.2.1	Laser source power composed of a single laser diode	81
4.2.2.2	Laser source power composed of nine laser diodes	83
4.2.2.3	Laser source efficiency	86
4.2.2.4	Comparison between the full laser source and that of a single laser diode	87
4.2.2.5	Optical signal of the full laser source	88
4.3	Conclusion	90
5	Possible Improvements	91
5.1	Enhance Laser Source Performances	91
5.2	Facilitate Laser Source Use	92
5.2.1	Graphical User Interface	92
5.2.2	Temperature sensor	93
6	Final Conclusion	94
	Appendices	A1
A	Altium Complete Schematics	A1

B Complete PCB	A9
B.1 3D PCB - Front view	A9
B.2 3D PCB - Back view	A10
B.3 2D PCB - Top Layer	A11
B.4 2D PCB - Plane Layer 1	A12
B.5 2D PCB - Plane Layer 2	A13
B.6 2D PCB - Bottom Layer	A14
B.7 Real PCB - Front view before soldering	A15
B.8 Real PCB - Back view before soldering	A16
B.9 Real PCB - Front view after soldering	A17
B.10 Real PCB - Back view after soldering	A18
C Further Explanations on the Software Part	A19
D Graphical User Interface	A24

List of Figures

1.1	Time-of-Flight (ToF) principle.	1
1.2	64×64 pixel dual-mode SPAD sensor.	3
1.3	Emission of light from the LED [23].	4
1.4	Constructional detail of LED [23], [27].	5
1.5	Absorption process [32].	7
1.6	Spontaneous emission process [32].	7
1.7	Stimulated emission process [32].	8
1.8	Constructional detail of laser diode [35],[32].	9
1.9	Fermi Level in conduction and valence band [38].	9
1.10	L-I curve for Laser Diode and LED.	11
1.11	Previous 3D PCB model.	13
2.1	Illustration of an electrical schematic and a PCB created by Altium Designer.	16
2.2	Representation of the Arduino Nano 33 IoT programmable board.	18
2.3	I ² C Bus Interface [54].	19
2.4	I ² C Bus Communication Protocol [57].	20
2.5	Example of an I ² C communication in write mode [59].	21
3.1	Block diagram of the complete electrical system.	23
3.2	Electrical schematic of LM1084 Low Dropout Positive Regulator.	28
3.3	Electrical schematic of LM3478 Step-Up Converter.	32
3.4	Electrical schematic of MCP4562 Single Digital Rheostat.	34
3.5	Electrical schematic of INA225 Current Sense Amplifier.	36
3.6	Electrical schematic of the first TPS82085 Step-Down Converter: $5\text{ V} \rightarrow 3.3\text{ V}$	38
3.7	Electrical schematic of the second TPS82085 Step-Down Converter: $5\text{ V} \rightarrow 1.8\text{ V}$	38
3.8	Beam Divergence: $P_{opt} = f(\Theta); T = 25^\circ\text{C}$ [43].	40
3.9	Electrical Internal Circuit [43].	41
3.10	Electrical schematic of three PLT5 450B Laser Diodes (LD1 refers to the first driver).	41
3.11	Block Diagram of iC-HSB Laser Driver [46].	42
3.12	Electrical schematic of iC-HSB Laser Driver.	44
3.13	Block Diagram of Si5340 Clock Generator [81].	47
3.14	Electrical schematic of Si5340 Clock Generator.	49
3.15	Electrical schematic of U.FL Coaxial Connector.	50
3.16	Block Diagram of LMK00301 Differential Clock Buffer [84].	52
3.17	Electrical schematic of LMK00301 Differential Clock Buffer.	54
3.18	Electrical schematic of Arduino Nano 33 IoT.	56
3.19	Footprints designed on Altium.	57
3.20	3D PCB model.	58

3.21	Different layers of the PCB.	60
3.22	Heat sink designed on Fusion 360.	64
4.1	Optical test setup.	74
4.2	Main laser source configurations.	77
4.3	Current consumption [mA] of the main generator, the source meter and the total current consumption of the PCB as a function of the laser source configuration at a frequency of 10 MHz.	78
4.4	Signal at the Clock Generator output when it is configured to have a 10 kHz frequency output signal.	80
4.5	Signal at the Clock Generator output when it is configured to have a 110 MHz frequency output signal.	80
4.6	Optical power [mW] of a single laser diode as a function of its distance [cm] from the power sensor and the signal frequency [MHz].	82
4.7	Irradiance [mW/cm ²] of a single laser diode as a function of its distance [cm] from the power sensor and the signal frequency [MHz].	83
4.8	Optical power [mW] of the full laser source as a function of its distance [cm] from the power sensor and the signal frequency [MHz].	84
4.9	Irradiance [mW/cm ²] of the full laser source as a function of its distance [cm] from the power sensor and the signal frequency [MHz].	85
4.10	Efficiency [%] of a single laser diode and the full laser source as a function of distance between the laser source and the power sensor at a frequency of 10 MHz.	87
4.11	Signal received by the photodetector when a 1 MHz frequency signal is generated. . . .	89
4.12	Signal received by the photodetector when a 10 MHz frequency signal is generated. . .	89
4.13	Signal received by the photodetector when a 100 MHz frequency signal is generated. .	89
5.1	Laser source emitted on a convergent lens.	92

List of Tables

4.1	Current consumption [mA] of the source meter, the main generator and the total current consumption of the PCB as a function of the laser source configuration at a frequency of 10 MHz.	78
4.2	Current consumption as a function of frequency when all nine laser diodes are turned on.	79
4.3	Optical power [mW] of a single laser diode as a function of its distance [cm] from the power sensor and the signal frequency [MHz].	81
4.4	Irradiance [mW/cm ²] of a single laser diode as a function of its distance [cm] from the power sensor and the signal frequency [MHz].	82
4.5	Optical power [mW] of the full laser source as a function of its distance [cm] from the power sensor and the signal frequency [MHz].	84
4.6	Irradiance [mW/cm ²] of the full laser source as a function of its distance [cm] from the power sensor and the signal frequency [MHz].	85
4.7	Efficiency [%] of a single laser diode and the full laser source as a function of distance between the laser source and the power sensor at a frequency of 10 MHz.	86

List of Abbreviations

AEL Accessible Emission Limit.

CMOS Complementary Metal Oxide Semiconductor.

FPGA Field-Programmable Gate Array.

GND Ground.

GUI Graphical User Interface.

IC Integrated Circuit.

ICs Integrated Circuits.

IDE Integrated Development Environment.

IEC International Electrotechnical Commission.

IoT Internet of Things.

I²C Inter Integrated Circuit.

LDA Laser Diode Anode.

LDK Laser Diode Cathode.

LDO Low Dropout.

LED Light-Emitting Diode.

LIDAR Light Detection and Ranging.

LSB Least Significant Bit.

LVDS Low Voltage Differential Signaling.

MPE Maximum Permissible Exposure.

MSB Most Significant Bit.

PCB Printed Circuit Board.

PLL Phase Lock Loop.

PSM Power Save Mode.

PVT Process, Voltage and Temperature.

PWM Pulse Width Modulation.

SCL Serial Clock Line.

SDA Serial Data Line.

SPAD Single Photon Avalanche Diode.

TAC Time-to-Amplitude Converters.

TDC Time-to-Digital Converters.

THT Through-Hole Technology.

TII Triple Integration Interpolator.

TIM Thermal Interface Material.

ToF Time-of-Flight.

UMCC Ultra Miniature Coax Connectors.

USB Universal Serial Bus.

VCO Voltage Controlled Oscillator.

Chapter 1

Introduction

1.1 Context of the Project

A very interesting principle consisting in measuring the time needed for light to travel between a sensor and a target in order to provide an accurate distance measurement is the Time-of-Flight (ToF) principle [1], [2]. An optical sensor using the ToF principle is used with an emitter of light wave or pulse. When this signal hits the target, it is then reflected back to the sensor. This sensor measures the lapse of time between the moment of emission and the moment of reflection of the signal. The distance between the target and the sensor is directly proportional to the measured lapse of time, knowing that the speed of light is constant in air [3]. Figure 1.1 below illustrates this ToF principle.

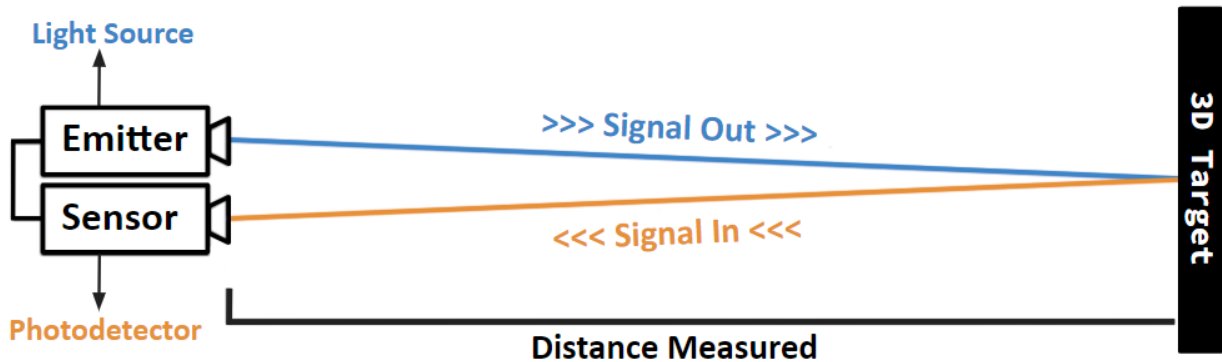


Figure 1.1: Time-of-Flight (ToF) principle.

Other optical techniques exist to measure distances without requiring contact [4]. However, these techniques suffer from some disadvantages such as lower accuracy, very complex calculations, etc. This is why the ToF principle has become the most widely used technique for distance detection. There are two categories of ToF sensors. The first one is direct ToF sensors, which directly measure the ToF of a light pulse [5]. The second category is indirect ToF sensors that measure the light intensity [6]. This second category is not covered in this project.

Another important concept is the Single Photon Avalanche Diode (SPAD), which is a photodetector device [7]. This device consists of a P-N junction reverse biased above its breakdown voltage. When a single photon impacts the junction in this unstable state, it triggers an avalanche which generates a current flow. SPADs have some interesting characteristics. One feature is that they have a probability of photon detection, *i.e.* a probability of breakdown for each incident photon. They also have high sensitivity and short response times.

Light Detection and Ranging (LIDAR) has always been of particular interest, especially for classical scanning LIDAR systems used to detect vehicles but also pedestrians [8], [9]. LIDAR works on the basis of the direct ToF principle.

Mechanical systems to physically scan a laser beam across the field of view have been used by conventional LIDAR implementations. All this by taking a series of measurements at a single point and building an image over time [10]. In recent years, an extension of these classical scanning systems has been proposed. It is about flash LIDAR [11] where a two-dimensional (2D) array of SPADs and an optical lens are used to capture a depth image using a semiconductor sensor [12]. Compared to classical scanning systems, this technique has a lot of benefits. The main benefits are that it brings:

- Greater reliability since no mechanical components are required.
- Higher data throughput since a full set of sensors can capture depth simultaneously.

However, this also requires that each pixel in the captured image has access to a synchronization circuit that controls the events of the photon [13]. The ability to assemble SPADs and Complementary Metal Oxide Semiconductor (CMOS) [14] circuits into a single sensor has led to great advances in the design of flash LIDAR sensors [15], [16].

Several different synchronisation circuit architectures exist in the literature. However, none have been found to be optimal for flash LIDAR systems. In the concept of a direct ToF sensor, the lapse of time between the emission of the light wave or pulse and the reflection is directly measured using a synchronisation circuit. On the one hand, digital synchronisation techniques, known as Time-to-Digital Converters (TDC), are the most common and varied of the proposed flash LIDAR sensors [12].

On the other hand, analogue techniques, known as Time-to-Amplitude Converters (TAC), have proved capable of achieving higher temporal resolution and linearity at the cost of large integration areas which are not feasible for pixel synchronisation circuits [17]. Since TACs use analogue techniques, they have certain disadvantages compared to TDCs:

- They are more sensitive to noise.
- They have a limited dynamic range.
- They are vulnerable to capacitive discharges.

This is why it is the TDCs that are most often used for flash LIDAR.

More recently, great progress has been made in sensor manufacturing processes, the optimisation of TDCs and in light emission and processing devices. This is leading to three-dimensional (3D) array of SPADs that could become the standard for depth cameras [18]. They are indeed beginning to be introduced in electronic products including those using the direct ToF. For time-dependent applications, such as 3D imaging [19], SPADs are excellent photodetector devices.

In the context of 3D imaging applications, the light pulse travels to the target and is reflected back to the sensor. The distance d between the sensor and the target is given by the following formula [3]:

$$d = \frac{c \times t_m}{2} \quad (1.1)$$

where c is the speed of light and t_m is the time measured by the sensor.

In [20], an analogue Triple Integration Interpolator (TII) timing technique has been introduced. This technique has the potential for higher reliability than conventional analogue synchronisation techniques with some other advantages:

- A common mode noise rejection.
- A Process, Voltage and Temperature (PVT) invariant
- An immunity to capacitive discharges.

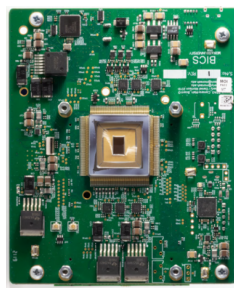
These properties of TII improve the resolution and linearity advantages of other analogue synchronisation techniques but can be accommodated in a much smaller area. However, TII still suffers from the limited dynamic range characteristic of analogue synchronisation techniques.

The equipment at the Microsys laboratory of the University of Liege is a fully functional 64×64 pixel dual-mode SPAD sensor, *i.e.* each pixel contains a SPAD sensor and acts as a proof of concept for the application of the TII scheme in flash LIDAR systems [12]. In addition to the TII, the synchronisation technique uses both a Time-to-Digital Converter (TDC) and a Time-to-Amplitude Converter (TAC). The sensor has two modes of operation:

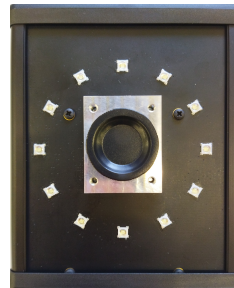
- Either in direct image-based ToF mode, where the timestamp of the first photon event in each pixel is recorded.
- Or in photon counting mode where the number of photon events is counted over a given interval, for each pixel. It is therefore an image intensity that is measured in this second mode.

The sensor has been integrated onto an interface board, as shown in figure 1.2a. The interface board contains all the necessary power supplies, SPAD bias voltage generation and peripheral circuits required by the sensor and uses a Field-Programmable Gate Array (FPGA) module as the main processing unit to drive the sensor control signals.

The complete camera system is integrated into a case, with provisions for mounting a lens to focus the image on the sensor. The light source is a laser consisting of 12 Light-Emitting Diodes (LEDs) to illuminate the target when operating in ToF. The entire box, therefore, serves as both a light emitter and a sensor. This case is shown in figure 1.2b below.



(a) Sensor integrated onto an interface board [12]



(b) Case with the complete camera system

Figure 1.2: 64×64 pixel dual-mode SPAD sensor.

1.1.1 Theory of operation of a LED

The Light-Emitting Diode (LED) [21] is a P-N junction diode that emits light when an electric current flows through it in the forward direction, *i.e.* the positive terminal of the current source on the P-type material and the negative terminal on the N-type material. The current flow is due to the movement of electrons in the opposite direction [22].

The emission of light from the LED is shown in figure 1.3. When an external voltage is applied to the electrons in the valence band (valence electrons), they gain sufficient energy and break the bond with the parent atom. These electrons are called free electrons. When the valence electron leaves the parent atom, it leaves an empty space in the valence shell which is called a hole [23].

The electrons in the valence band, *i.e.* the valence electrons, have almost the same energy level. Similarly, the electrons in the conduction band, *i.e.* the free electrons, also have almost the same energy level.

The energy level of electrons and holes in the valence band is lower than that of free electrons in the conduction band. Therefore, in order to recombine with the holes in the valence band, the free electrons must lose energy.

The free electrons emit electromagnetic energy in the form of photons and recombine with holes in the valence band after a short time.

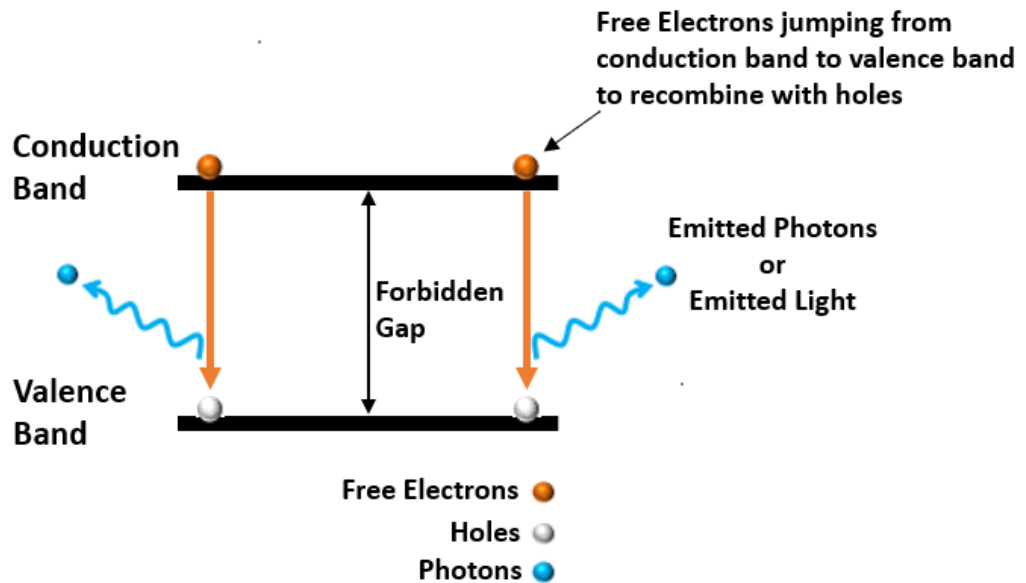


Figure 1.3: Emission of light from the LED [23].

The light energy depends on the distance between the conduction band and the valence band. The larger the gap, the higher the light intensity, because the electrons have to release more energy to recombine with the holes. The forbidden gap corresponds to the energy values that the electron cannot take [24].

The brightness of the light emitted also depends on the material used to construct the LED and the direct current flow through the LED.

It is possible to increase the conductivity of a semiconductor by a chemical process, called doping, which consists in inserting impurities into the semiconductor [25].

To obtain an N-type material, the semiconductor material is doped with a higher valence element (having more electrons than the semiconductor), such as Phosphorus, to add electrons to the conduction band. Conduction is then achieved by the movement of these electrons.

To obtain a P-type material, the semiconductor material is doped with an element of lower valence, such as Boron, in order to decrease the number of electrons in the valence band. Conduction is then ensured by the displacement of positively charged carriers, the holes [26].

Figure 1.4 shows the basic construction of a LED. This figure shows that when the LED, and therefore the P-N junction, is in direct polarisation, there is a growth in the minority carrier population in each zone, *i.e.* the majority electrons in the N-type region are injected into the P-type region where they recombine with the holes. The opposite phenomenon with the majority holes also occurs. As the mobility of electrons is much greater than that of holes, the rate of injection of electrons into the P-type region is greater than the rate of injection of holes into the N-type region [24], [26].

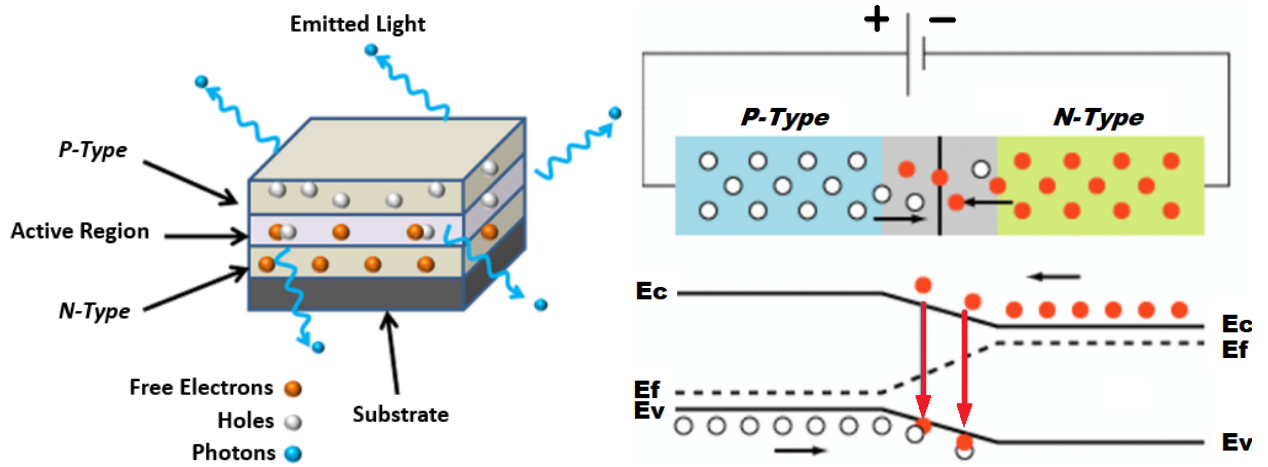


Figure 1.4: Constructional detail of LED [23], [27].

The LED therefore consists of P-doped material on the one hand and N-doped material on the other. It is at the interface of these two materials that electron-hole recombinations are possible. This interface is the active region of the semiconductor, also called the depletion zone, where the photons resulting from these recombinations are generated. Doping results in a decrease in the depletion zone. This decrease is more important in the P-type region than in the N-type region, which again favours the injection of electrons over holes.

Photons interact with other materials used in the LED and the current flowing through it to emit visible light [26].

This property is called electroluminescence which is the definition of the LED technology.

Another thing to keep in mind is that when the LED is reverse biased, the free electrons (majority carriers) on the N-side and the holes (majority carriers) on the P-side move away from the junction. As a result, the width of the depletion zone increases and no charge carrier recombination occurs. Thus, no light is produced [23].

The semiconductor materials used for visible LEDs are gallium phosphide (GaP), gallium arsenide phosphide (GaAsP) and gallium nitride (GaN). LEDs emit light of different colours such as red, green, yellow, blue, orange, etc. GaAsP emits red or yellow light. GaP emits red or green light and GaN emits blue light. The best semiconductor material used to make infrared (IR) LEDs is gallium arsenide (GaAs) [28].

1.1.2 Theory of operation of a Laser Diode

LASER stands for Light Amplification by Stimulated Emission of Radiation. Here too, the current flows through the gallium compounds at the P-N junction [29].

But in the case of laser diodes, the photon emissions are stimulated to create a feedback loop. All photons are in phase with each other and have the same wavelength, *i.e.* monochromatic [30].

Essentially, a beam of photons is responsible for progressively filling a cavity composed of mirror surfaces. This mirror surface reflects the photons back to the atoms inside the cavity, exciting their electrons. These electrons in an excited state want to release the extra energy, which again appears as a photon. This newly released photon is added to the photon beam inside the cavity, amplifying the reflection and excitation process. Once enough photons are released, a small light escape gap allows a narrow, bright, focused beam of laser light to be emitted. All this occurs in three steps [26], [31], [32]:

First Step: Absorption

When electrical energy is supplied to the electron, the additional energy supplied to it is consumed by the jump from the valence band to the conduction band. The process is known as absorption and explained in figure 1.5.

Let us consider two energy levels:

- E1, the lower energy level (valence band).
- E2, the higher energy level (conduction band).

Initially, it is assumed that the electron is in the lower energy state. To move from a lower energy level to a higher one, the electron must overcome the energy difference between the two levels, given by $E2 - E1$. In laser diodes, electrical energy or DC voltage is used as the external energy source. When this external energy source provides sufficient energy to the valence electrons, they break the bond with the parent atom and jump into the conduction band. The electrons in the conduction band are called free electrons.

When the valence electron leaves the valence shell, an empty space is created at the point where the electron leaves. This empty space in the valence shell is called a hole.

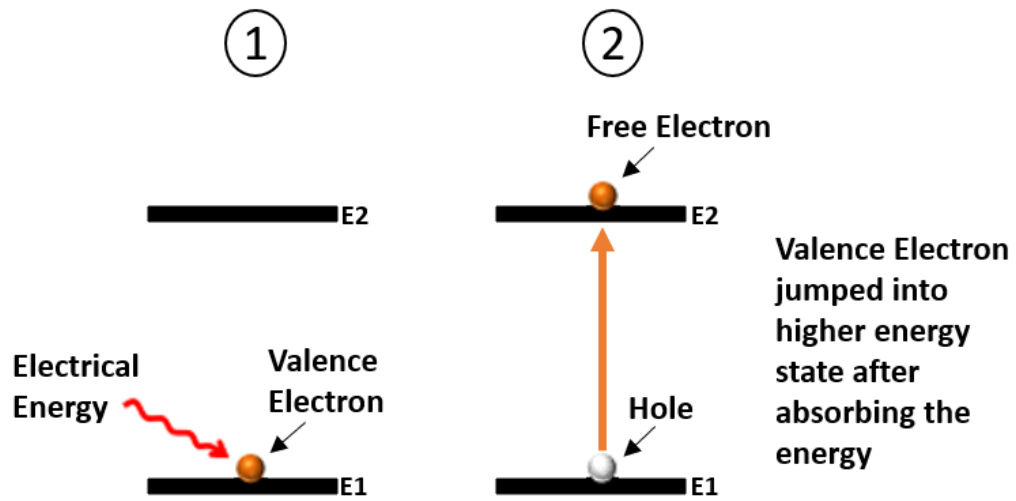


Figure 1.5: Absorption process [32].

Second Step: Spontaneous Emission

Then the process of spontaneous emission occurs, shown in figure 1.6. Due to absorption, electrons are present in the E2 energy level. The electrons in the conduction band, the free electrons, are in the higher energy state. Therefore, the free electrons have more energy than the holes.

The free electrons must lose their extra energy to recombine with the holes in the valence band. Free electrons in the conduction band will not stay for long. After a short time, they recombine with the lower energy holes releasing energy in the form of photons.

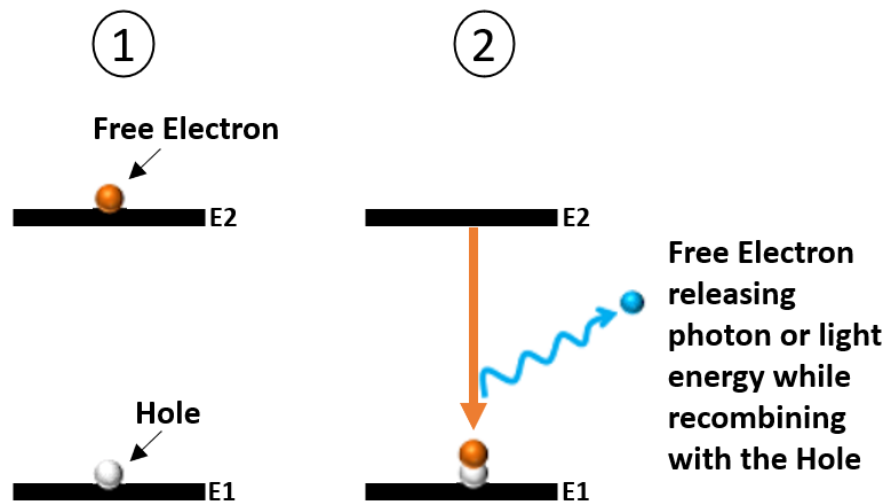


Figure 1.6: Spontaneous emission process [32].

Third Step: Stimulated Emission

Finally comes the last step which is the stimulated emission shown in figure 1.7. In stimulated emission, the excited or free electrons do not have to wait until the end of their lifetime. Before the end of their lifetime, incident or external photons will force the free electrons to recombine with holes, thus causing the release of another photon. As the forward current increases, more electrons enter the depletion zone and cause more photons to be emitted, the avalanche effect [33]. All the photons generated by the stimulated emission travel in the same direction and with the same phase, thus generating a monochromatic bright light. As a result, a narrow beam of high-intensity laser light is produced. The light generated by the stimulated emission travels parallel to the junction.

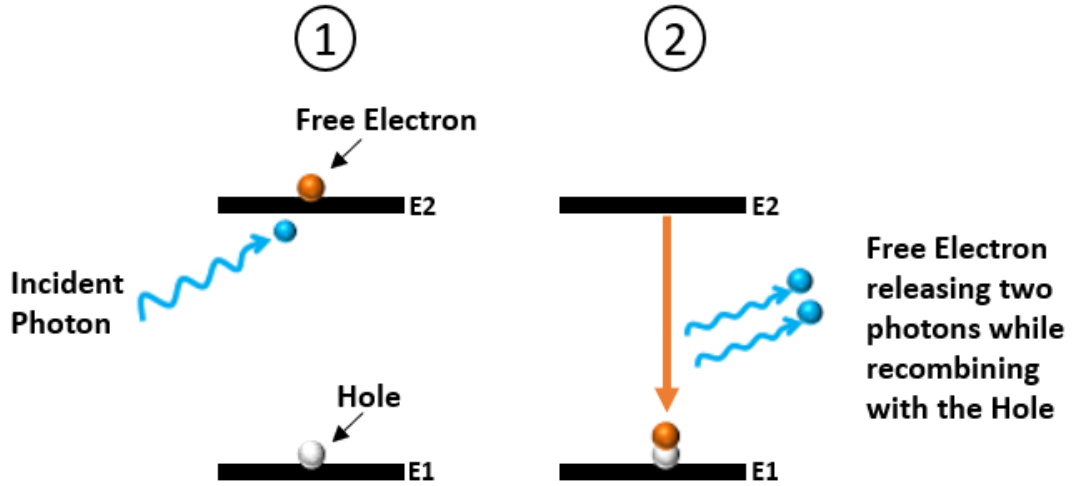


Figure 1.7: Stimulated emission process [32].

This efficiency results in the laser heating up considerably. The optical output power of a laser diode is between 1 mW and 500 mW, depending on the safety class [34]. These safety classes are described in section 1.1.4.

Figure 1.8 below shows the basic construction of a laser diode. In their configuration, polishing at both ends of the junction (both ends are optically reflective) is performed to provide a mirror-like surface, a resonant cavity for the photons. The light generated in the P-N junction will bounce back and forth (hundreds of times) between the two reflective surfaces. However, one must be fully reflective while the other must be partially reflective. The fully reflective end will reflect the light completely while the partially reflective end will reflect most of the light but allow a small amount of light [30]. The laser output comes from the active region of the laser diode [35].

As a result, a huge optical gain is achieved. By reflection from this surface, more electron and hole pairs are produced. This produces more radiation through the device [30].

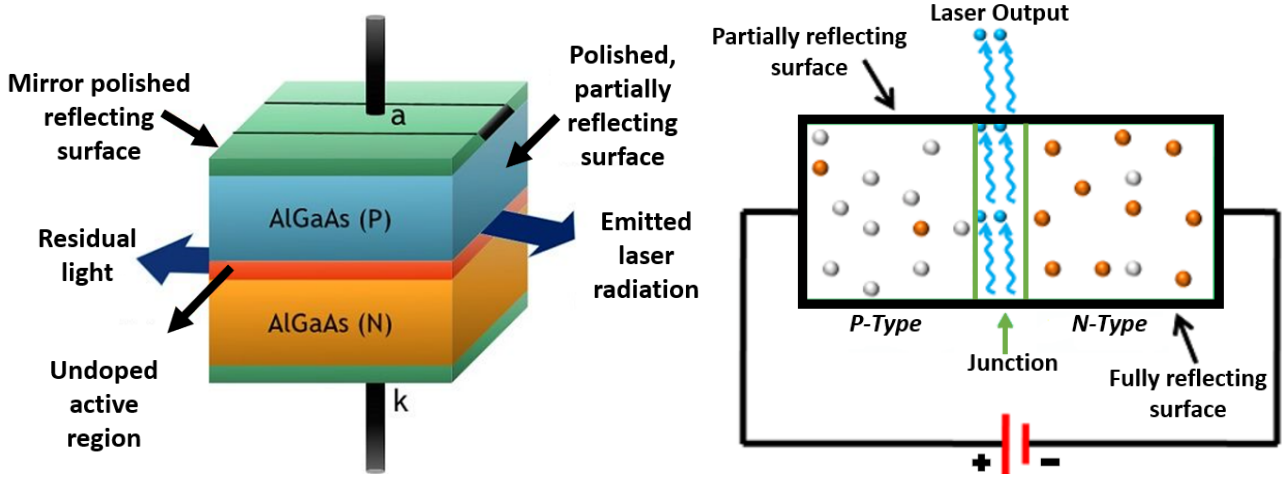


Figure 1.8: Constructional detail of laser diode [35],[32].

This construction is formed by doping aluminium or silicon onto a gallium arsenide (GaAs) material to generate an N-type and P-type layer. At the same time, an additional active layer of undoped GaAs is placed between the two layers. The thickness of this active layer is a few nanometres.

The purpose of placing this layer between the P-type and N-type layers is to increase the surface area for combining electrons and holes and to increase the emitted radiation accordingly. This means that many electron-hole pairs must be created in the material. An injection of many electrons into the P-type region is therefore carried out. This is done precisely by means of the P-N junction. The P-type region is heavily doped so that at equilibrium the Fermi level of the holes is in the valence band. The N-type region is heavily doped so that the density of electrons injected into the P-type region under the action of the bias voltage is such that the Fermi level of the electrons is in the conduction band [26]. This is illustrated in figure 1.9. The Fermi level (dotted line in the figure below) is an energy level for the collection of particles at the temperature of absolute zero. It is therefore the surface of a conductor defined at absolute zero where no electron will have enough energy to rise above the surface. If this level is in the valence and conduction band, electron-hole recombinations will be possible [36], [37].

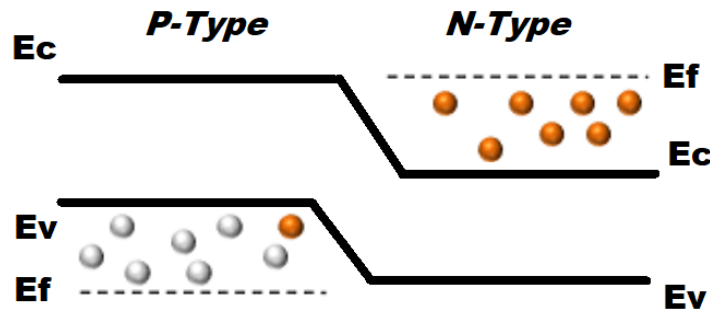


Figure 1.9: Fermi Level in conduction and valence band [38].

1.1.3 Differences between a LED and a Laser Diode

Firstly, the important distinction between a Light-Emitting Diode (LED) and a Laser Diode lies in the theory of operation [30]:

- A LED emits light as a result of charge carriers recombining around the P-N junction, whereas a laser diode emits light as a result of photons entering the atom, which forces them to release identical photons.
- A LED operates on the principle of electroluminescence and a laser diode operates on the theory of stimulated emission.

Then, the junction area is another main distinction between a LED and a laser diode. On the one hand, in the case of a laser diode, the junction field is very small and light can enter from a very small area. On the other hand, the junction field of a LED is larger. Light is therefore allowed to pass through a large field.

Afterwards, in terms of the way the light is emitted and the characteristics of this light, a LED and a laser diode are different:

- Both a LED and a laser diode emit photons to produce light. On the one hand, the light from a LED is more scattered and multidirectional, so this light is called incoherent, *i.e.* divergent. On the other hand, the light from a laser diode is very focused, so this light is qualified as coherent, *i.e.* convergent. While a LED reflects on a square of 1 mm, a laser diode focuses on a square of only 10 microns (= 0.01 mm) [39].
- The spectral width of a LED is greater than that of a laser diode. A larger spectral width allows for a larger link bandwidth. For a LED, the spectral width is about 80 nm when operating at 1310 nm and 40 nm at 850 nm. The spectral width of a laser diode is 3 nm when operating at 1310 nm and 1 nm at 850 nm [38].
- A LED has several wavelengths and is polychromatic whereas a laser diode is monochromatic [40].
- The line width of the output spectrum is obviously the narrowest for a laser diode since the optical cavity and the optical gain characteristics of a laser diode structure define the resonant wavelengths that lead to lasing emission. The optical efficiency of a laser diode is, therefore, higher than that of a LED [39]. However, the use of a laser diode is more complex and requires more precision to achieve a certain efficiency.

Furthermore, the response time of a laser diode is much shorter than that of a LED. Therefore, laser diodes are used in optics and electronics, while LEDs are used for lighting.

Finally, the operation of a LED and a laser diode is different depending on the current supplied to them:

- A laser diode can be characterized in terms of its threshold current, I_{th} which indicates the value of current at which stimulated emission overcomes the spontaneous emission as shown by the Light-Current (L-I) curve in figure 1.10. Indeed, this curve clearly shows that for a laser

diode, a progressive increase in power is noticed until a threshold point is reached [31]. After the threshold value, the emission is stimulated. A rapid increase in power is observed even for a small increase in current. A laser diode does not work until a minimum current is applied. A laser diode requires a higher current to maintain the high energy state of the electrons [41].

- A LED starts to emit light at only about 50 mA. In a LED, the light output increases steadily as the diode current increases. The output power of a LED, which is proportional to the input current, is lower than that of a laser diode.

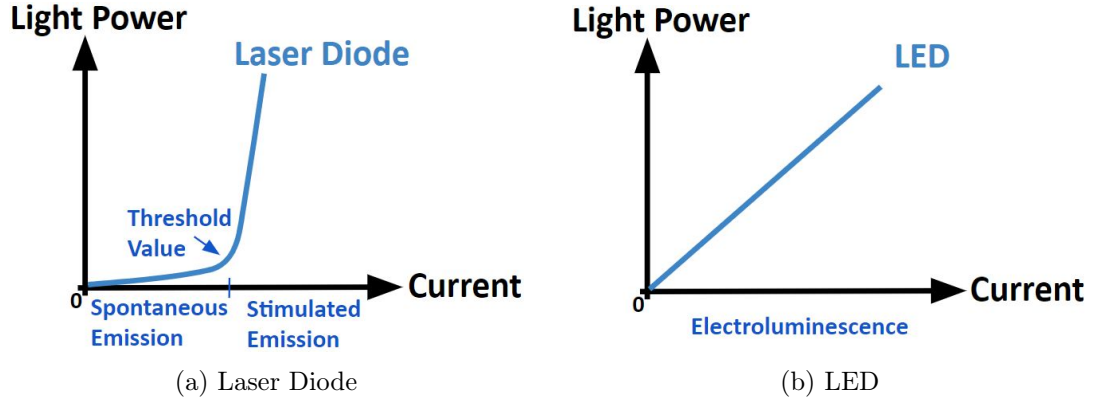


Figure 1.10: L-I curve for Laser Diode and LED.

A drawback with laser diodes is that the emission of photons is very temperature-dependent. The laser diode is already operating close to its limit and, therefore, becomes quite hot. If it gets too hot, this can change its amount of light emitted and its current. A heat sink is therefore often necessary. This is the case in this project. Despite this, laser diodes are chosen because they are more suitable for the type of application in this work.

1.1.4 Laser safety classes

Firstly, it is important to know that there are different classes of laser devices [42]. Some precautions must be taken due to IEC 60825-1 which is the primary standard that describes the safety of laser products developed and published by the International Electrotechnical Commission (IEC). The main objective of this document is to introduce a classification system for lasers and laser products that emit radiation in the 180 nm to 1 mm wavelength range, according to their optical radiation hazard rating, to facilitate risk assessment and help determine user control measures.

The classification is based on calculations and determined by the Accessible Emission Limit (AEL) which is the maximum allowable emission in a particular class, but also incorporates observational conditions such as Maximum Permissible Exposure (MPE) which is the level of laser radiation to which people can be exposed under normal conditions without suffering harmful effects:

- Class 1: Laser devices that are safe during use, even when viewed directly into the beam over a long period of time, even when exposure occurs when using telescopic devices.
- Class 1M: Laser devices emitting in the wavelength range of 302.5 nm to 4000 nm that are safe under reasonably predictable conditions of use. However, this limit may be exceeded and eye damage may occur after exposure to an optical device.
- Class 1C: Laser devices intended for direct application of laser radiation to the skin or internal body tissue for medical or other procedures. The level of skin exposure depends on the application.
- Class 2: Laser devices emitting visible radiation in the wavelength range of 400 nm to 700 nm, with an output power of less than 1 mW, where protection of the eye is normally provided by defence reflexes including the palpebral reflex (eye closure reflex). However, they can be dangerous for deliberate exposure to the beam.
- Class 2M: Laser devices emitting visible beams in the wavelength range of 400 nm to 700 nm and which are safe for short-term exposure only, to the naked eye. MPE may be exceeded and eye damage may occur after exposure to an optical device.
- Class 3R: Laser devices with an output power between 1 mW and 5 mW, emitting in the wavelength range from 302.5 nm to 10^6 nm. They, therefore, emit radiation that may exceed the MPE for direct vision in the beam, but the risk of injury, increasing with the duration of exposure, is in most cases relatively low.
- Class 3B: Laser devices of 5 mW to 500 mW output power, which are normally dangerous when ocular exposure in the beam occurs, including accidental short-term exposure. Viewing diffuse reflections is normally safe.
- Class 4: Laser devices where the view into the beam is dangerous. Viewing diffuse reflections is also dangerous. These lasers can cause skin damage and can also be a fire danger. Extreme care must be taken when using them.

1.2 The Project

1.2.1 State of the project before this thesis

As explained in section 1.1, the equipment available in the laboratory is a 64×64 pixel dual-mode SPAD sensor. However, this instrument is no longer used due to its sub-optimal efficiency. This is why two PhD students from the Microsys laboratory, Mister Hervé Pierre and Mister François Piron, quickly developed their own optical laser source which they need.

Globally, this laser source is made up of a single PLT5 450B Laser Diode [43] as well as a single ONET1151L Current Driver [44]. As for the power part, the LMR62421 Voltage Regulator [45] is used. SMA Coaxial Connectors, white components at the top of the figure 1.11a, directly connected to the driver allow the driver to receive a signal from an external clock generator. A 3D representation of the Printed Circuit Board (PCB) consisting of this laser diode and the current driver is shown in figure 1.11 below. The dimensions are $70 \text{ mm} \times 79.9 \text{ mm}$ ($\approx 5590 \text{ mm}^2$) with a total of 47 components.

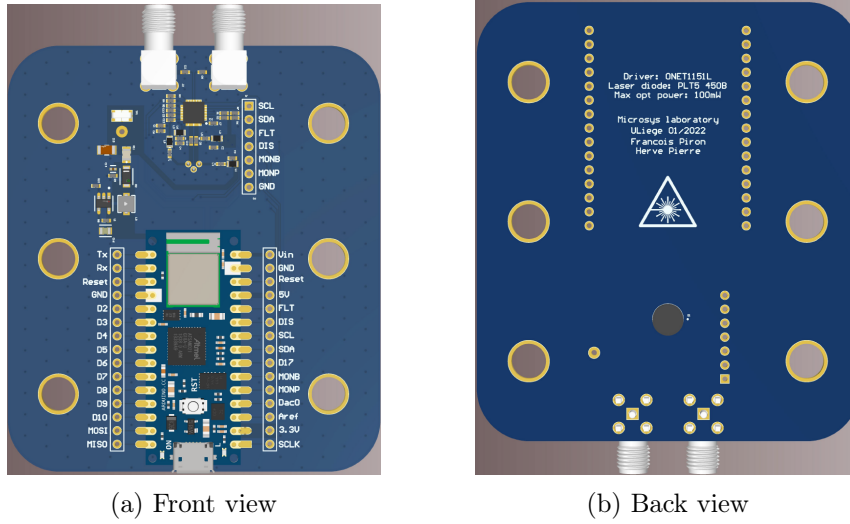


Figure 1.11: Previous 3D PCB model.

The two main disadvantages of this optical laser source are, firstly, its low power at long distances and secondly, the small area covered by the light it emits. This is due to the use of a single laser diode. A third disadvantage is that it is not configurable. Indeed, as the single laser diode is always supplied with the same current value, the laser source always produces the same light. This is mainly due to the fact that the **Current Driver** used is not optimal for this particular application.

Various optical tests were performed by Mr. Hervé Pierre and myself in order to verify the operation of this laser source. I accompanied Mr. Hervé Pierre in this process in order, on the one hand, to familiarise myself with the use of a laser source and, on the other hand, to observe the performances of this same laser source. The setup of the optical test is similar to that used to perform the laser source tests in this Master's Thesis. It is fully detailed in figure 4.1 of section 4.1.

The PLT5 450B Laser Diode used has an optical output power of 100 mW, which represents a Class 3B laser. Precautions such as wearing protective glasses and isolating in a closed room where no one can look have been taken.

1.2.2 Objectives and constraints of this thesis

It was agreed that the two main objectives of this work are to conceive an optical laser source that, on the one hand, has a higher power and, on the other hand, emits light over a wider area than that developed by the two PhD students of the Microsys laboratory. The latter is composed of a single **PLT5 450B Laser Diode** with a theoretical optical output power of 100 mW and emits over a small area even at short distances. As these performances are not sufficient, the new optical laser source conceived within the framework of this project is composed of nine **PLT5 450B Laser Diodes**, which makes it possible, on the one hand, to increase the power and, on the other hand, to emit light over a wider area. The different performances of this new laser source are experimented in chapter 4.

In addition, a third objective of this new laser source is that it must be configurable (configure the number of laser diodes turned on and off, the current that supplies these laser diodes, etc.) and not always emit the same light continuously. For this reason, an amount of additional devices and components are added to handle these nine **Laser Diodes** and hence the laser source. The structure of this optical laser source is fully described in chapter 3.

The steps to achieve the objectives of this thesis are therefore the following:

- To carry out the entire electrical system.
- To conceive and assemble the PCB containing the entire electrical system.
- To design a heat sink and then use CNC machining to manufacture it.
- To implement the Arduino code to establish the Inter Integrated Circuit (I²C) communication protocol.
- To perform the various tests of the optical laser source to examine its performances.
- To implement the Graphical User Interface (GUI) in order to facilitate the laser source use if time allows. This last part is therefore a bonus if time permits¹.

In the long run, this new optical laser source, composed of **Laser Diodes**, and no longer from LEDs like the 64 x 64 pixel dual-mode SPAD sensor, will be used to meet two specific functions required:

- To measure the distance between a sensor and a target according to the principle of ToF explained in section 1.1. It is for this first function that the power must be higher in order to be able to reach targets located at longer distances.
- To realize a three-dimensional camera that can observe a whole area of the same target as the first function. It is for this second function that the laser source must emit light over a wide area, *i.e.* cover a certain angle, rather than converge on a single point.

The development of the new laser source considers the subsequent integration of the above two specific functions. The optical laser source conceived in this thesis will be integrated onto an interface board developed by a PhD student in the Microsys laboratory in the near future. This interface board contains an integrated sensor and the peripheral circuits required by this board and sensor. An FPGA module is also present on this board and acts as the main processing unit to drive the various control

¹The design of the GUI was started but due to lack of time could not be finalised.

signals. As the PhD student's interface board is not yet achieved, the integration of the laser source and consequently the testing of the above two functions cannot yet be performed.

The main constraint of this project is therefore to consider the subsequent integration of the two specific functions described above.

A second constraint is to find and use current drivers that are made for this type of application, *i.e.* the conception of an optical laser source. Indeed, there are a lot of types of current drivers but very few are capable of handling the current for laser diodes. After a long research, it is the **iC-HSB Ultrafast Laser Drivers** [46] which are devices still in preliminary development phase that are chosen. These three **iC-HSB Drivers** each supply three **PLT5 450B Laser Diodes**. This is explained in section 3.2.5.

A third constraint is that it must be the possibility to send a signal into the system either by an internal signal generator or by an external signal generator. Therefore, it is necessary to have the devices that are able to realize these two possibilities.

A final constraint is to optimize the spaces and the size of the PCB. Indeed, the PCB must not exceed a specific size which is $80\text{ mm} \times 110\text{ mm}$ ($= 8800\text{ mm}^2$). However, fixing holes, as for the old laser source in figure 1.11, are essential on the PCB in order to be able to fix it to a table which is part of the optical tests setup. This further reduces the amount of space available on the PCB for devices and components. This constraint must be respected in order to be able, firstly, to integrate the optical laser source onto the interface board and, secondly, to correctly place and calibrate the PCB, as has been done in figure 4.1, enabling the optical tests to be feasible.

1.2.3 Structure of this thesis

A number of tools had to be used in order to achieve the desired objectives. After the presentation of these different tools, a full description of the electrical system, *i.e.* the electrical schematics and the PCB, will be discussed including the relevant different devices and components, the way they will be added to the system and will mutually interact. the methods used to improve the thermal dissipation of the PCB and the implementation of the software architecture will also be described. Afterwards, there will be a discussion of the various optical laser source tests carried out and their analyse, this in order to observe the performances of the laser source. Finally, the possible improvements to this project, which could make it more optimal, will be examined before ending with a conclusion.

The end of the document is punctuated by four appendices: the first one contains all the electrical schematics carried out for this project. The second one represents the PCB under all the different possible views. The third one offers further explanations on the implemented software part. The fourth one contains the GUI which should have been used if time had allowed.

Chapter 2

Tools

Before starting any research, it is important to find out about the different available tools. This chapter presents the main tools that were used for both the hardware and software aspects of this project.

2.1 Altium Designer

The Altium Designer [47] software is used for the design of PCBs. This software offers a complete design environment that allows a large amount of features such as circuit schematics, display and PCB creation. Everything is available in the same environment, allowing the creation of high-quality PCBs.

An illustration of a wiring diagram and design of a PCB created by Altium Designer is shown in figure 2.1 below. The whole design is explained in chapter 3.

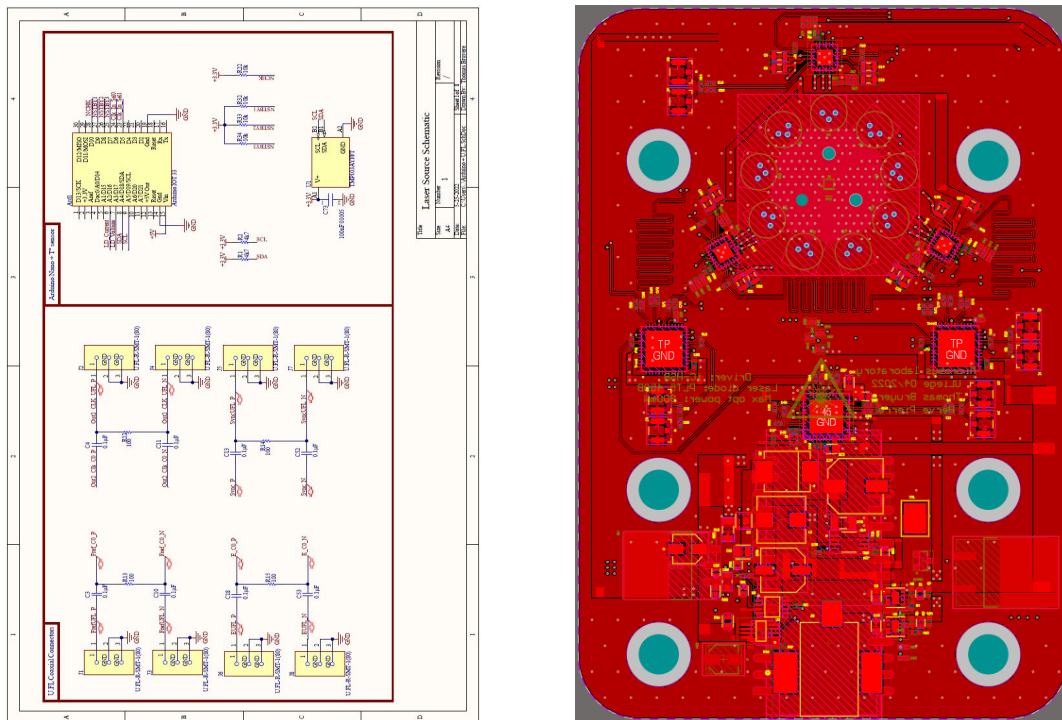


Figure 2.1: Illustration of an electrical schematic and a PCB created by Altium Designer. Extended view of all schematics and the PCB in appendix A and appendix B.

2.2 Python with PyQt

This section describes the specific features of PyQt [48] that are worth highlighting as they enable to elaborate a part of this project.

First of all, PyQt is a contraction of two words:

- On the one hand, Python [49] (the programming language used) is said to be very easy to learn.
- On the other hand, Qt [50] is an extremely complete framework (mainly for graphic interfaces).

PyQt serves as a bridge between these two worlds and brings Qt to the Python environment.

PyQt is therefore a set of Python bindings for the Qt application framework. The Qt library is one of the most powerful and popular GUI libraries. PyQt is implemented as a set of Python modules. It is a cross-platform toolkit that runs on all major operating systems.

Finally, PyQt has over 620 classes and 6000 functions and methods. In addition, it has a large amount of modules which themselves contain all the graphical commands but also non-GUI features for working with files, directories, etc. PyQt was therefore used to create a GUI to communicate easily with the whole project. Indeed, this interface allows to modify some input parameters (like the current for instance) very easily and to return the values of other interesting parameters (like the output voltage for example).

The design of the graphical user interface has started. However, there was not enough time to complete it and therefore to use it. This is explained in section 5.2.1.

2.3 Arduino

Arduino [51] is a rapid prototyping platform: a set of tools developed to facilitate the design of microcontroller-based assemblies, without wasting too much time learning the ins and outs. Arduino is therefore several things:

- A programmable board.
- A software that allows the programming of the card, the communication and integrates numerous function libraries.
- A community.

Firstly, the programmable board used in this project is the **Arduino Nano 33 Internet of Things (IoT)** [52]. IoT means the interconnection between the Internet and physical objects, places and environments. The representation of this programmable map is shown in figure 2.2. As this card has many connectors, it is possible to connect all sorts of things (LEDs, laser diodes, small electric motors, etc.) but also many sensors (humidity, light, temperature, etc.). It is thus possible to realize a lot of electronic, interactive or autonomous projects.

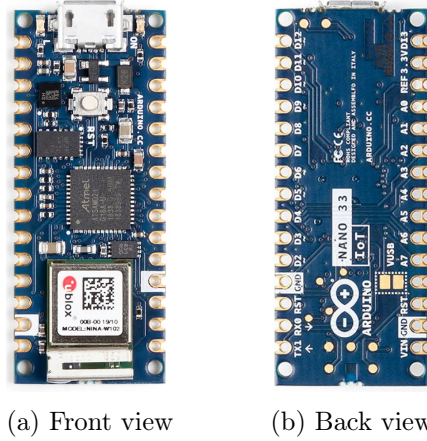


Figure 2.2: Representation of the Arduino Nano 33 IoT programmable board.

Then, the software, called Arduino Integrated Development Environment (IDE), is open source. This software provides everything needed to edit a program and check its syntax. Then, it is used to send the programs to the board, connected to the computer via a Universal Serial Bus (USB) cable. The programming language is very similar to C++, which is one of the most common languages.

Finally, the major advantage of the Arduino is its community because it is open-source software. There are many resources, tutorials, books, forums, etc. around Arduino.

An additional, and not least, plus of using an Arduino is that the I²C protocol can be used. This protocol, described in the following section 2.4, allows a wide range of electronic components to inter-communicate.

It is for all these reasons that Arduino was chosen for this project. All the pins of the Arduino Nano 33 IoT used to communicate with all the components are detailed in section 3.2.9.

2.4 I²C Communication Protocol

2.4.1 I²C Bus Interface

A bus is a device for linking and communicating between several hardware components. The I²C bus [53] belongs to the serial buses, *i.e.* it simply needs two connections to communicate and transmit the entire information between electronic components. These two connections are the following:

- The Serial Data Line (SDA): used by the master and slave to send and receive data.
- The Serial Clock Line (SCL): used to transmit a synchronous clock signal, *i.e.* a signal that indicates the rate of change of the SDA.

Of course, we need two more connections for a supply voltage (V_{DD}) and an electrical reference signal (Ground (GND)).

Therefore, the I²C bus consists of two bidirectional “open-drain” lines, SDA and SCL, pulled up with resistors R_p as shown in figure 2.3 below. This means that the devices connected to the I²C bus can pull any of these two lines down, but they cannot pull them up. If one of the devices ever wanted to drive the lines high, it would simply drop that line, and it would be driven high by the pull-up resistors.

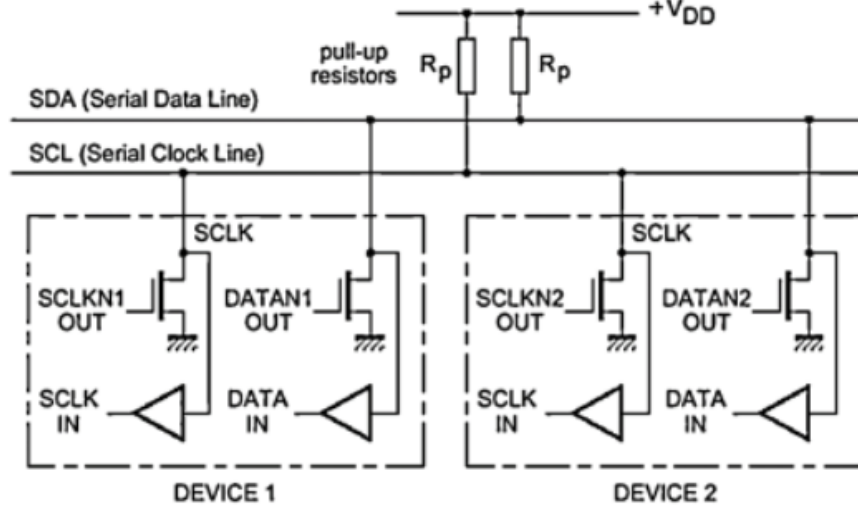


Figure 2.3: I²C Bus Interface [54].

The picture above shows the NMOS transistors inside the devices. For the device to pull any of the two lines low, a high voltage to the transistor gate is necessary. If the gate voltage is low, the NMOS transistor is not activated and the corresponding line is driven high.

All the devices connected to the bus are classified as either being Master or Slave. Master is the device that initiates the transfer and drives the clock line SCL. With I²C, you can connect multiple slaves to a single master and you can have multiple masters controlling single, or multiple slaves. In this project, the master is the **Arduino Nano 33 IoT** and the slaves are the other devices that communicate in I²C with the Arduino. There is therefore one master and several slaves [55].

As mentioned earlier, this is a serial link, which means that the transfer speed will be lower (data transferred bit by bit) than with a parallel bus (data transferred by several bits at a time). But in many cases, speed is not the predominant factor. The use of an I²C bus reduces the complexity of the printed circuit boards to be built.

The voltages associated with the logic levels will depend on the technology of the circuits involved. All circuits connected to the I²C bus must use the same potentials to define the high and low levels. Ultimately, this implies that all devices connected to the same bus must be powered in the same way. This does not mean that the devices must use the same power source. The supply voltage just has to be the same for all devices, with the GND wire unifying the references. The I²C supports a wide range of voltage levels but the most widely used are +5V and +3.3V. This gives values between 1 k Ω and 47 k Ω for pull-up resistors but values below 10 k Ω are generally preferable.

2.4.2 I²C Bus Communication

Before taking control of the bus, a circuit must check that the SDA and SCL lines are inactive, *i.e.* in the high state. If this is the case, the circuit indicates that it is taking control of the bus by setting the SDA line low, while SCL is still high. Therefore, other circuits know that the bus is busy and should not attempt to take control of it. The circuit that has just taken control of the bus becomes the master, marking the start of communication with the slaves. To stop this communication, the same principle applies. When SDA goes from low to high while SCL is still high, this marks the end of the communication between the master and the slaves.

I²C transfers 8 data bits, *i.e.* 1 data byte at a time. The lowest bit, *i.e.* the *D0* or *A0* bit on the figure 2.4, is the Least Significant Bit (LSB). The strongest bit, *i.e.* the *D7* or *A6* bit on the figure 2.4, is the Most Significant Bit (MSB). Firstly, to transmit the bits correctly on the SDA line, the master must therefore first set the SCL line to the low state. Then the master can set the SDA line to the level corresponding to the bit to be transmitted and set the SCL line high to indicate that the bit is present on the SDA line. The same operation will be repeated as many times as necessary to transmit the 8 data bits. Note that the most significant bit is transmitted first.

Then, once the transfer of each byte is complete, the slave must acknowledge it by returning an ACK bit to the master on the SDA line. To achieve this, when the SCL line is low after the eight SCL clock impulses, the master releases the SDA line, *i.e.* the SDA line becomes high for the ACK clock impulse. The slave is forced to generate an acknowledgement after each byte sent by the master by pulling the SDA line low during the ACK clock impulse. Since the outputs of each are open collectors, the master sees the 0 (low) of the slave and can then move on. Otherwise, there is an error and the master must generate the stop condition [56].

In total, therefore, nine SCL clock impulses are required to transmit one byte of data. This is illustrated in figure 2.4.

As far more than two components can be connected to an I²C bus, the master must be able to choose which slave is to receive the data. Each device connected to the bus has an unique address. The first data transmission is therefore always sent by the master and consists of addressing the correct slave. According to the I²C specifications, this address is either 7 bits or 10 bits (this is more uncommon).

When we have an address of 7 bits, we can have up to a maximum of $2^7 = 128$ devices connected to the I²C bus, with addresses 0 to 127. Now, when the master calls the slave(s), it still has to send 8 data bits. In this case, the master adds an extra bit to the 7 address bits to indicate whether it is requesting a read from the slave (R) or forcing a write to the slave (W). For read, $R/W = 1$, whereas for write, $R/W = 0$. Now the data sent looks something like the figure 2.4 below.

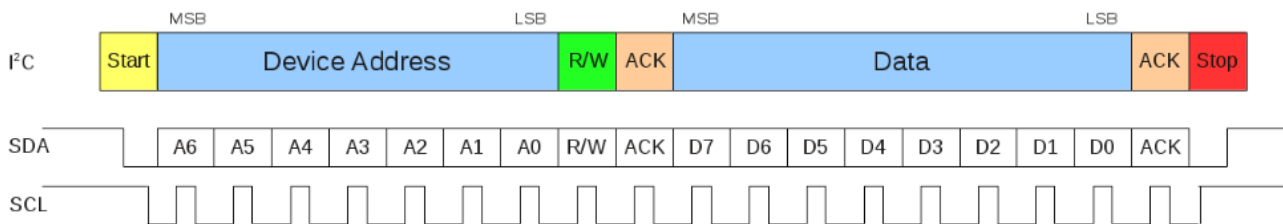


Figure 2.4: I²C Bus Communication Protocol [57].

If the R/W bit previously sent was 0, this means that the master must write one or more data bytes. After each valid ACK bit, the master can continue to send bytes to the slave or terminate with a stop condition. If the master is in writing mode, it writes the address of the slave register to the SDA line, followed by the value it wants to write to that specified register.

If the R/W bit transmitted together with the address is 1, this means that the master wants to read data from the slave. After the ACK bit of the address, the slave will keep control of the SDA line but the SCL clock signal is still generated by the master. To do this, the master will set its own SDA output high to allow the slave to take control of the SDA line. The slave must wait for the SCL line to go low to change the state of the SDA line otherwise the master will detect a stop condition and abort the transfer [58].

Once the slave has transmitted the 8 data bits, the master will generate an acknowledgement bit. If the master wants to read more bytes, it will set the acknowledgement bit to 0. If the master decides that the reading is finished, it will set the ACK bit to 1. If the master is in reading mode, it also writes the address of the slave register it wants to read and the slave writes the corresponding value to the specified register immediately after.

An example is given in the following figure 2.4. As the R/W bit = 0, the master forces a write to the slave. The address of the slave device is *0x6C*. The value *0xE2* is therefore written to register *0x09*.

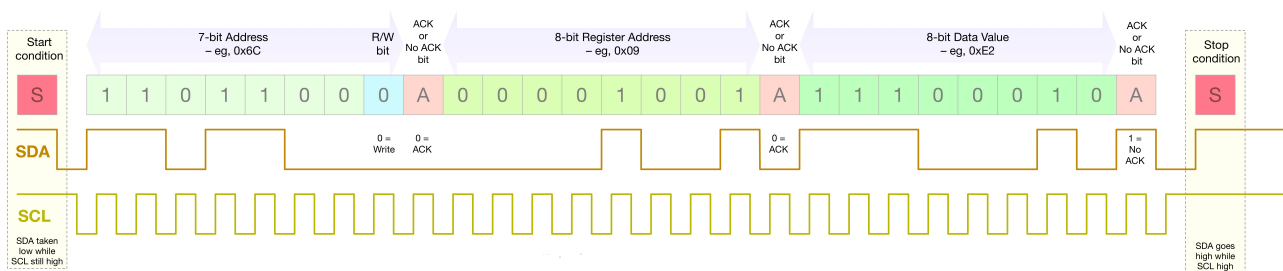


Figure 2.5: Example of an I²C communication in write mode [59].

In addition to that, some additional features are present in the I²C protocol. For instance, if the master is going too fast for the slave (the frequency of SCL is too high) the slave can stop the transaction momentarily by keeping SCL low so that it has the time to be ready for the rest of the transmission, this is called clock stretching.

The I²C bus protocol, therefore, defines the succession of possible states on the SDA and SCL lines and enables the communication between the elements to be managed [60].

The **Arduino Nano 33 IoT** programmable board shown in figure 2.2 and used for this project has the necessary pins (SDA and SCL) in order to adopt this protocol I²C. The association of the two thus makes it possible to carry out this project. All of this and how the protocol was exactly used for this project is described in detail in chapter 3.

Chapter 3

Electrical System

The objective of the electrical part is to assemble the different devices and components and make them communicate with each other in order to achieve the objective which is to conceive the optical laser source. The first section is composed of a block diagram that presents a sketch of the interactions between the different parts of the system. The second section describes the different devices and components used and the different connections they establish. The third section is devoted to the explanation of the conception of the PCB, which is the final hardware. The fourth section presents the methods used to improve the thermal dissipation of the PCB and more specifically of the laser diodes. The fifth section features the implementation of the software architecture that allows to establish the I²C communication protocol between the devices forming the laser source. And last but not least, the chapter ends with a presentation of the problems encountered during the carrying out of this part and a conclusion.

Since the Covid-19 period, some components have been out of stock. Indeed, between the beginning of the conception of the PCB and the moment of ordering the devices and components, some often had to be replaced or even removed because the delivery time was too long.

The devices and components for the PCB were purchased by Microsys laboratory from Montefiore, the two main electronic component distributors being Mouser [61] and Farnell [62].

3.1 Block Diagram

Figure 3.1 below presents a first sketch of the interactions between the different devices and components of the electrical system. Each of these elements is described in the following sections.

Each of the colours on the block diagram has a meaning which is explained below:

- Yellow connections: These connections mean that the signal is produced by an external **Clock Generator** to the PCB. This **Clock Generator** is connected to the **Differential Clock Buffers** through **Coaxial Connectors**. This method is used for all tests of the laser source. This is why the connections between **Differential Clock Buffers** and the **iC-HSB Drivers** are also yellow. However, there is a second method which is explained in the next point.
- Green connections: These connections mean that the signal is produced by an internal **Clock Generator** to the PCB. This **Clock Generator** is directly connected to the **Differential Clock Buffers**. This method is tested to ensure that the device is functioning correctly. However, this method will only be used when the laser source will be integrated onto the interface board composed of an integrated sensor, peripheral circuits and an FPGA module.

- Blue connections: These connections replace the SDA and SCL pins for better visibility of the diagram. They represent the I²C bus that is connected to devices that are capable to communicate using the I²C protocol.

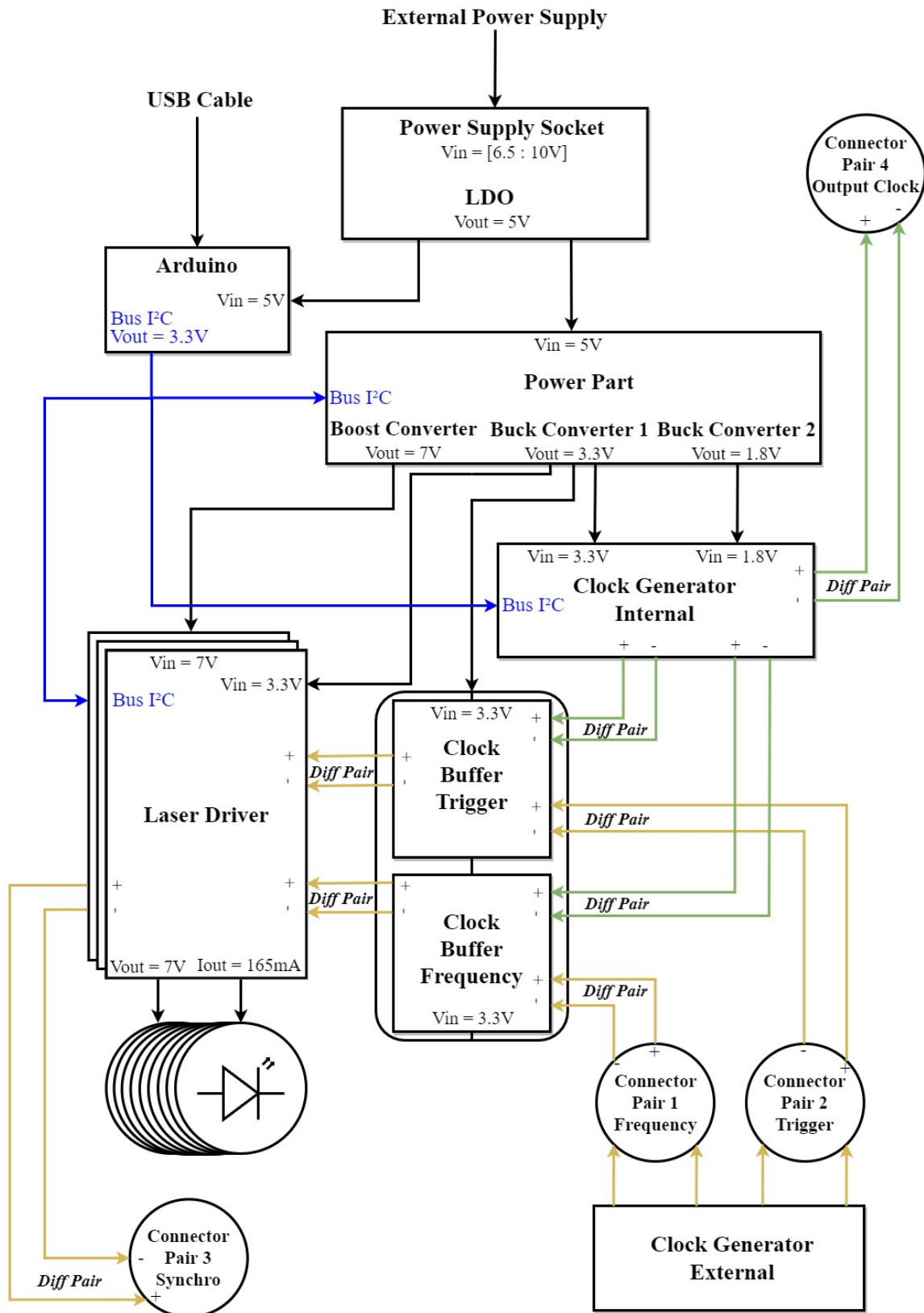


Figure 3.1: Block diagram of the complete electrical system.

3.2 Devices and Components of the Electrical System

Before describing all the devices and components used in this project and the different connections they establish, it is important to make a few remarks and define certain elements so that they do not have to be repeated in each section of this chapter.

Pull-up resistors

As explained in section 2.4, the I²C bus consists of two bidirectional “open-drain” lines, SDA and SCL, pulled up by resistors. This means that devices connected to the I²C bus can pull one of these two lines down, but cannot pull them up. If one of the devices wants to pull the lines up, it must simply drop that line, which is then pulled up by the pull-up resistors. The value of the pull-up resistors must therefore be chosen carefully to find a compromise between the current consumption and the time it takes for the lines to rise to the high state when one of the devices drops a line. The larger the pull-up resistor values, the longer it takes for the bus lines to go from low to high and the lower the current consumption, and vice versa. The pull-up resistor values in this project are 4.7 k Ω which is the standard value for I²C pull-up resistors. Obviously, only one pull-up resistor must be placed per line.

Pull-down resistors

Unlike pull-up resistors that pull the lines up when a device drops them, pull-down resistors pull the lines down when a device drops them. Indeed, the pull-down resistors are connected between the pins and the GND and can therefore pull the lines down. It is the opposite role of the pull-up, but the principle is the same.

Load termination resistor

In electronics, electrical termination is the termination of a transmission line with a termination resistor that corresponds to the characteristic impedance of the line. A termination resistor is a simple component that ensures the integrity of the signal, especially during high-speed transmission. In addition, a termination resistor is used to prevent signal reflections that cause signal distortion and power loss. In other words, a termination resistor placed at the end of a transmission line prevents the signal from bouncing. In the framework of this project, a load termination resistor is placed in parallel between two connection tracks of a differential pair.

When selecting the value of the termination resistor, the characteristic impedance of the differential pair must be taken into account. In fact, the resistance must be equal to this characteristic impedance. Therefore, in this project, the value of each of the termination resistors on the differential pairs is 100 Ω . The characteristic impedance is explained later in this chapter.

Non-populated resistors

In the electrical schematics, some resistors are placed and are “non-populated (NP)”. This means that they are resistors with a value of 0 Ω but are not directly soldered to the PCB. Indeed, the purpose of placing these 0 Ω resistors in the electrical schematics is to have the slots already provided on the PCB. So, if a few resistors are needed to, for example, change the address of a device or form a shortcut, it is quite possible to solder a 0 Ω resistor but also several hundred Ω if the footprint matches. This means that it is not necessary to remake a new PCB if some resistors must be added.

Decoupling capacitors

An important thing to remember is that decoupling capacitors are used and placed next to the power pins of any digital electronic device. Decoupling capacitors are very important components when it comes to logic circuits. The power supplies that supply voltage to the circuit are not always clean [63].

Decoupling capacitors are used to prevent noise from entering the system by shunting it to the GND. They are therefore placed between the supply voltage pins and GND (low impedance GND for efficient operation) to eliminate unwanted signals from the power supply. They must be placed as close as possible to the power and GND terminals of the unit. In operation, the capacitors short any type of AC signal to the GND, so that AC noise in a DC signal is eliminated, resulting in a cleaner and purer DC signal. This, therefore, helps to protect the different Integrated Circuits (ICs).

For low-frequency noise, the value of the decoupling capacitor is usually between 1 μF and 100 μF . For high-frequency noise, the value is between 0.01 μF and 0.1 μF . In the framework of this project, the values of these decoupling capacitors are not always the same. They will therefore be specified in each case.

Coupling capacitors

The main function of a coupling capacitor is the transmission of the AC signal from one circuit to another, but does not pass the DC frequency. They are therefore useful in circuits where AC signals (high-frequencies) are the desired signals to be output, while DC signals (low-frequencies) are only used to power certain devices of the circuit but should not appear in the output. Indeed, for low-frequency signals, it has a very high reactance, so that low-frequency signals are blocked. For high-frequency signals, it has a low reactance, so that high-frequency signals are easily passed through [63].

In the framework of this project, a coupling capacitor is placed in series on each track of the differential pair. The value of the capacitor depends on the frequency of the AC signal passed through. The higher the frequency, the lower the reactance given by the capacitor. Therefore, a low capacitance value is required to pass high-frequency signals. Therefore, the value of each of the coupling capacitors is 0.1 μF .

3.2.1 LM1084 Low Dropout Positive Regulator

The power supply for a design is essential. In the case of this project, the specific main voltage is 5 V. Indeed, the input supply voltage of the **Step-Up Converter** described in section 3.2.2, as well as the two **Step-Down Converters** described in section 3.2.3, is 5 V. It is, therefore, necessary to be as precise as possible in order to have this desired voltage value. For this purpose, there are low dropout voltage regulators.

A Low Dropout (LDO) Voltage Regulator is an indispensable element for managing the power supply of an integrated circuit [64]. An LDO voltage regulator is also called a step-down DC-DC converter with a variable input voltage. Indeed, the LDO voltage regulator is a type of linear voltage regulator that can operate at a very low potential difference between the input and the output to reduce the power dissipated as heat and increase the voltage conversion efficiency. This potential difference is called the dropout voltage and is noted $V_{Dropout}$. This dropout voltage is therefore the minimum voltage difference at the terminals of the regulator for proper regulation. When the voltage difference between the input and output falls below the dropout voltage, the regulator stops regulating because it cannot maintain a stable operation. Therefore, the output voltage decreases.

LDO voltage regulators are therefore more efficient than conventional linear regulators. They are distinguished by their ability to maintain regulation with small differences between supply voltage and load voltage. The output voltage of an LDO voltage regulator is independent of load impedance, input voltage variations, temperature and time. In addition, they are tiny and generate low noise.

Another characteristic of voltage regulators is the quiescent current noted I_q . It corresponds to the current consumed by the internal system of the LDO voltage regulator when it is in stand-by mode with a constant input supply voltage and when no load or very light load is connected. It is the current flowing in the GND pin. This quiescent current is calculated as the difference between the input current (I_{in}) and the output current (I_{out}). Since quiescent current does not flow through the output, it affects the efficiency of the regulator. In low power systems, a low quiescent current provides maximum efficiency.

The efficiency of an LDO voltage regulator depends on the quiescent current (I_q), the output current (I_{out}) the input voltage (V_{in}) and also the output voltage (V_{out}). It is calculated as follows:

$$Efficiency = \frac{V_{out} \times I_{out}}{(I_q + I_{out}) \times V_{in}} \times 100\% \quad (3.1)$$

The power dissipated by an LDO voltage regulator is calculated as follows:

$$P_{Dissipated} = (V_{in} - V_{out}) \times I_{out} + (V_{in} \times I_q) \quad (3.2)$$

Figure 3.2 below shows the electrical schematic of several different devices.

The first device, on the left of the figure, is an external DC power socket. For this project, the power socket is a RASM712_BKZ [65]. It is to this **Power Socket** that an external generator can be connected. Consequently, it is possible to inject an input voltage as well as an input current into the circuit.

The second device, on the right of the figure, is the LDO voltage regulator. For this project, it is the LM1084 Low Dropout Positive Regulator [66] that is used. The operation of this LDO is to have a feedback loop made up of a voltage divider which aims to decrease the output voltage. This output voltage is then compared to the reference voltage by an error amplifier. This error amplifier should consume as little current as possible. The first input to the error amplifier is therefore the output voltage reduced by the voltage divider. The second input is the reference voltage, *i.e.* the input voltage. After comparison, the error amplifier then adjusts the resistance of the pass element to ensure that the output voltage of the LDO is maintained at the desired voltage. This LDO uses a single N-type transistor. This allows for a lower dropout voltage. This transistor is called the pass element. This pass element is responsible for transferring current from the input to the load.

The range of the input voltage of this LDO in order to have a 5 V output voltage is [6.5: 20 V]. This LDO is guaranteed to provide a minimum voltage drop of 1.5 V. Therefore, the difference between the input voltage and the output voltage of the LDO voltage regulator must be at least equal to 1.5 V in order to have a stable operation. For this reason, the input voltage V_{in} , *i.e.* the voltage in the **Power Socket**, must be at least equal to the following value:

$$\begin{aligned} V_{Dropout} &= V_{in} - V_{out} \\ \Leftrightarrow 1.5V &= V_{in} - 5V \\ \Leftrightarrow V_{in} &= 6.5V \end{aligned} \tag{3.3}$$

On the one hand, for tests performed with an input voltage lower than 6.5 V, the output voltage is lower than 5 V. On the other hand, for the tests performed with an input voltage going up to 10 V, the output voltage is well equal to 5 V.

However, in typical use of the laser source, *i.e.* when the laser source is fully turned on mode and a frequency of 10 MHz is produced by a **Clock Generator** (test explained in chapter 4), 740 mA is drained, *i.e.* consumed, at the input of the LDO. Moreover, the output current of the LDO is 735 mA. It is therefore possible to calculate the quiescent current as follows:

$$I_q = I_{in} - I_{out} = 740mA - 735mA = 5mA \tag{3.4}$$

This value corresponds to the value indicated in the datasheet of the LM1084 Low Dropout Positive Regulators.

The power dissipated by the LDO voltage regulator is therefore:

$$\begin{aligned} P_{Dissipated} &= (V_{in} - V_{out}) \times I_{out} + (V_{in} \times I_q) \\ &= (7V - 5V) \times 0.735A + (7V \times 0.005A) \\ &= 1.505W \end{aligned} \tag{3.5}$$

which is quite high.

The **Low Dropout Positive Regulators** of this project is a high-efficiency linear regulator. Indeed, using the voltage values as well as the current values, it is possible to calculate the efficiency of the LDO voltage regulator. The efficiency is calculated as follows:

$$\begin{aligned}
 Efficiency &= \frac{V_{out} \times I_{out}}{(I_q + I_{out}) \times V_{in}} \times 100\% \\
 &= \frac{5V \times 0.735A}{(0.005A + 0.735A) \times 7V} \times 100\% \\
 &\approx 71\%
 \end{aligned} \tag{3.6}$$

The last device, between the **Power Socket** and the LDO voltage regulator, is a P-type MOSFET (PNP) [29]. The latter is the **IRF9640 MOSFET P-type** [67]. The pins of a P-type MOSFET are a Drain (D), a Source (S) and a Gate (G). For this circuit, the drain pin of the P-type MOSFET is connected directly to the **Power Socket**, the gate pin is connected to the GND and the source pin is connected to the LDO. This component is a Reverse Polarity Protection. Indeed, if the power supply of the circuit connected to the **Power Socket** is reversed, *i.e.* the positive wire to GND and the negative wire to V_{dd} , it can have consequences on the global circuit. For example, the circuit may burn out or the power supply itself may be destroyed as well.

This is why the **IRF9640 P-type MOSFET** is used as reverse polarity protection. It works by connecting or disconnecting the supply load depending on whether the supply is connected correctly or not. On the one hand, with correct polarity, the P-type MOSFET turns on when its V_{GS} ¹ is appropriate. On the other hand, with a reverse polarity, the load is disconnected from the input power supply because the V_{GS} voltage of the P-type MOSFET is too low and therefore it does not turn on. Another advantage of using the P-type MOSFET as a reverse polarity protection is its low power loss. Indeed, the drain-source resistance of this P-type MOSFET is typically $R_{DS} = 0.35\Omega$. If the current through this transistor is 0.740 A, its power loss is then:

$$P_{Loss} = I^2 \times R_{DS} = 0.740^2 A \times 0.35\Omega \approx 0.191W \tag{3.7}$$

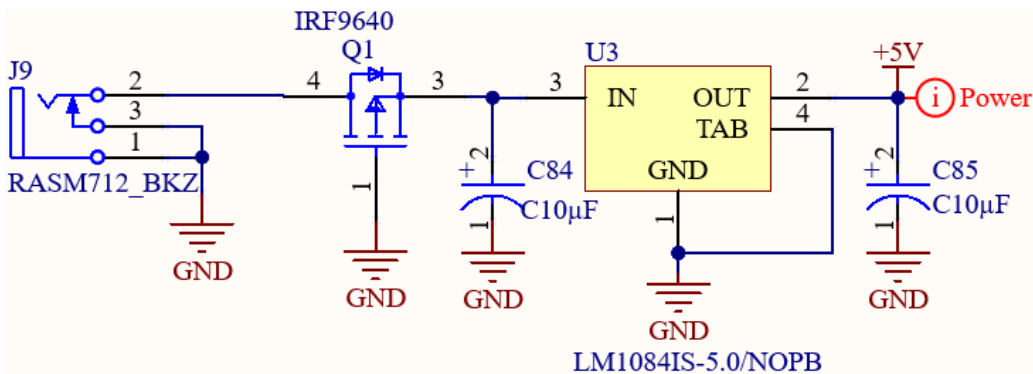


Figure 3.2: Electrical schematic of LM1084 Low Dropout Positive Regulator.

It is also possible to see from the above figure 3.2 that there is an input capacitor and an output capacitor for the LDO voltage regulator.

¹Gate to Source Voltage.

The input capacitor filters out the noise overlaid on the input voltage. This capacitor has a value of 10 μF and must be placed at the input to bypass the noise.

The output capacitor is an important component in an LDO voltage regulator. If the load current demand increases, the output capacitor has the role of supplying the current. This changes the output voltage. This modification is detected by the feedback loop. So while the error amplifier is responsible for passing more current through the pass element, *i.e.* the N-type transistor, the output capacitor is responsible for supplying the current. This capacitor has a value of 10 μF .

A characteristic of the **LM1084 Low Dropout Positive Regulator** is that it has a load regulation of 0.1%. The load regulation of an LDO voltage regulator is its ability to maintain a stable output voltage while being subject to load current variations. The lower the load regulation, the more stable and reliable the output voltage. With a value of 0.1% being low, the operation around the output capacitor is efficient.

3.2.2 LM3478 Step-Up Converter

As explained in the previous section, the power supply for this project is essential and is 5 V. However, the forward voltage, V_f , of a laser diode is the positive voltage applied between its anode and cathode. The laser diodes used in this project, **PLT5 450B Laser Diodes** which are explained in detail in section 3.2.4, have a forward voltage typically 5.5 V and can be as high as 7 V. Consequently, a step-up converter, also called boost converter, is useful in the framework of this project.

In the first place, the whole circuit involved in the operation of the step-up converter is designed to be supplied with an input voltage of 5 V adjusted by the LDO voltage regulator and to have an output voltage of 7 V to supply the **Laser Diodes**. Moreover, the output current is 2 A. These values are therefore constant because the other devices and components that make up this part of the circuit are fixed.

In the second place, a resistor in the circuit is replaced by a variable resistor which allows the output voltage and current of the step-up converter to be modified if necessary. However, the description below is made before the addition of the variable resistor. The benefits of adding the variable resistor are explained later.

The step-up converter used in this project is the **LM3478 High-Efficiency Step-Up Converter** [68]. Its electrical schematic is shown in figure 3.3. The latter has interesting features for this project.

Firstly, a **Step-Up Converter** is a simple type of switching converter. It, therefore, takes an input voltage and provides an output voltage greater than the input voltage. There is therefore a conversion from DC input to DC output, *i.e.* a fixed DC voltage is transformed into an adjustable DC voltage. The **LM3478 Step-Up Converter** has built-in features such as thermal shutdown, shortcut protection, overvoltage protection, etc. It has a wide range of supply voltages from 2.97 V to 40 V and an adjustable clock frequency from 100 kHz to 1 MHz.

Then, this device is supplied with a voltage of 5 V on the V_{in} input pin of the power supply. The overvoltage protection is triggered if the input voltage exceeds 7.2 V. An input capacitor and a decoupling capacitor are required. A value of less than 10 μF for the input capacitor can cause problems with impedance interactions or switching noise and thus affect the **Step-Up Converter**.

For this reason, the input capacitor has a value of 100 μF . The decoupling capacitor connected between the V_{in} pin and GND has a typical value of 0.1 μF .

Moreover, the DR pin represents the control pin. The voltage on this pin is equal to the input voltage when the input voltage is below 7.2 V. So, for voltages V_{in} below 7.2 V, the internal bias of the Integrated Circuit (IC) is the voltage V_{in} . This pin must be connected to the gate of an external MOSFET. The Q2 MOSFET used in this circuit is CSD17313Q2Q1 N-type MOSFET [69]. The maximum drain to source voltage, $V_{DS,MAX}$, must be greater than the output voltage. This is the case as $V_{DS,MAX} = 30\text{ V}$. There is also an Inductor [70] between the V_{in} pin and the drain of the N-type MOSFET. The Inductor is an energy storage element in the Step-Up Converter. This L1 Inductor has a value of 4.7 μH . A final component that is essential is a Schottky Rectifier Diode [71]. Indeed, by observing the electrical schematic, it is possible to notice that, on the one hand, the average current through the D2 Schottky Diode is the average current of the load, *i.e.* the three iC-HSB Drivers described in section 3.2.5. On the other hand, the peak current through the D2 Schottky Diode, *i.e.* the current that the diode is capable of delivering for short periods of time, is the peak current through the Inductor.

All of these components are needed in this system because the Step-Up Converter operates in two states.

In the first operating state, the N-type MOSFET is turned on and energy is stored in the Inductor. During this state, the Schottky Diode is reverse biased and the charging current is supplied by the output capacitor. Indeed, an output capacitor is necessary because it is the one that provides all the output current when the Inductor is charging. Therefore, it receives very large ripple currents. It must be able to handle the maximum current and therefore this capacitor in this project has a value of 180 μF .

In the second state, the N-type MOSFET is disabled, *i.e.* turned off, and the Schottky Diode is forward biased. The energy stored in the Inductor is transferred to the load and the output capacitor. The ratio of the switch-on time to the total period is the duty cycle D, as shown in the following equation:

$$D = 1 - \left(\frac{V_{in} - V_{Q2}}{V_{out} + V_{D2}} \right) = 1 - \left(\frac{5\text{V} - 0.85\text{V}}{7\text{V} + 0.5\text{V}} \right) = 0.44667 = 44.667\% \quad (3.8)$$

where $V_{D2} = 0.5\text{ V}$ is the forward voltage drop of the Schottky Diode and $V_{Q2} = 0.85\text{ V}$ is the voltage drop across the N-type MOSFET when it is turned on.

In addition, the ISEN pin is the current sense input pin. The voltage generated across an external shunt resistor is fed into this pin. This is because the maximum amount of current that can be delivered to the load is set by the shunt resistor. The current limit occurs when the voltage generated across the shunt resistor equals the current sense threshold voltage, V_{Sense} which is typically 156 mV when $V_{in} = 5\text{ V}$. When this threshold is reached, the N-type MOSFET is disabled until the next cycle. The value of the shunt resistor, R19 resistor which is connected to the source of the N-type MOSFET in figure 3.3, is calculated as follows:

$$\begin{aligned} R19 &= \frac{V_{Sense} - (D \times V_{Sense} \times V_{SL, ratio})}{I_{SW} Limit} \\ &= \frac{0.156\text{V} - (0.44667 \times 0.156\text{V} \times 0.78)}{4.075\text{A}} \\ &= 24.9\text{m}\Omega \end{aligned} \quad (3.9)$$

where $V_{SL, ratio}$ is the ratio between the internal compensation ramp voltage (V_{SL}) and the threshold voltage (V_{Sense}) and where ISW_{Limit} is the peak switch current limit which is calculated as follows:

$$\begin{aligned} ISW_{Limit} &= \left(\frac{I_{out}}{1-D} \right) + \left(\frac{D \times V_{in}}{2 \times F_s \times L1} \right) \\ &= \left(\frac{2A}{1-0.44667} \right) + \left(\frac{0.44667 \times 5V}{2 \times 515kHz \times 4.7\mu F} \right) \\ &= 4.075A \end{aligned} \quad (3.10)$$

where $F_s \approx 515kHz$ is the switching frequency and $L1$ is the **Inductor** that must meet the following condition:

$$\begin{aligned} L1 &> \frac{D \times (1-D) \times V_{in}}{2 \times I_{out} \times F_s} \\ \Leftrightarrow L1 &> \frac{0.44667 \times (1-0.44667) \times 5V}{2 \times 2A \times 515kHz} \\ \Leftrightarrow L1 &> 0.6\mu F \end{aligned} \quad (3.11)$$

A value of $20m\Omega$ is selected for the $R19$ shunt resistor as it is an acceptable value for this project. A value of $4.7\mu F$ is chosen for the $L1$ **Inductor** because it is a standard value for an inductor that respects the above condition.

As for the resistor $R20 = 100\Omega$ and the capacitor $C31 = 10pF$ connected to the ISEN pin, these two components form an RC filter to filter the noise on the ISEN pin. The values of these components are those proposed in the datasheet.

Finally, the FB pin is the feedback pin. The output voltage must be adjusted with a resistor divider to provide $1.26V$ to this pin. It is also on this pin that the overvoltage can be detected. If at any time the voltage on the feedback pin rises to $V_{FB} + V_{OVP} = 1.26V + 0.1V = 1.36V$ where V_{OVP} is the output overvoltage protection, the overvoltage protection is triggered. This then forces the **N-type MOSFET** to turn off. In the circuit, the peak current through the $Q2$ **N-type MOSFET** is sensed by the external $R19$ shunt resistor. The voltage across this resistor is passed to the ISEN pin. The output voltage is also sensed by an external feedback resistor divider network and fed to the negative input of the error amplifier which is the FB feedback pin. Initially, this resistor network consists of the $R21$ resistor and a second resistor nicknamed R_{Second} ². In order to calculate the values of these two resistors that form the external feedback resistor divider network, the following equation is used:

$$\begin{aligned} R_{Second} &= \frac{V_{FB} \times R21}{V_{out} - V_{FB}} \\ &= \frac{1.26V \times 4.53k\Omega}{7V - 1.26V} \\ &= 994.3\Omega \end{aligned} \quad (3.12)$$

where $R21$ is the resistance between the output voltage and the feedback pin and R_{Second} is the resistance between the feedback pin and the GND. Therefore, in order to have an output voltage $V_{out} = 7V$ and a voltage at the FB pin $V_{FB} = 1.26V$, a value of $4.53k\Omega$ is chosen for the $R21$ resistor. This gives a value of $994.3\Omega \approx 1k\Omega$ for the R_{Second} resistor.

²This resistor no longer appears on the electrical schematic because it has been replaced by a variable resistor.

However, as explained at the beginning of this section, this electrical schematic has been modified and the R_{Second} resistor is replaced by a variable resistor. This variable resistor is the MCP4562 Single Rheostat connected to the FB pin as shown³ in figure 3.3 below. The operation of this variable resistor is described later in this section. This FB pin, after the $R21$ resistor, is connected to the output voltage. It is also to this same location that the INA225 Current Sense Amplifier is connected⁴. The output voltage of the Step-Up Converter is at this location, so the iC-HSB Drivers are also connected to the same location. The operation of this device is also described later in this section.

The output voltage can be programmed using the resistor divider between the output and the FB pin. Indeed, as the constant value R_{Second} resistor is substituted by the variable $R_{Rheostat}$ resistor which is the MCP4562 Single Rheostat, it is now possible to program the output voltage to the desired value. As the resistors are chosen so that the voltage on the FB pin is always 1.26V, the following equation can be written:

$$R_{Rheostat} = \frac{1.26V \times R21}{V_{out} - 1.26V} = \frac{1.26V \times 4.53k\Omega}{V_{out} - 1.26V} \quad (3.13)$$

where $R21 = 4.53k\Omega$ is the resistance between the output voltage and the feedback pin and $R_{Rheostat}$ is the variable resistance between the feedback pin and the GND. Thanks to the Rheostat, which is a variable resistor, it is, therefore, possible to program the desired output voltage.

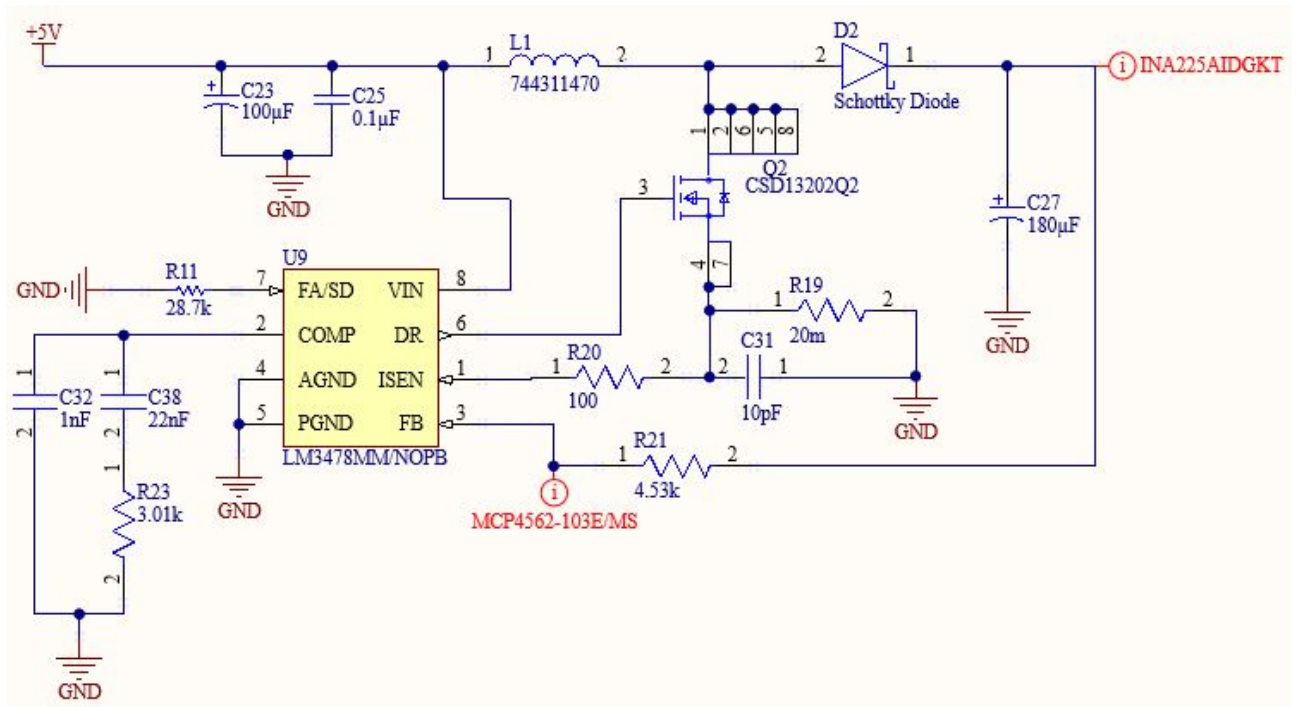


Figure 3.3: Electrical schematic of LM3478 Step-Up Converter.

The function of each of the last pins shown in figure 3.3 is as follows:

- FA/SD Pin: This pin is used to adjust the switching frequency of the device. This frequency can be adjusted between 100 kHz and 1 MHz using a single external resistor. This resistor is connected between this pin and GND. To calculate its value, the equation $R11 = 4.503 \times 10^{11} \times f_s^{-1.26}$ is

³The connection is made at the location of the (i) MCP4562-103E/MS indicator.

⁴The connection is made at the location of the (i) INA225AIDGKT indicator.

used. The resistance is therefore $28.7\text{ k}\Omega$ in order to have a switching frequency $F_s \approx 515\text{ kHz}$. This pin also functions as a shutdown pin. A high-level signal ($> 1.35\text{ V}$) for more than $30\text{ }\mu\text{s}$ will turn the device off which reduces the total supply current to the IC to less than $10\text{ }\mu\text{A}$.

- **AGND and PGND Pins:** These are the analogue GND pin and the power GND pin respectively. These pins are connected to the same GND at a single point to avoid GND loop currents, *i.e.* currents that cause noise or interference when the two pins are connected to GND by different paths.
- **COMP Pin:** This pin is a compensation pin. Any DC-DC converter that regulates the output voltage uses a negative feedback loop to ensure good accuracy. In order to provide compensation for this feedback loop, a combination of a resistor and capacitor is connected to this pin. An incorrect compensation scheme can result in a phase reversal of the loop, causing positive feedback and therefore an uncontrolled and inaccurate output. A 22 nF capacitor is connected in series with a $3.01\text{ k}\Omega$ resistor. Another 1 nF capacitor is placed in parallel with the other two components. The assembly is then connected to the GND. The values chosen are those recommended in the datasheet.

As mentioned earlier, the **Step-Up Converter** is connected to two other devices. Indeed, in figure 3.3 above, the **Step-Up Converter** is connected to a single **Rheostat** and a **Current Sense Amplifier**⁵. These two devices are described below.

The first device is therefore the **MCP4562** [72] and its electrical schematic is illustrated in figure 3.4. The device uses the I²C interface and supports 7-bit resistor networks and rheostat pinouts.

Firstly, in this project, this device acts as a **Single Digital Rheostat**. The **Rheostat** is a two-terminal variable resistor that is connected in series. It is used to control the flow of electric current by increasing or decreasing the resistance while keeping the voltage constant. But it can also be used to control the output voltage by increasing or decreasing the resistance while keeping the flow of electric current constant. The fact is that a current in an electric circuit depends on both the voltage applied in the circuit and the total resistance of the circuit. On the one hand, according to Ohm's law [73], to increase the current flow in the circuit, the resistance of the circuit must be reduced. On the other hand, to decrease the current flow in the circuit, the resistance of the circuit must be increased. The same principle, based on Ohm's law, is applied to vary the voltage.

It is therefore thanks to this **Rheostat** that it is possible to control the current flow in the overall circuit of this project.

Next, the I²C protocol is available because the SDA and SCL pins are available on this **Rheostat**. It is by using the I²C interface, and therefore not manually, that it is possible to modify this variable resistance.

Finally, the V_{DD} pin of this device is the positive input supply. This supply at the V_{DD} pin is a 5 V voltage. The input power supply is relative to the V_{SS} pin which is the GND reference of the device. There is a $0.1\text{ }\mu\text{F}$ decoupling capacitor between the 5 V and the GND.

⁵The connections are made at the locations of the ⓘ indicators.

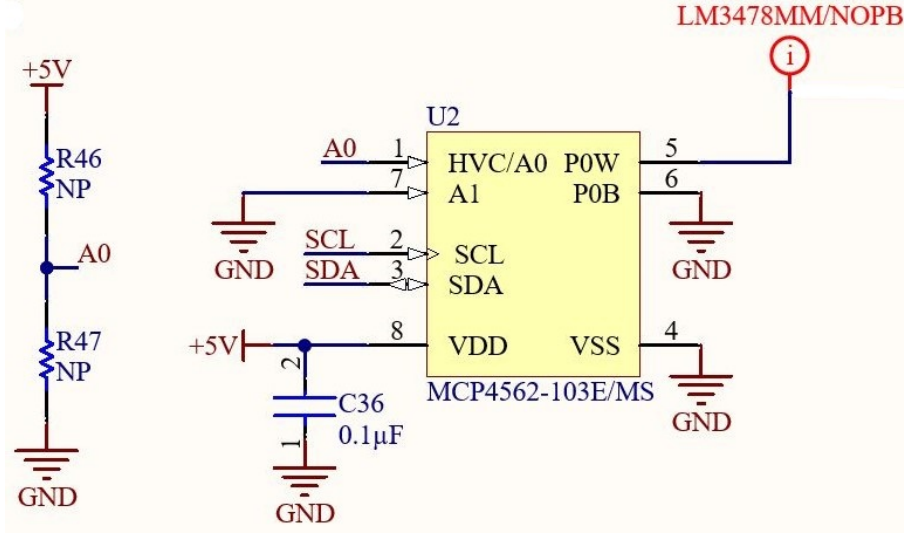


Figure 3.4: Electrical schematic of MCP4562 Single Digital Rheostat.

The function of each of the other pins shown in figure 3.4 is as follows:

- **A0 and A1 Pins:** These are the two pins that are used to specify the address of that device. The A0 pin corresponds to bit 0 of the address and the A1 pin to bit 1. They are therefore used for the I²C interface. In the figure, A1 is connected to GND and is therefore in the low state (0). For pin A0, there are two resistors $R46$ and $R47$ that have no value, *i.e.* they are unpopulated, and so initially, no resistors are placed on the PCB at these non-populated locations. When selecting the address for the **Rheostat**, a single 0Ω resistor is placed for $R47$ resistor. This resistor, therefore, forms a shortcut to GND. The status of pin A0 is therefore low (0). The I²C address of this device is $0x2C$.
- **P0W Pin:** This pin is connected to the “W” terminal of the internal **Rheostat**. It corresponds to the wiper of the **Rheostat**. This pin can carry both positive and negative current as it has no polarity to the other terminals. The voltage on the “W” terminal is always between V_{DD} and V_{SS} . The “W” terminal is therefore the adjustable terminal that is connected to the wiper and therefore changes the value of this variable resistor. It is through this pin that the connection is made between the **Rheostat** and the **Step-Up Converter**.
- **P0B Pin:** This pin is connected to the B terminal of the internal **Rheostat**. It corresponds to the permanent connection to the zero value of the **Rheostat** wiper, *i.e.* the lowest value of the resistance. This pin can also carry positive and negative current as it has no polarity to the other terminals. As with the “W” terminal, the voltage on the “B” terminal must be between V_{DD} and V_{SS} . P0B Pin is connected directly to GND.

As mentioned in the description of the **Step-Up Converter** above, the output voltage is programmable thanks to the variable resistance. Indeed, with the equation 3.13, it is possible to calculate the value of the resistance of the **Rheostat**, $R_{Rheostat}$, necessary to have the required output voltage. However, for all the tests, the **Rheostat** is programmed to have a resistance of $1\text{ k}\Omega$ as for the R_{Second} resistance of the equation 3.12. This device was therefore added in case it became necessary to change the supply voltage of the **iC-HSB Drivers**.

The second device is the INA225 [74] and its electrical schematic is illustrated in figure 3.5. This device is a **Current Sense Amplifier**, also called a **Current Shunt Monitor**. It is designed to monitor the current flow in both directions by measuring the common-mode voltage drop across a sensing element which is a shunt resistor.

First and foremost, the common-mode voltage refers to the average voltage applied to the amplifier inputs. This **Current Sense Amplifier** supports common-mode voltages ranging from 2.7 V to 36 V while operating on a 5 V supply. Indeed, the voltage applied to the V_S supply terminal is 5 V. The CMRR, *i.e.* the ability of the device to reject common-mode signals, is 105 dB. This CMRR is high which means that the current sense amplifier can detect a tiny common-mode signal [64]. A 0.1 μ F decoupling capacitor placed between the 5 V pin and GND is required for stability. As far as current is concerned, this device supports a maximum current, *i.e.* the full-scale current I_{MAX} , of 2 A.

Furthermore, there are four discrete gain levels that can be selected via the two pins GS0 and GS1. For each of these two pins, two valueless, *i.e.* non-populated, resistor slots are placed on the PCB. Depending on the selected gain, the appropriate resistors are added to the PCB. The selected gain is that of 25 V/V. Consequently, a shortcut is required between pin GS0 and the GND and another shortcut between pin GS1 and GND. Therefore, a 0Ω resistor is placed to the $R30$ and $R31$ resistors.

Finally, as mentioned previously, a sensing element which is a shunt resistor is used [75]. This resistor is connected to the terminals IN+ which is on the supply side of the shunt resistor and IN- which is on the load side, *i.e.* the three **iC-HSB Drivers** that supply the nine **Laser Diodes**, of the shunt resistor. It generates a slight voltage drop when current flows through it. This is based on Ohm's law. Varying the value of the shunt resistor has an impact:

- Increasing its value increases the differential voltage developed across it when current flows through it. However, it also increases the power that is dissipated across it.
- Decreasing its value reduces the power dissipated across it. However, this increases the measurement errors resulting from the decrease in the input signal.

Consequently, several factors come into play in order to calculate the maximum value of the shunt resistor. These factors are the maximum current to be measured (full-scale current), the maximum output voltage of the circuit (full-scale output voltage) that follows this device and the gain of the selected device. The full-scale current I_{MAX} is 2 A, the full-scale voltage output V_{out} is 5 V and the selected gain is 25 V/V. Therefore, the ideal maximum differential input voltage is:

$$V_{Diff} = \frac{V_{out}}{Gain} = \frac{5V}{25V/V} = 0.2V \quad (3.14)$$

Using this value, the shunt resistor value is calculated as follows:

$$R_{Shunt} = \frac{V_{Diff}}{I_{MAX}} = \frac{0.2V}{2A} = 100m\Omega \quad (3.15)$$

Therefore, the power dissipation of the shunt resistor is:

$$P_{Shunt} = R_{Shunt} \times I_{MAX}^2 = 100m\Omega \times 2^2 A = 400mW \quad (3.16)$$

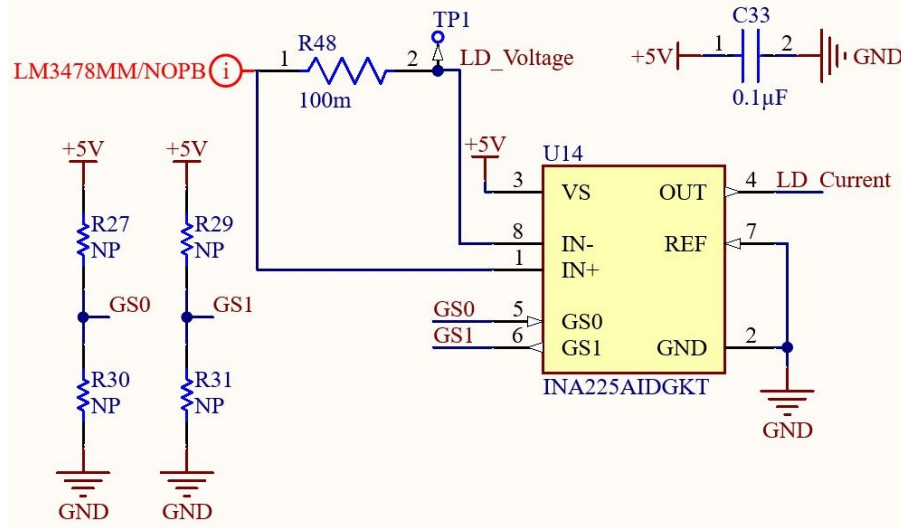


Figure 3.5: Electrical schematic of INA225 Current Sense Amplifier.

Some clarification of some of the pins in figure 3.5 above is necessary:

- **IN+ Pin:** It is through this pin that the connection is made between the **Current Sense Amplifier** and the **Step-Up Converter**.
- **IN- Pin:** It is through this pin that it is possible to get indications on the supply voltage value of the three **iC-HSB Drivers**. In fact, this pin is connected to the VB pin of each of the three **iC-HSB Drivers** explained in section 3.2.5. This, therefore, supplies the three **iC-HSB Drivers** with the desired voltage and current which is managed by the **Rheostat**. It is also connected to the **Arduino Nano 33 IoT** explained in section 2.3 to control possible errors. It is essential to avoid overvoltage in the circuit, hence the importance of controlling the supply voltage.
- **OUT Pin:** It represents the output voltage. Like the IN- pin, it is through this pin that it is possible to get indications of the value of the current flowing in the circuit. It is connected directly to the **Arduino Nano 33 IoT** because the **INA225** is a current amplifier, so the current flowing through this device is the current flowing through the drivers. It is essential to avoid overcurrent in the circuit, and this is why this current control is important.
- **REF Pin:** It represents the reference voltage which is connected directly to GND.

In addition, there is a **S275I-46R Test Point [76]** (TP1 in figure 3.5) which is connected directly to the three **iC-HSB Drivers**. This allows the circuit to be externally supplied directly with the desired voltage and current. Indeed, in a first step, several tests explained in chapter 4, are performed with an external power supply in order to subject a voltage and a current in a very precise way to the **iC-HSB Drivers** and thus the laser diodes. Once these first verification tests are done, this **Test Point** is no longer used.

3.2.3 TPS82085 Step-Down Converter

As explained in section 3.2.1, the power supply is 5 V. However, some devices need a 3.3 V supply and others need 1.8 V. It is therefore essential to have step-down converters, also called buck converters, for the proper functioning of this project.

The step-down converters used in this project are the **TPS82085 High-Efficiency Step-Down Converter** [77]. The latter has some interesting features.

Firstly, the TPS82085 is an optimised **Step-Down Converter** with a small size and high-efficiency. The power module consists of a synchronous step-down converter and an inductor to simplify the design, reduce the number of external components and save PCB space. Therefore, the necessary power inductor is integrated into the device. The inductance has a value of 0.47 μH .

Then, to maximise efficiency, the **Step-Down Converter** operates in Pulse Width Modulation (PWM) mode for medium to heavy load conditions with a nominal switching frequency of 2.4 MHz. It can automatically switch to Power Save Mode (PSM) for light load currents. As the load current decreases, the switching frequency also decreases. Using the DCS-Control topology (Direct Control with Seamless transition into Power Save Mode), the device achieves excellent load transient performance and precise output voltage regulation, combined with low output voltage ripple.

Finally, it is robust and reliable due to overtemperature protection and shortcut protection. There is also a switching current limitation that prevents the device from having a high inductance current. Excessive current can occur in the event of a high load or shorted output circuit.

The function of each of the pins of the **Step-Down Converter** that are used is as follows:

- V_{in} Pins: These pins correspond to the input voltage. The range of this voltage is [2.5: 6 V]. In this project, the input voltage on these pins is 5 V.
- EN Pin: This is the activation pin. It can either be pulled up to activate the device or pulled down to deactivate it. This pin has an internal pull-down resistor of 400 k Ω when the device is disabled. It is connected, *i.e.* shorted, to the input supply voltage of 5 V. This activates the device and the pull-down resistor is therefore disconnected.
- FB Pin: This is the feedback reference pin. An external resistor divider connected to this pin programs the output voltage. This pin is therefore connected between two resistors but this is explained below. The typical feedback control voltage for PWM and PSM modes is 0.8V.

The output voltage, V_{out} of each **Step-down Converter** is set by an external resistor divider [78]. The value of the resistors in figures 3.6 and 3.7 is calculated respectively in equations 3.17 and 3.18 below. Note that the resistors $R4$ and $R10$ should not be greater than 180 k Ω so that sufficient high current flows through them. This improves the sensitivity to noise and the accuracy of the output voltage. As previously stated, the FB pin, *i.e.* the feedback reference pin, has a typical voltage of 0.8V.

For the first **Step-Down Converter**, to have an output voltage of 3.3 V, the calculation is as follows:

$$\begin{aligned}
 V_{out} &= V_{FB} \times \left(1 + \frac{R3}{R4} \right) \\
 \Leftrightarrow 3.3 &= 0.8V \times \left(1 + \frac{R3}{R4} \right) \\
 \Leftrightarrow R3 &= 31.25k\Omega \quad \text{and} \quad R4 = 10k\Omega
 \end{aligned}
 \tag{3.17}$$

There are of course other possible resistor combinations to achieve an output voltage of 3.3 V. However, these are simple resistor values to be found on the market and have been chosen.

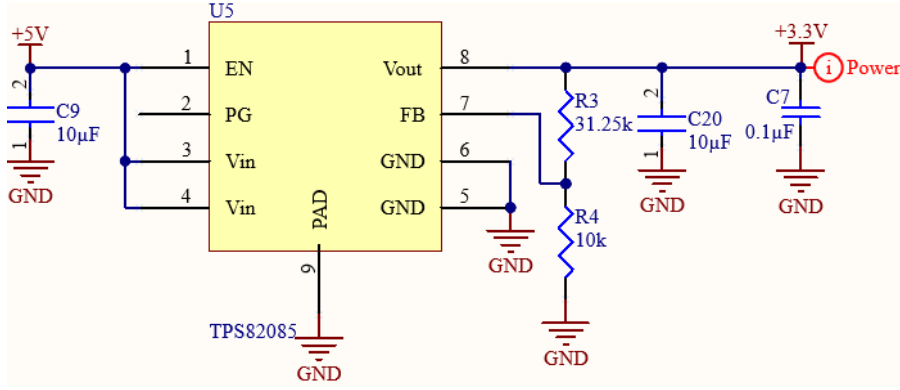


Figure 3.6: Electrical schematic of the first TPS82085 Step-Down Converter: 5 V \rightarrow 3.3 V.

For the second **Step-Down Converter**, to have an output voltage of 1.8 V, the calculation is as follows:

$$\begin{aligned}
 V_{out} &= V_{FB} \times \left(1 + \frac{R9}{R10} \right) \\
 \Leftrightarrow 1.8V &= 0.8V \times \left(1 + \frac{R9}{R10} \right) \\
 \Leftrightarrow R9 &= 200k\Omega \quad \text{and} \quad R10 = 160k\Omega
 \end{aligned}
 \tag{3.18}$$

There are of course other possible resistor combinations to achieve an output voltage of 1.8 V. However, these are simple resistor values to be found on the market and have been chosen.

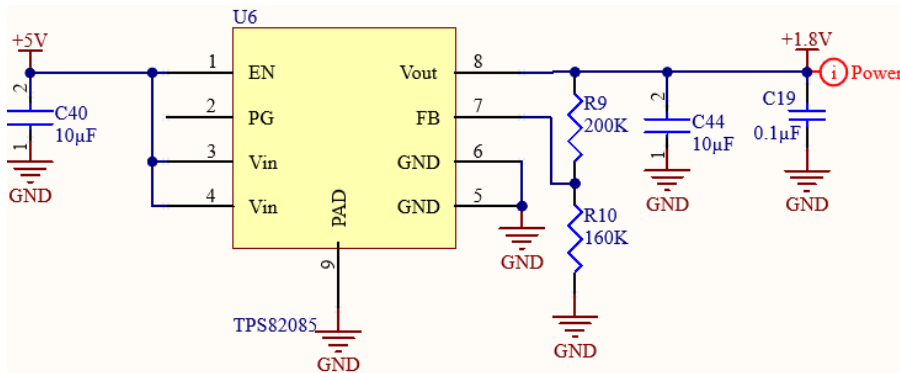


Figure 3.7: Electrical schematic of the second TPS82085 Step-Down Converter: 5 V \rightarrow 1.8 V.

As shown in the figures above, input and output capacitors are present as with the **Step-up Converter**. This is because, for optimal filtering of the input and output voltages, capacitors are required.

The input capacitor of each **Step-Down Converter** ($C9$ for the first and $C40$ for the second) minimises input voltage ripple and suppresses input voltage spikes. These input capacitors are therefore necessary and have a value of $10\text{ }\mu\text{F}$ as indicated in the datasheet.

The output capacitor of each **Step-Down Converter** ($C20$ for the first and $C44$ for the second) is also used to play the same role as the input capacitor but this time at the output of the converter. These output capacitors are therefore needed as well and have a typical value of $10\text{ }\mu\text{F}$.

There is also a decoupling capacitor between the 3.3 V or 1.8 V supply voltage, depending on **Step-Down Converter** ($C7$ for the first and $C19$ for the second), and the GND. These capacitors have a value of $0.1\text{ }\mu\text{F}$.

3.2.4 PLT5 450B Laser Diodes

As mentioned earlier, the choice of the laser diodes used in this project is PLT5 450B [43]. The general operation of a laser diode is explained in section 1.1.2. The advantages of using a **Laser Diode** over a LED are detailed in section 1.1.3. These **Laser Diodes** are chosen because of their characteristics. The characteristics of the PLT5 450B **Laser Diode** are as follows:

- The optical output power, P_{opt} , which is the energy per unit time carried by the laser beam from a single **Laser Diode**, is 100 mW ⁶ at a temperature of 25°C . The peak output power can however reach 120 mW .
- The range of the emission wavelength, λ_{peak} , is $[440: 460\text{ nm}]$ and the typical value is 450 nm . This wavelength belongs to the visible radiation range and corresponds to blue light.
- The range of the operating current, I_{op} , is $[90: 165\text{ mA}]$. For this project, the forward current, I_f , which is the amount of current flowing through the **Laser Diode** when operating in direct polarisation, is 165 mA .
- The forward voltage, V_f , which is a positive voltage applied between the anode of the **Laser Diode** and its cathode, is typically 5.5 V and can be as high as 7 V . For this project, the forward voltage is 7 V .
- The threshold current, I_{th} , is typically 17 mA and can be as high as 60 mA . the threshold current is approximately 18 mA for the laser diodes which constitute the new laser source.

One of the two objectives of this project is to obtain an optical laser source with high power. This is why there are nine **Laser Diodes** for the making of this laser. This gives a total output power of up to 900 mW when all nine **Laser Diodes** are focused on a single point. Great care must therefore be taken when carrying out the tests.

⁶ $100\text{ mW} = 0.1\text{ J/s}$.

For a single **Laser Diode**, the total power dissipation in the worst condition operates when the forward current is maximum (165 mA) and the forward voltage is also maximum (7 V). In this situation, the total power dissipated by a single laser diode is:

$$P_{1 \text{ diode}} = V_f \times I_f = 7 \times 0.165 = 1.155W \quad (3.19)$$

However, when the nine **Laser Diodes** are operated at the same time, the total power dissipated is:

$$P_{9 \text{ diodes}} = 9 \times P_{1 \text{ diode}} = 9 \times 1.155 = 10.395W \quad (3.20)$$

The power dissipation is therefore very high. This has major consequences for thermal dissipation, which is explained in detail in section 3.4.

As indicated in the characteristics of **Laser Diodes**, they are highly convergent. Indeed, the PLT5 450B **Laser Diode** has a beam divergence parallel to the P-N junction, $\Theta_{//}$, of typically 6.5° . The following figure 3.8 illustrates this beam divergence ⁷.

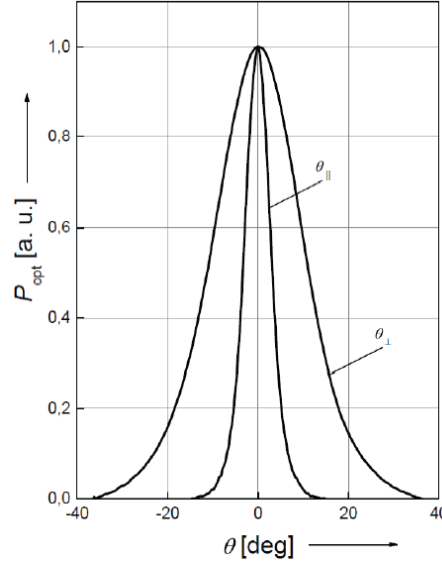


Figure 3.8: Beam Divergence: $P_{opt} = f(\Theta)$; $T = 25^\circ C$ [43].

Each of the **Laser Diode** is a light source whose intensity depends on the direction. This is also shown by the figure 3.8 above. From an angle of about 10° in one direction, the output power is almost zero. This light source is qualified as orthotropic, also known as Lambertian light source, as opposed to isotropic light sources which have a uniform light intensity in all directions. [79].

The current **iC-HSB Drivers**, described in section 3.2.5, are three in number. Each current **iC-HSB Drivers**, therefore, supplies three **Laser Diodes**. Placing twelve **Laser Diodes** connected to four current **iC-HSB Drivers** would not have been feasible due to the size constraint of the PCB. The different connections that are explained are for a single current **iC-HSB Driver** and therefore only three **Laser Diodes**. Indeed, the analysis is identical for the other two **iC-HSB Driver** and thus the other six **Laser Diodes**, which is therefore redundant.

⁷The atomic units (a.u.) on the graph form a system of units widely used to simplify formal or numerical calculations in quantum physics.

The internal electrical circuit of a Laser Diode is as follows:

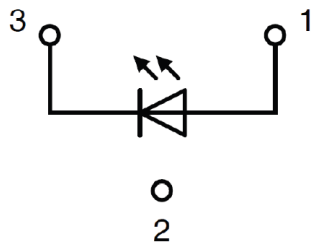


Figure 3.9: Electrical Internal Circuit [43].

- Pin 1 (LD1_A) is the anode: the anode of each Laser Diodes is connected to the pin Laser Diode Anode (LDA) of the iC-HSB Driver and the three anodes are thus connected to the same pin.
- Pin 2 is unused.
- Pin 3 (LD1_Kx⁸) is the cathode: the cathode of each Laser Diodes is connected to a pin Laser Diode Cathode (LDK) of the iC-HSB Driver and the three cathodes are thus connected to three different LDKx⁹ pins.

The block diagram of the current iC-HSB Driver consisting of all the pins is given in figure 3.11 and the electrical schematic of three Laser Diodes is presented in figure 3.10 below.

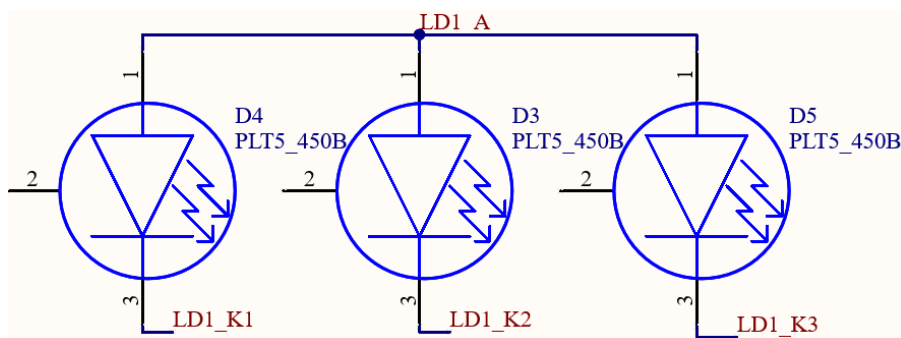


Figure 3.10: Electrical schematic of three PLT5 450B Laser Diodes (LD1 refers to the first driver).

⁸LD1_K1, LD1_K2 and LD1_K3.

⁹LDK1 (LD1_K1), LDK2 (LD1_K2) and LDK3 (LD1_K3).

3.2.5 iC-HSB Ultrafast Laser Drivers

To drive the Laser Diodes, the iC-HSB Ultrafast Laser Driver [46], whose block diagram is shown in figure 3.11, is used. This iC-HSB Driver is chosen because of its characteristics and applications. Indeed, this iC-HSB Driver is used for LIDARs as well as for the ToF principle, which is exactly one of the functions desired for the use of the optical laser source.

These iC-HSB Ultrafast Laser Drivers have several interesting features. These devices are extremely important in this project as it is through them that the laser source can be configured.

Firstly, in the event of overheating and overcurrent, the laser will turn off. Indeed, this project can be confronted with problems at the level of temperature and intensity. Another source of error is overenergy. There is also a safety feature for this. There is therefore a good security system for all current iC-HSB Drivers, which protects them fairly well. This is therefore an important point.

Then, the serial programming interface I²C is available. In the diagram in figure 3.11 are the pins SDA and SCL, which are essential for this project. An Low Voltage Differential Signaling (LVDS) synchronisation output and an LVDS trigger input are also available.

Finally, the iC-HSB Driver has a permitted supply voltage of 3.3 V to 5 V. In this project, the input pin for the supply voltage, V_{DD} , is 3.3 V. The V_{DD} pin is typically connected to the output of the Step-Down Converter which is described in section 3.2.3. Parallel 0.1 μ F decoupling capacitors are connected to the V_{DD} pin. The output current range at the pins that supply the Laser Diodes, $I(LDKx)$, is [120: 200 mA]. This range is consistent with the fact that the Laser Diodes are supplied with a forward current of 165 mA.

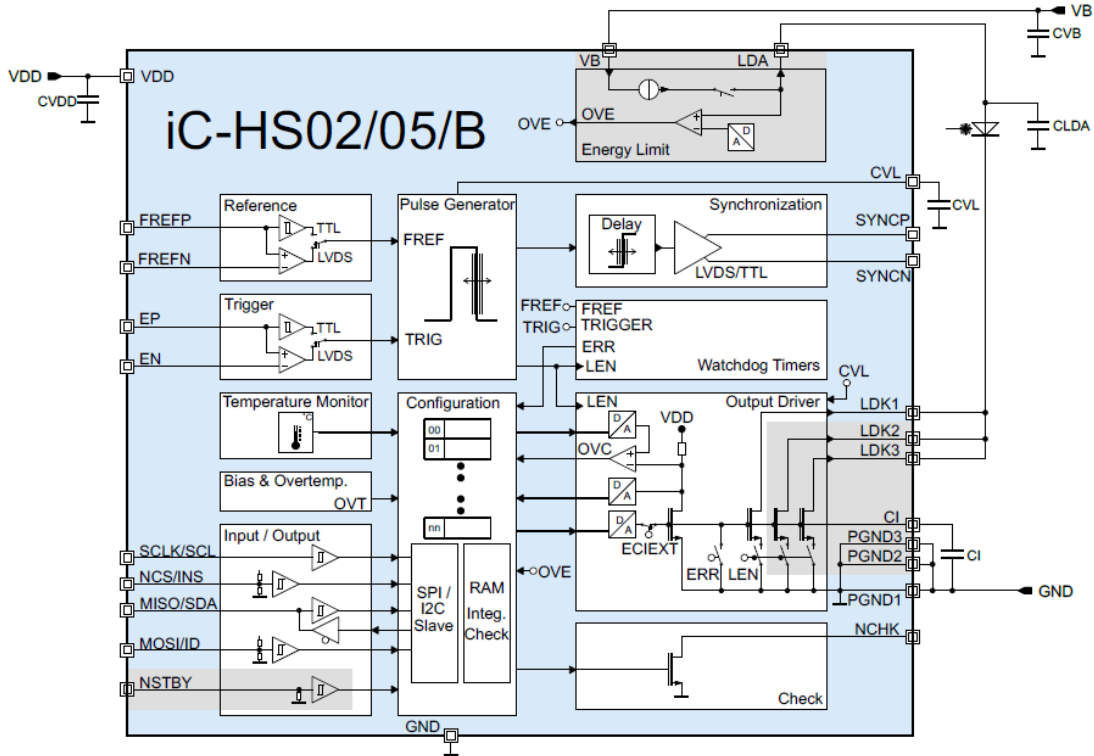


Figure 3.11: Block Diagram of iC-HSB Laser Driver [46].

However, all the pins are in use and each has a specific function. Their function is as follows (the name of each pin described below is as shown in figure 3.12):

- **CVL Pin:** Pin representing the logic supply voltage regulator. In normal mode, a 100 nF capacitor is connected to this pin and to the GND (value provided in the datasheet).
- **CI Pin:** The amplitude of the output current impulses is set through the **iC-HSB Driver** node CI. The IC voltage can be defined with the CI(9:0) register. Depending on this register, the output will drive the maximum current (range [120: 200 mA]) or minimum, typically 10% of the maximum current (range [5: 40 mA]). The current delivered by the output driver can be related to the value of CI(9:0) register with the following formula:

$$I(LDKx) = ILDKx_{min} + CI(9 : 0) \times \Delta ILDKx \quad (3.21)$$

where $ILDKx_{min}$ is the output current when CI(9:0) is defined at its lowest value, and $\Delta ILDKx$ is the current increment of 1 LSB in CI(9:0). A 100 nF capacitor is connected to this pin and to the GND (value provided in the datasheet).

- **EN and EP Pins:** Pins representing the negative and positive triggering of the LVDS input. The trigger signal for laser activation is input on these two pins. These inputs enable differential LVDS mode. The maximum input frequency is 200 MHz. These pins are connected by differential pairs to the first **LMK00301 Differential Clock Buffer** which is described in section 3.2.8.
- **FrefN and FrefP Pins:** Pins representing the negative and positive reference frequency of the LVDS input. A reference frequency clock for the impulse generator is provided on these pins. These inputs enable differential LVDS mode. The maximum input frequency is 200 MHz. These pins are connected by differential pairs to the second **LMK00301 Differential Clock Buffer** which is described in section 3.2.8.
- **SyncN and SyncP Pins:** These outputs generate a differential impulse for each impulse generated by the output **iC-HSB Driver**. This impulse can be used for synchronisation in ToF applications. Each of these pins is connected to a **U.FL Coaxial Connector** which are described in section 3.2.7.
- **LDA Pin:** As explained in the previous section, the LDA pin of each **iC-HSB Driver** is connected to the anode of each of the three **Laser Diodes**. A 47 nF **CLDA** capacitor is connected to this pin and to the GND (value provided in the datasheet). The **iC-HSB Driver** includes an energy limiting circuit for safety. It is through the **CLDA** capacitor that the pulsed laser current is supplied. This capacitor is charged with a programmable constant current source supplied by the VB pin, as shown in figure 3.11. The energy available to the laser is established by the current supplied to the **CLDA** capacitor. When **CLDA** supplies the laser current, it starts to discharge and so there will be a voltage drop at LDA. The magnitude of this voltage drop depends on the amplitude and length of the output current impulse. If the average current demand of the **Laser Diodes** is greater than the current supplied by the LDA pin, the laser will turn off because the voltage at the LDA pin generated by the capacitor will decrease.
- **VB (LD_Voltage) Pin:** Pin representing the supply voltage of the energy limit. As mentioned in the previous point (LDA Pin), the VB pin provides a constant current source which charges the **CLDA** capacitor. Indeed, the VB pin is connected to **Step-Up Converter**. As explained in section 3.2.2, the output voltage and output current of the **Step-Up Converter** are initially

7 V and 2 A. The voltage at the VB pin is therefore 7 V which is acceptable as the permissible voltage range at VB is [3.5: 15 V]. This is the same permissible voltage range for the LDA pin. The VB pin is also connected to **Arduino Nano 33 IoT** (section 3.2.9). A 4.7 μF CVB capacitor is connected to this pin and to GND which is the value provided in the datasheet.

- **NCHK Pin:** Pin representing the check request. Several errors can prevent the driver from working properly (overheating, CI pin overvoltage, LDKx pin overcurrent, etc.). All these errors are signalled at the open-drain output NCHK. This pin is connected directly to the **Arduino Nano 33 IoT**.
- **NSTBY Pin:** Pin representing the stand-by mode. The **iC-HSB Driver** has a low power consumption sleep mode. Thanks to this pin it is possible to use this stand-by mode. This pin is connected directly to the **Arduino Nano 33 IoT**.
- **ID Pin:** Thanks to this pin it is possible to have different addresses for the **iC-HSB Drivers** which are the slaves in the I²C protocol. Indeed, on figure 3.12, resistors $R4$ and $R5$ have no value (they are non-populated). Initially, no resistors are placed on the PCB at these non-populated locations. It is only afterwards, when the addresses are chosen, that the resistors are placed. Depending on the value of these resistors, the drivers have different addresses (an identification code (ID)). The datasheet shows the four different possible addresses. The first is when $R6$ resistor is at $0\ \Omega$ and $R5$ resistor is not placed. The ID pin is then directly connected to the GND. The second is when $R5$ resistor is at $0\ \Omega$ and $R6$ resistor is not placed. The ID pin is then directly connected to the V_{DD} . The third is when $R5 = 10\ \text{k}\Omega$ and $R6 = 6.6\ \text{k}\Omega$. The last one is when $R5 = 6.6\ \text{k}\Omega$ and $R6 = 10\ \text{k}\Omega$. The last two possibilities are therefore the formation of a voltage divider bridge.

All of what is mentioned in this section applies exactly to the other two **iC-HSB Drivers**. A representation of the electrical schematic of an **iC-HSB Driver** is shown in figure 3.12 below (appendix A for the representation of the other two).

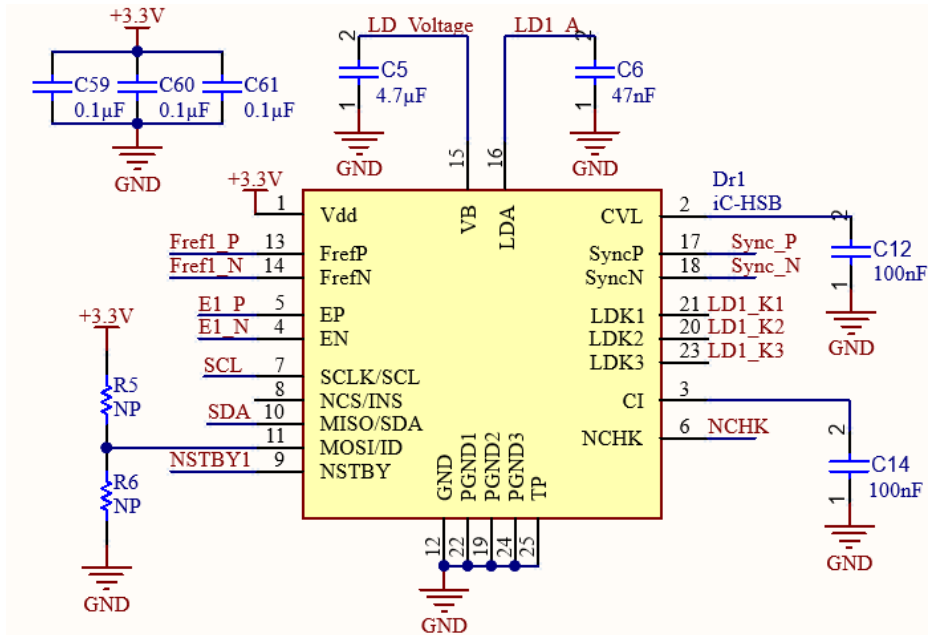


Figure 3.12: Electrical schematic of iC-HSB Laser Driver.

In the case of this project, three I²C addresses are therefore chosen:

- **iC-HSB Ultrafast Laser Driver 1:** The two resistors are $R5$ and $R6$. The value of the resistor $R6 = 0\Omega$ and no resistor is placed on the PCB for $R5$. The ID pin is then directly connected to the GND. This gives an I²C address that is $0x70$ for this iC-HSB Ultrafast Laser Driver 1.
- **iC-HSB Ultrafast Laser Driver 2:** The two resistors are $R24$ and $R26$. The resistor values are $R24 = 10\text{ k}\Omega$ and $R26 = 6.6\text{ k}\Omega$. Pin ID is therefore connected to both GND and V_{dd} , forming a voltage divider bridge. This gives an I²C address that is $0x71$ for this iC-HSB Ultrafast Laser Driver 2.
- **iC-HSB Ultrafast Laser Driver 3:** The two resistors are $R35$ and $R37$. The resistor value $R35 = 0\Omega$ and no resistor is placed on the PCB for $R37$. The ID pin is then directly connected to the V_{DD} . This gives an I²C address that is $0x73$ for this iC-HSB Ultrafast Laser Driver 3.

The addressing of the devices is discussed in detail in section 3.5.

3.2.6 Si5340 Clock Generator

To generate signals at a specific frequency, a frequency generator is used. In this project, an external frequency generator to the PCB is used. However, a frequency generator internal to the PCB will be required when the laser source will be integrated onto the interface board containing the FPGA module. For this reason, a frequency generator is included in the PCB circuit schematics.

A frequency generator, also called clock generator, is an electronic oscillator that produces a clock signal used to synchronise the operation of a circuit. A clock generator is always composed of a Phase Lock Loop (PLL). A PLL is an electronic circuit made up of analogue and digital components, including a Voltage Controlled Oscillator (VCO) that constantly adjusts to match the frequency of an input signal.

The main purpose of a PLL circuit is to synchronise the frequency of an oscillator output signal to a reference signal. Hence, a PLL reduces the phase errors between the output and input frequencies. When the phase difference between the two signals is zero, the system is said to be “locked”. A PLL helps to achieve both frequency and phase locks in a circuit [80].

In the framework of this project, the clock generator is the Si5340 [81]. As can be seen in figure 3.13, the block diagram of the PLL found in the Si5340 Clock Generator consists of a fractional feedback voltage divider, a phase detector, a low pass filter and a VCO [64]. A frequency signal is generated by dividing the output frequency using a frequency divider circuit. This signal is compared to the input reference signal by the phase detector. The output voltage of the phase detector is a function of the phase difference of the two input signals, *i.e.* the reference input signal and the output signal of the VCO. This is where the frequency divider is useful as the input reference signal is often at a lower frequency than the VCO output signal. The frequency divider, therefore, reduces the frequency of the output signal before the phase detector makes the comparison. The low-pass filtered output of the phase detector is used to control the frequency of the oscillator (VCO). It is also possible to see that there is a zero delay mode connected to the PLL. This mode, which is described later in this section, is used in this project.

The **Clock Generator** included in the electrical schematic of this project has some useful features. These characteristics can be observed in figure 3.13.

First and foremost, the main feature of the **Clock Generator** is that it generates any combination of output frequencies from any input frequency. It has four inputs and four outputs. Each input/output is represented by two pins. In this project, all four outputs are used but only one input is needed. The two pins of the only input used are connected to **Crystal Clock Oscillator**. This has a standard frequency range of [7: 80 MHz]. However, the supply voltage, V_{DD} , is 1.8 V for this **Crystal Clock Oscillator** in this project. The frequency range is thus [20: 50 MHz] [82]. With this input frequency range, the output frequency range is [100 Hz: 350 MHz]. The connections between the pins are described later in the section.

Secondly, the **Clock Generator** uses MultiSynth technology to provide the most flexible frequency clock generator. The PLL locks to an external input on pins IN0 and IN0B. The external input is the **Crystal Clock Oscillator**. The input frequency of the **Crystal Clock Oscillator** is divided by the MultiSynth stage and some output integer dividers as shown in the diagram. The function of the PLL is to phase lock to the selected input and provide a common reference for all the output MultiSynth dividers. High-resolution MultiSynth fractional dividers allow true input at any frequency to any frequency on any output. The output drivers offer flexible output formats that are independently configurable on each output. Additional dividers provide additional frequency division if required.

Afterwards, the I²C protocol is feasible as the SDA and SCL pins are available on this **Clock Generator**. However, for this device, one pin is used to select the I²C mode. Indeed, in addition to having the SDA and SCL pins, the I2C_SEL pin must select the serial interface mode as I²C by setting I2C_SEL = 1 (high state). This pin is pulled high internally by a $\approx 20\text{ k}\Omega$ resistor. This device has an I²C address that is $0x76$. In terms of supply voltages, the VDDAx¹⁰ pins of the core supply require a 3.3 V power source. The core of the device operates from a supply voltage of 1.8 V (VDDx¹¹ pins). The supply voltage for the OUTx¹² outputs is also 3.3 V. For each of these supply voltages, a 1 μF decoupling capacitor is connected.

Lastly, a zero delay mode is available. This mode is configured by opening the internal feedback loop and closing it externally. It is used for applications that require a fixed and constant minimum delay between the input and selected outputs. The purpose of this mode is to eliminate all possible internal delays that are introduced by the different stages of the **Clock Generator**, *i.e.* dividers, crosspoint, input and output drivers. The connections made for this zero delay mode are explained later in the section.

¹⁰VDDA1 and VDDA2.

¹¹VDD1, VDD2, VDD3 and VDD4.

¹²OUT0, OUT1, OUT2 and OUT3.

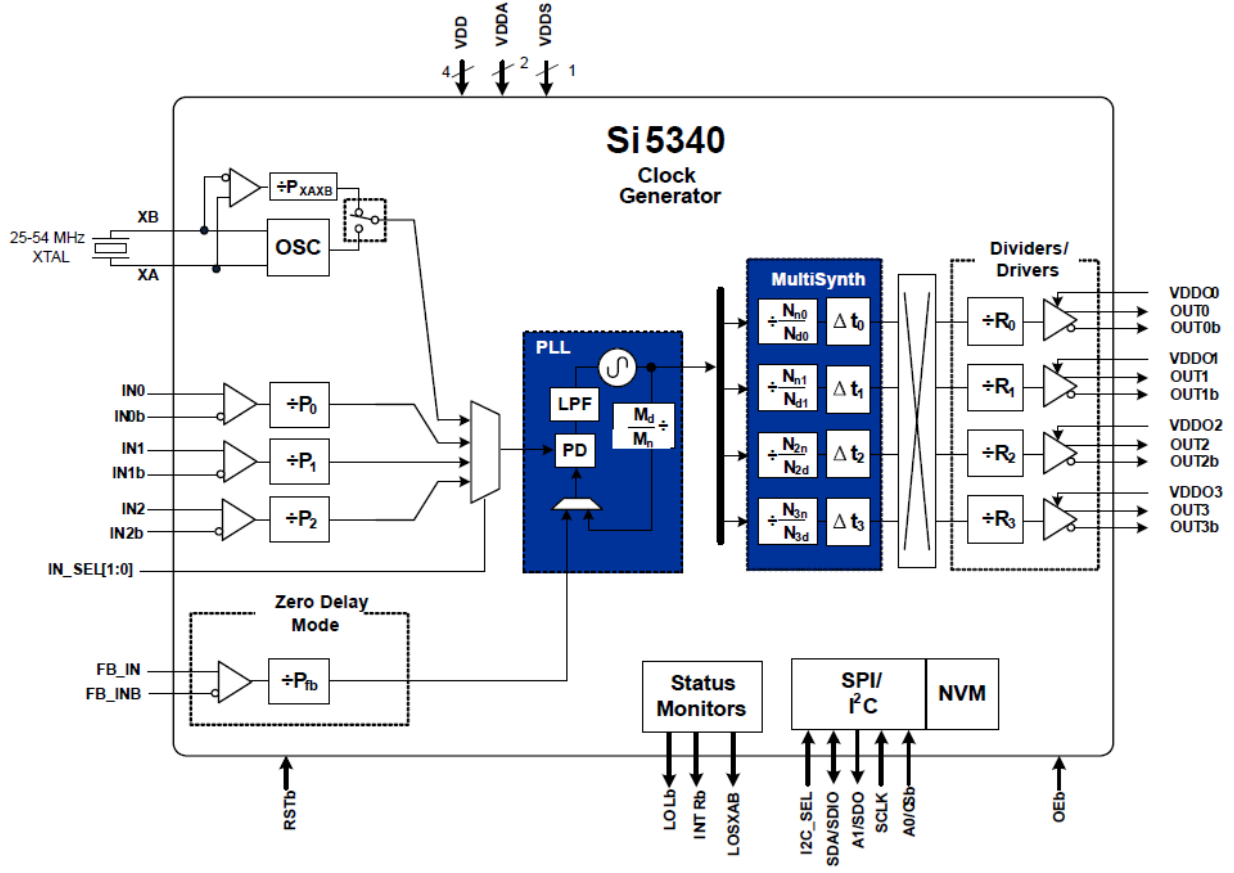


Figure 3.13: Block Diagram of Si5340 Clock Generator [81].

The different connections between the **Clock Generator** pins and the other devices are as follows (the name of each pin described below is as shown in figure 3.14):

- **IN0 and IN0B Pins:** As mentioned earlier, the PLL locks to an external input. This external input is the **Crystal Clock Oscillator**. The power supply, V_{DD} , of this **Crystal Clock Oscillator** is 1.8 V. For this supply, a 470 nF decoupling capacitor is connected to V_{DD} . The output pin of this **Crystal Clock Oscillator** provides a frequency in the range [20: 50 MHz] to the IN0 pin of the **Si5340 Clock Generator**. A 0.1 μ F coupling capacitor is placed in series with this connection. Since it is an asymmetrical clock that is applied to the IN0 pin, the IN0B pin is connected to GND. As recommended in the datasheet, a 0.1 μ F coupling capacitor is also placed between pin IN0B and GND.
- **IN_SEL0 and IN_SEL1 Pins:** These pins handle the selection of the input reference. Indeed, the IN_SELx pins are used in the manual pin control mode to select the active clock input. These pins are pulled high internally with a ≈ 20 k Ω resistor depending on the selected voltage and can be left unconnected when not in use. For the laser source conceived in this project, the only input that is selected is the IN0 input represented by the IN0 and IN0B pins. To select this input, the IN_SEL0 and IN_SEL1 pins must be in the low (0) state. To accomplish this, these two pins are shorted directly to GND.

- **A0 and A1 Pins:** These are the pins representing address selection. Indeed, the two address selection bits (A0, A1) are provided through these two pins. This allows four I²C address choices for the **Clock Generator** so that there is no overlapping I²C addresses. The A0 address input pin is pulled high internally by a $\approx 20\text{ k}\Omega$ resistor depending on the voltage selected. The A1 address input pin does not have an internal pull-up or pull-down resistor. The address chosen for this slave is *0x76*. For this address, the A0 bit is low (0) and the A1 bit is high (1). Therefore, pin A0 is shorted to GND while pin A1 is shorted to a 3.3 V supply.
- **OUT0 (Out2_Clk_P) and OUT0B (Out2_Clk_N) Pins:** These two pins represent an output clock. This output clock supports a programmable signal amplitude because it is configured as a differential output. Each of these two output pins is connected to a **Coaxial Connector** in order to be able to analyse the signals generated by the **Clock Generator** for other devices. The desired output signal is configurable through register control.
- **OUT1 (FrefPll_P) and OUT1B (FrefPll_N) Pins:** These two pins represent an output clock. This output clock supports a programmable signal amplitude because it is configured as a differential output. These two pins are connected to two inputs of the second **Differential Clock Buffer** to generate the desired output signal. This desired signal is the reference frequency clock for the impulse generator (FrefN and FrefP) which is configurable through register control.
- **OUT2 (EPll_P) and OUT2B (EPll_N) Pins:** These two pins represent an output clock. This output clock supports a programmable signal amplitude because it is configured as a differential output. These two pins are connected to two inputs of the first **Differential Clock Buffer** to generate the desired output signal. This desired signal is the trigger signal for laser activation which is configurable through register control.
- **OUT3 (Out3_Clk_P) and OUT3B (Out2_Clk_P) Pins:** As previously mentioned, a zero delay mode is available. Note that the FB_IN and FB_INb pins are used as external feedback inputs for the Si5340's zero delay mode. Any of the outputs can be fed back to the FB_IN (Feedback_Clk_P) and FB_INB (Feedback_Clk_N) pins. However, to minimise the input-output delay, the length of the tracks that are connected to these pins should be minimised. Pins OUT3 and OUT3B are therefore used to connect the FB_IN and FB_INB pins. The FB_IN and FB_INB input pins are terminated and AC-coupled when zero delay mode is used. A differential connection of the external feedback path is required for best performance.

As shown in the electrical diagram below, both load termination resistors and coupling capacitors are present. Indeed, to connect each of the clock outputs of the Si5340, a load termination resistor between the two tracks of the differential pairs is required. This resistor is equal to the global impedance of the circuit, *i.e.* $100\ \Omega$. The value of each of the coupling capacitors on each differential pair track is $0.1\ \mu\text{F}$.

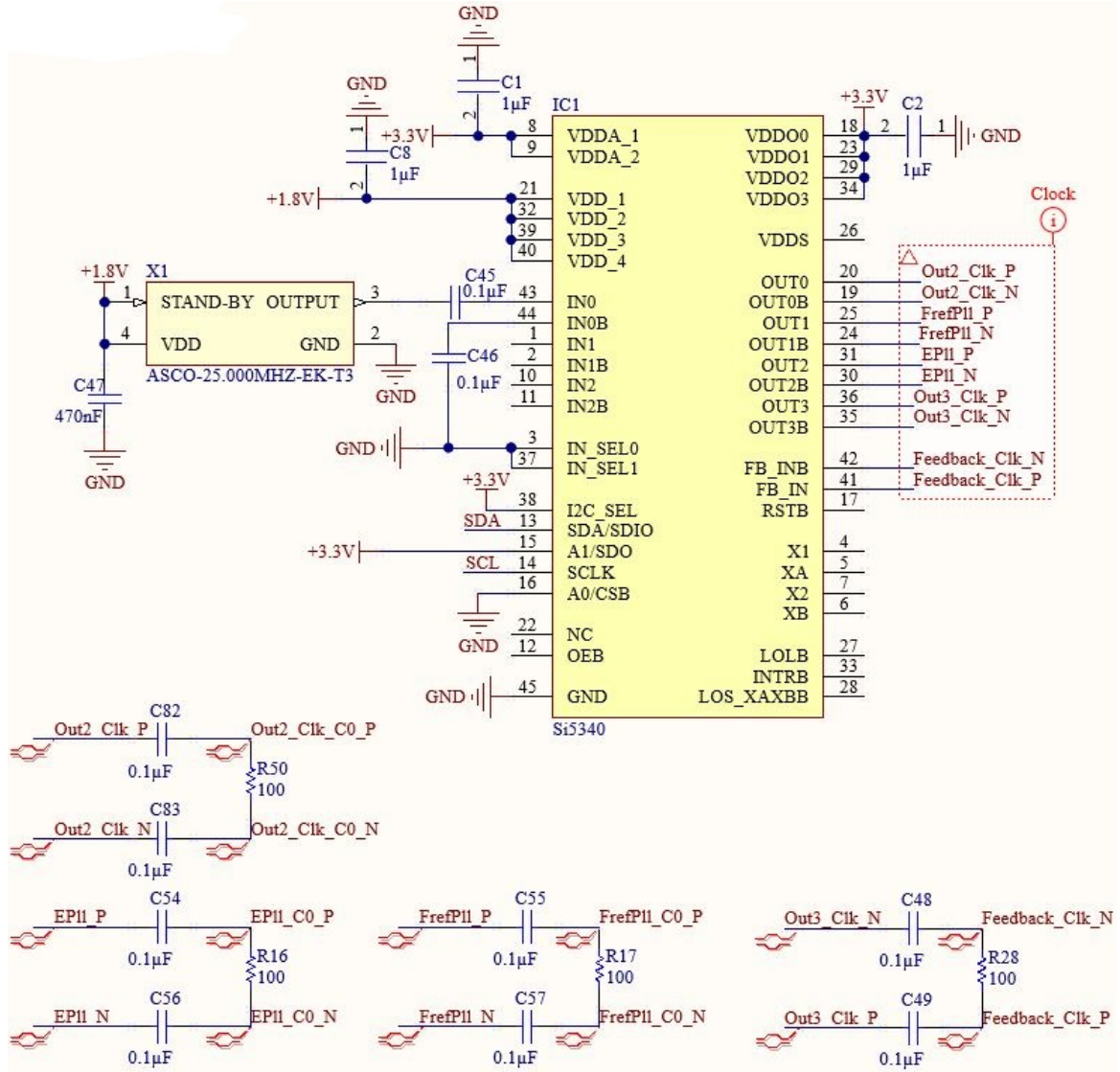


Figure 3.14: Electrical schematic of Si5340 Clock Generator.

3.2.7 Ultra Miniature Coaxial Connectors

Coaxial Connectors are metal objects that are used to terminate coaxial cables. In the framework of this project, they provide the connection between the PCB and an oscilloscope or between an external frequency generator and the PCB while maintaining an external shield against interference. A coaxial cable is secure against all types of noise and interference.

In this project, height Ultra Miniature Coax Connectors (UMCC)¹³ [83] are used. They play a role in the electrical communication system. The different connections are as follows:

- Two connectors are each connected to an output pin of a single iC-HSB Driver. The two pins connected are SyncN and SyncP which generate a differential impulse for each impulse generated by the output driver. These two Coaxial Connectors are used to display the individual differential impulses on the oscilloscope and then analyse them. It is therefore possible to analyse the signals at the output of the iC-HSB Driver.

¹³UMCC is equivalent to U.FL Coaxial Connector.

- Two connectors are each connected to a pin of the Si5340 Clock Generator. The two pins connected are OUT0 and OUT0B which are the output clock of the Clock Generator. These two Coaxial Connectors are used to visualize the clock signals of the Clock Generator output on the oscilloscope in order to analyse them.
- Two connectors are each connected to a pin of the first Differential Clock Buffer. The two pins connected are CLKIn0 and CLKIn0* which constitute the input clock. This input clock manages the trigger signals for the laser activation of the different iC-HSB Drivers. These two Coaxial Connectors are used to generate an external signal to the first Differential Clock Buffer.
- Two connectors are each connected to a pin on the second LMK00301 Differential Clock Buffer. The two pins connected are CLKIn0 and CLKIn0*, which constitute the input clock. This input clock manages the reference frequency clock for the impulse generator of the different iC-HSB Drivers. These two Coaxial Connectors are used to generate an external signal to the second Differential Clock Buffer.

The first two pairs of Coaxial Connectors are therefore connected to the outputs of devices (either the Clock Generator or the iC-HSB Driver) in order to display and analyse the different signals transmitted in the circuit. The Coaxial Connectors connected to the iC-HSB Driver are useful throughout the project. However, those connected to the Clock Generator are used simply to test if this device operates correctly.

The last two pairs of Coaxial Connectors have a different role. Indeed, they are connected to the inputs of devices (either the first or the second Differential Clock Buffer). These Coaxial Connectors are therefore useful for generating an external signal to the two Differential Clock Buffer. These Coaxial Connectors are used throughout the various tests. Indeed, during the tests, the Clock Generator is not used. The various tests are explained in chapter 4.

A representation of the electrical schematic of two Coaxial Connectors is shown in figure 3.15 below. The others are made exactly the same way.

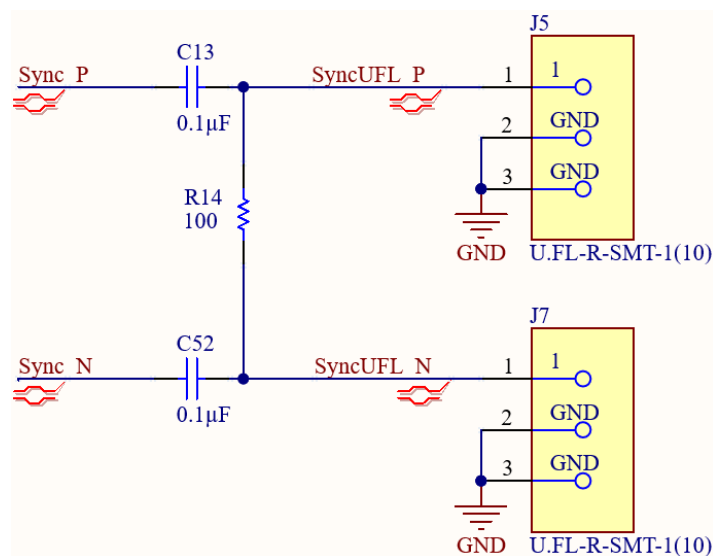


Figure 3.15: Electrical schematic of U.FL Coaxial Connector.

The connections are established in differential pairs to be able to transfer data streams of the same amplitude and opposite polarity at a very high speed. Moreover, the impedance of each **Coaxial Connector** is 50Ω . Since the differential impedance is in odd mode (section 3.3.5), the impedance of the differential pairs is simply twice the impedance of each track. Therefore, using the differential pairs allows you to have an overall impedance of 100Ω .

As shown in figure 3.15, a load termination resistor is placed in parallel between the two connection tracks of the differential pair. As explained at the beginning of this chapter, the resistance value is 100Ω since the characteristic impedance of differential pairs is 100Ω . In addition, as also mentioned, a $0.1\mu\text{F}$ coupling capacitor is placed in series on each track of the differential pair.

When routing the PCB, the resistor and the two capacitors should be placed as close as possible to the **Coaxial Connectors**. Indeed, reducing the length of the tracks between these components as much as possible reduces the risks of electromagnetic interference and signal reflections.

3.2.8 LMK00301 Differential Clock Buffer

A buffer is an element that produces an output signal, which has the same value as the input signal. It is also referred to as a repeater of the signal it receives. Clock buffers are therefore designed to have good properties for clock distribution networks, *i.e.* clock trees. An important property is that there is no delay between clock signals. A differential clock buffer is therefore the distribution of clocks over differential pairs.

The two differential clock buffers used in this project are **LMK00301 Differential Clock Buffers** [84]. The block diagram of these **LMK00301 Differential Clock Buffers** is shown at figure 3.16.

Obviously, the two **Differential Clock Buffers** have identical characteristics since they are the same devices. However, the connections with the different components that constitute this project are not identical for both **Differential Clock Buffers**. On the one hand, the first one is connected to different components through the pins representing the negative and positive triggering of the LVDS. On the other hand, the second one is connected to different components through the pins representing the negative and positive reference frequency of the LVDS. This is described later in this section when the different pins are presented.

To start with, the **Differential Clock Buffer** has some main features for the purpose of managing the different signals. These characteristics can be observed in figure 3.16.

Firstly, it includes an input multiplexer. A multiplexer is used to transmit information from several sources on the same link. This is done by means of logic gates. The present multiplexer is a 3:1, which means that there are three input lines and one output line. Of the three input lines, two are universal inputs that operate at up to 3.1 GHz and support LVDS mode. Therefore, the two universal input lines are each represented by a pair of pins. These are **CLKIn0/CLKIn0*** and **CLKIn1/CLKIn1*** respectively. In this project, only these two universal input lines are used (the third input line **OSCI**n is not used). The input clock can be selected from these two pin pairs. This selection is controlled using two particular pins. Indeed, the **Differential Clock Buffer** also has two selection lines which are each represented by a single input pin. The two pins are **ClkInSel0** and **ClkInSel1**.

Then, the selected input clock is distributed to two banks, A and B, of five differential outputs. Both differential output banks can be independently configured as LVDS. In this project, bank B is used because it is configured by default for LVDS. Three pairs of output pins are used (ClkB0/ClkB0*, ClkB1/ClkB1*, ClkB2/ClkB2*) and the other two are unused. Any unused output pins must be left floating to minimise capacity and reduce power consumption.

One final feature is that it operates from a $V_{cc} = 3.3\text{ V}$ core supply. In addition, it has three independent 3.3 V output power supplies. However, only V_{ccob} is used. On the two supply pins, V_{cc} and V_{ccob} , there is a decoupling capacitor of 0.1 μF . The Differential Clock Buffer offers high performance, versatility and energy efficiency.

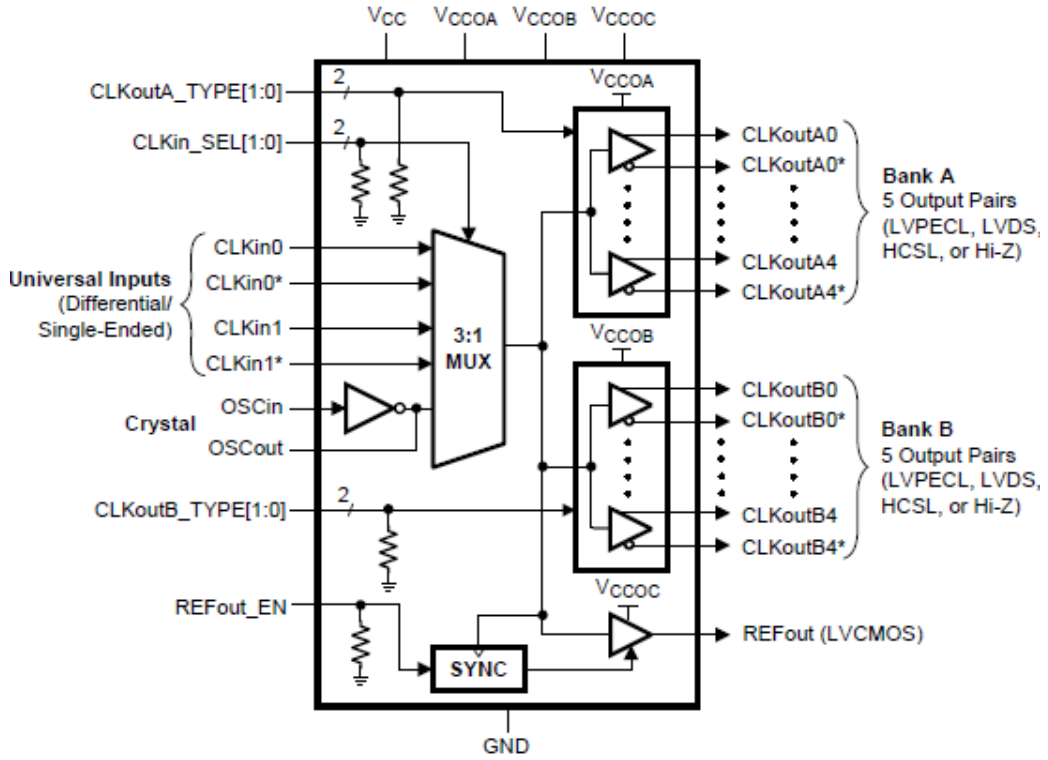


Figure 3.16: Block Diagram of LMK00301 Differential Clock Buffer [84].

Then, as explained at the beginning of the section, the two Differential Clock Buffers have the same characteristics. However, from one Differential Clock Buffer to another, the same pin does not perform the same connection. Indeed, the function of the different pins is the following (the name of each pin described below is as shown in figure 3.17):

- ClkInSel0 (Clk_In_Sel0) and ClkInSel1 (Clk_In_Sel1) Pins: These two pins of the first Differential Clock Buffer are connected to their counterpart of the second one. The two Differential Clock Buffers are connected directly to Arduino Nano 33 IoT through these pins. The input clock can be selected from the CLKin0/CLKIn0* or CLKin1/CLKIn1* pin pairs¹⁴ for each of the Differential Clock Buffer. This input clock selection is therefore controlled by the input pins ClkInSel0 and ClkInSel1. Indeed, depending on the high and low states of these two lines, one of the two input clocks is selected. There are pull-down resistors integrated into the device

¹⁴CLKIn0* = $\overline{CLKIn0}$ and CLKIn1* = $\overline{CLKIn1}$, both notations exist.

connected to these two lines. Therefore, the states of these two lines depend on these pull-down resistors and it is through the **Arduino Nano 33 IoT** that it is possible to change the state. The states of these two lines are initially low (0). Two options are therefore possible. The first one, **CLKin0/CLKin0***, is selected when **ClkInSel0** and **ClkInSel1** are in the low state (0). In this first case, the pull-down resistors pull their respective lines low and are therefore in their initial state. The second one, **CLKin1/CLKin1***, is selected when **ClkInSel0** is in the high state (1) and **ClkInSel1** is in the low state (0). In this second case, the **ClkInSel0** line is pulled up by the device while the **ClkInSel1** line is dropped by the device, therefore the pull-down resistor pulls the line low which is its initial state.

- **ClkTypB0 (Clk_Out_B0) and ClkTypB1 (Clk_Out_B1) Pins:** These two pins of the first **Differential Clock Buffer** are connected to their counterpart of the second one. As mentioned earlier, bank B is used because it is configured by default for LVDS. The differential output buffer type for bank B outputs can be configured using the **ClkTypB0** and **ClkTypB1** inputs. Indeed, there are pull-down resistors integrated into the device connected to these two lines. Therefore, the states of these two lines are initially low (0). The LVDS mode is selected when **ClkTypB0** is in the high state (1) and **ClkTypB1** is in the low state (0). In this case, the **ClkTypB0** line is pulled high while the **ClkTypB1** line is dropped by the device and, consequently, the pull-down resistor pulls the line low which is its initial state. For **ClkTypB0** to be pulled high, a shortcut is created between this pin and 3.3 V.
- **CLKin0/CLKin0* (E_C0_P/E_C0_N for the first one and Fref_C0_P/Fref_C0_N for the second one) Pins:** These two pins represent the first universal input clock. The connections for these pins are differential pairs. For the first **Differential Clock Buffer**, each pin is connected to a **Coaxial Connector** described in section 3.2.7. For this first one, it is the trigger signal for laser activation that is present at these two pins. It is the same connection settings for the second **Differential Clock Buffer**, but with different **Coaxial Connectors**. For this second one, it is the reference frequency clock for the impulse generator that is present at these two pins. The **Coaxial Connectors** connected to these universal inputs are therefore used to analyse either the trigger signal or the reference frequency.
- **CLKin1/CLKin1* (EPll_C0_P/EPll_C0_N for the first one and FrefPll_C0_P/FrefPll_C0_N for the second one) Pins:** These two pins represent the second universal input clock. The connections for these pins are differential pairs. For the two **Differential Clock Buffers**, the pins are connected to the **Clock Generator** described in section 3.2.6. Indeed, the **Clock Generator** sends clocks to the two **Differential Clock Buffers**, *i.e.* the clock trees, through differential pairs. The latter will then manage the distribution of clocks at their output, *i.e.* for the three **iC-HSB Drivers**
- **Bank B (ClkB0/ClkB0*, ClkB1/ClkB1*, ClkB2/ClkB2*) Pins:** Each pair of pins is connected to one **iC-HSB Driver**. For the first **Differential Clock Buffer**, the different pairs are connected to the pins where the trigger signal for laser activation is provided (**EN** and **EP** pins of each laser driver). For the second one, the different pairs are connected to the pins where a reference frequency clock for the impulse generator is provided (**FrefN** and **FrefP** pins of each laser driver). As they are **Differential Clock Buffers**, the output signals have the same value as the input signals. This allows the different signals to be distributed where they are needed, *i.e.* to the three **iC-HSB Drivers**.

A representation of the electrical schematic of an LMK00301 Differential Clock Buffer is shown in figure 3.17 below. What differs from the representation of the second LMK00301 Differential Clock Buffer is the name of some pins. Therefore, the connections of these pins also vary, as explained just above. However, the characteristics remain the same. A representation of the electrical schematic of the second one is available in appendix A.

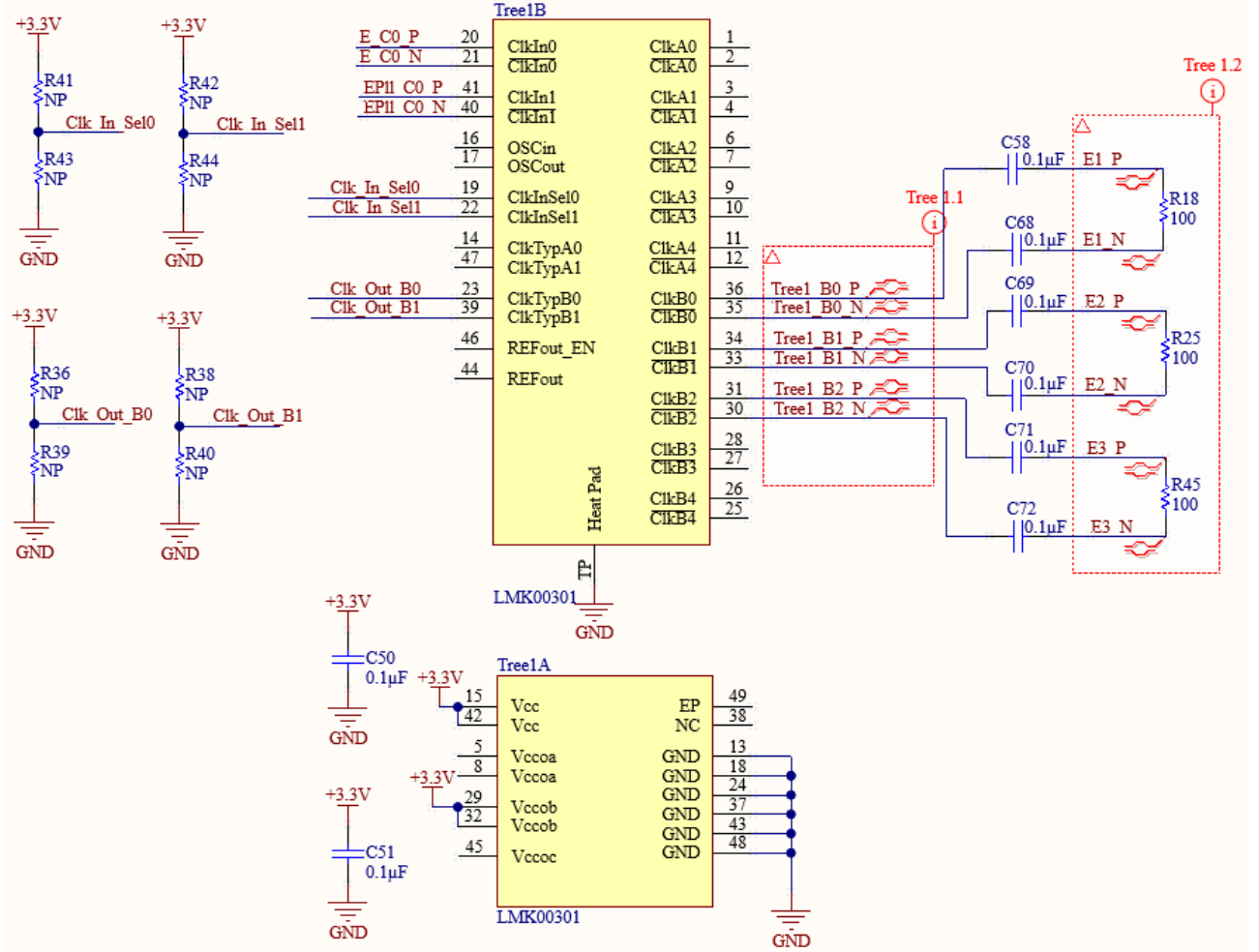


Figure 3.17: Electrical schematic of LMK00301 Differential Clock Buffer.

In figure 3.17 above the resistors are non-populated, as explained at the beginning of this section. In this case, it is necessary to create a shortcut between the ClkTypB0 pin and 3.3V. This is done by adding a 0Ω resistor to the R36 resistor. This shortcut allows the ClkTypB0 line to go high. The other unpopulated resistors are not needed. Their location on the PCB is therefore left empty.

To realize the connections between the iC-HSB Drivers and the pins of the Bank B, *i.e.* the right-hand connections on the figure 3.17, they are also differential pairs. Indeed, this is to have an overall impedance of 100Ω. A 100Ω load termination resistor is therefore placed in parallel between the two connection tracks of the differential pair. In addition, a 0.1 μF coupling capacitor is placed in series on each track of the differential pair. This is achieved by following the same logic described in section 3.2.7 when describing the differential pairs of U.FL Coaxial Connectors.

3.2.9 Arduino Nano 33 IoT

The core of this project is the **Arduino Nano 33 IoT** [52]. Indeed, to perform an I²C communication between several devices, an electronic device such as the **Arduino** is very often necessary. It is therefore this electronic device that executes the codes and is thus the master of this project. The other devices that have the necessary pins to communicate through the I²C protocol, *i.e.* the SDA and SCL pins, which are described in the previous sections, are therefore the slave devices.

The main features of the **Arduino Nano 33 IoT** are important in the framework of this project.

In the first instance, it is a miniature size module (45 mm x 18 mm). Indeed, this **Arduino Nano** is the smallest with a USB interface. This is a great advantage given the size constraints of the PCB. **Arduino** is the name of the board powered by a 32-bit low consumption microcontroller. The advantage over a microcontroller alone is its programming language which is easier to use. There is also the presence of a micro-USB port. **Arduino** also has all the advantages mentioned in section 2.3.

Moreover, there are a total of 22 digital input/output pins on the board. Out of these 22 pins, 14 are specific digital pins and 8 are analogue pins. The digital pins can read or write two possible values high or low (1 or 0). They can be used as inputs and outputs. The analogue inputs can read a value between 0 and 1023 and write a value between 0 and 255. They are only inputs.

In the last instance, the I²C serial programming interface is available. On the figure 3.18 are indeed the SDA and SCL pins. As the **Arduino Nano** is the master in the I²C protocol, these two pins are essential otherwise communication is impossible. As it is possible to see, the pull-up resistors $R1 = R2 = 4.7\text{ k}\Omega$ are also present. In terms of supply voltages, the **Arduino Nano** has several power supply pins: two output pins of 3.3 V and 5 V as well as one input pin V_{in} . The latter is used and is directly supplied with 5 V but the operating voltage of the circuit is 3.3 V. This is possible thanks to the device's internal pull-up resistors.

However, other pins are also essential and have a very specific function. These pins are the following (the name of each pin described below is as shown in figure 3.18):

- D16 (LD_Current) Pin: This pin is connected to the **Current Sense Amplifier** device which is described in section 3.2.2. As explained, this pin is therefore used to give an indication of the value of the current flows in the circuit. What is interesting for this project is the value of the current flowing to the **iC-HSB Drivers** and **Laser Diodes**.
- D17 (LD_Voltage) Pin: This pin is also connected to the **Current Sense Amplifier** device as well as to the three **iC-HSB Drivers** which are described in section 3.2.5. As explained, this pin is therefore used to give indications about the value of the voltage in the circuit. What is interesting for this project is the voltage value at the **iC-HSB Drivers** and **Laser Diodes**.
- D10 (NCHK) Pin: This pin is connected to the NCHK pin of each of the three **iC-HSB Drivers**. Indeed, it is thanks to this pin that it is possible to identify the different errors present on the drivers and consequently to be able to adjust them.

- D9, D8 and D7 (NSTBYx¹⁵) Pins: Each pin controls the stand-by mode of their respective iC-HSB Driver. It is, therefore, possible to operate the iC-HSB Drivers independently and therefore to activate, for example, only three or six laser diodes at the same time.
- D6 (Clk_In_Sel0) and D5 (Clk_In_Sel1) Pins: These pins are directly connected to the two Differential Clock Buffers. As said in section 3.2.8, it is thanks to these pins that the selection of the input clock of the Differential Clock Buffers is controlled. Indeed, there are pull-down resistors integrated into the device connected to these two lines. It is with the Arduino Nano that the high and low states of these lines are managed.

On the one hand, the LD_Current, LD_Voltage and NCHK pins are therefore pins of the Arduino Nano 33 IoT which allow to give information on the global circuit of this project. They are not used to control anything of the circuit, but rather to inform the user. On the other hand, the NSTBYx pins are used to control the operating mode of the three iC-HSB Drivers and allow them to be placed in stand-by mode, so they are not used to give information.

A representation of the electrical schematic of the Arduino Nano connections is given in figure 3.18 below.

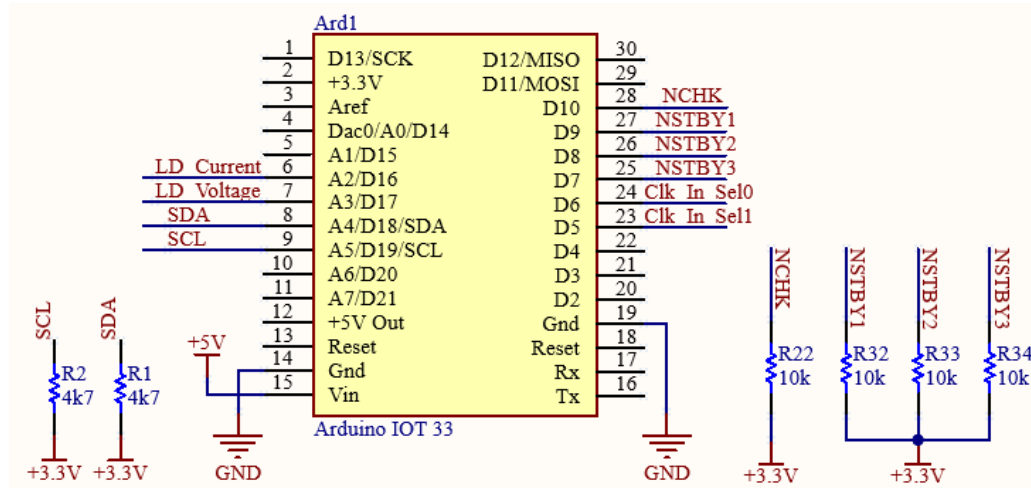


Figure 3.18: Electrical schematic of Arduino Nano 33 IoT.

In addition to the pull-up resistors connected to the SCL and SDA lines, there are also pull-up resistors for the NCHK and NSTBYx lines. On the one hand, the pull-up resistors on the NSTBYx lines are used to switch from stand-by mode (low) to operational mode (high) for the iC-HSB Drivers. On the other hand, the pull-up resistor on the NCHK line is used to switch from check request mode (low) to non-check request mode (high) for iC-HSB Drivers as well.

The principle of these pull-up resistors is exactly the same as for the I²C bus pull-up resistors. When the NSTBx and NCHK lines are high, the stand-by mode as well as the check request mode are disabled. The larger the pull-up resistor values, the longer the lines take to go from low to high and the lower the current consumption. Here, the time taken to go from low to high is less important than for the SDA and SCL lines. Indeed, the NCHK line is most often in the low state (check request mode) and the NSTBYx lines are most often in the high state (operational mode). Therefore the pull-up resistors are $R22 = R32 = R33 = R34 = 10\text{ k}\Omega$ in order to favour a low current consumption.

¹⁵NSTBY1, NSTBY2 and NSTBY3.

3.3 PCB Design

Once the devices and components are chosen and after having carried out the electronic schematics representing the connections between all electronic devices and components, the practical implementation of the circuit on a PCB has to be conceived. The conception of a PCB consists in placing the footprints of the different electronic devices and components and connecting them correctly by tracks and vias. The tracks are made of conductive metal and correspond to the circuit wires while vias consist of holes filled with conductive metal so that different layers of the PCB can be connected to each other. As mentioned in chapter 2, the PCB of the system is designed with the software Altium.

For this project, all 174 devices and components are positioned on the same PCB. Each component has its own place and is not all located on the same layer. This is discussed in section 3.3.2 and section 3.3.3 below.

3.3.1 Components footprint

Firstly, the footprint of each component must be declared. Most of the footprints that are used for this project are already in the Microsys laboratory libraries. The component footprints are designed in Altium using their datasheets. As an example, the footprints of a driver and a laser diode are shown on the left and right of the figure 3.19 respectively.

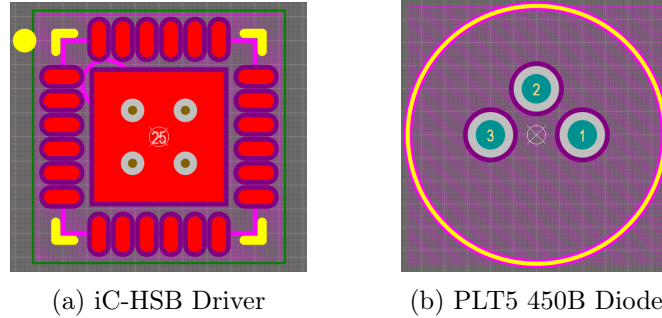


Figure 3.19: Footprints designed on Altium.

3.3.2 Components placement

Then, once all the components have a footprint, they are placed correctly to facilitate the connections on the PCB. On the one hand, to increase noise immunity, the length of the lead wires must be reduced. On the other hand, as explained in section 1.2.2, the PCB must respect some dimensions in order to be integrated onto the interface board and to perform the various laser tests. Appropriate placement is therefore very useful and essential.

Some remarks deserve to be mentioned:

- The positioning and orientation of the **Laser Diodes** are important. Indeed, these laser diodes must be placed in such a way that they form a circle. They must also be as close as possible (smallest diameter circle, $\varnothing = 28$ mm) in order for the laser to be as focused as possible and does not diverge too much from the target as the light emitted is orthotropic and is initially already deflected.

- In the next section, section 3.4, it is explained why a heat sink is added at the nine **Laser Diodes**. But many vias are also added at this same place, under the heat sink and therefore in the circle formed by the **Laser Diodes**, to improve this heat dissipation. They are covered with copper and allow heat to pass through the different layers by conduction.
- A default track width has been set at 0.2 mm to minimise the overall size of the PCB. However, the smaller the track width, the higher their resistance and the greater the Joule heat generated. Thus, for some wires that carry a higher current, a width of up to 0.5 mm is preferable. Indeed, the Joule effect is not desirable because the heat can propagate in the board, which can cause the malfunction of some components. For example, as mentioned in section 3.2.4, the laser diodes are supplied with a current of 165 mA. These wires are therefore wider in order to decrease the overall resistance of the wire (Pouillet's law [73]).
- For the same reasons as above, the power lines (+5 V, +3.3 V and +1.8 V) should be wider too. In this project, the power lines are even replaced by wide power planes to avoid the Joule effect as much as possible.
- A **Test Point** (TP1 [85]) is added to simplify the PCB testing process. It is used to test the quality and functionality of the PCB. It also allows various tests to be performed by connecting an external generator directly to it.
- The connecting wires used to connect the **Differential Clock Buffer** (section 3.2.8) to other components are differential pairs. The usefulness of differential pairs is described in section 3.3.4.

Taking this into account, the PCB library with all components is made. In order to verify the footprints, 3D models of each component are used to see if they fit. Then the routing of all components is done to obtain the 3D model of the PCB in figure 3.20.

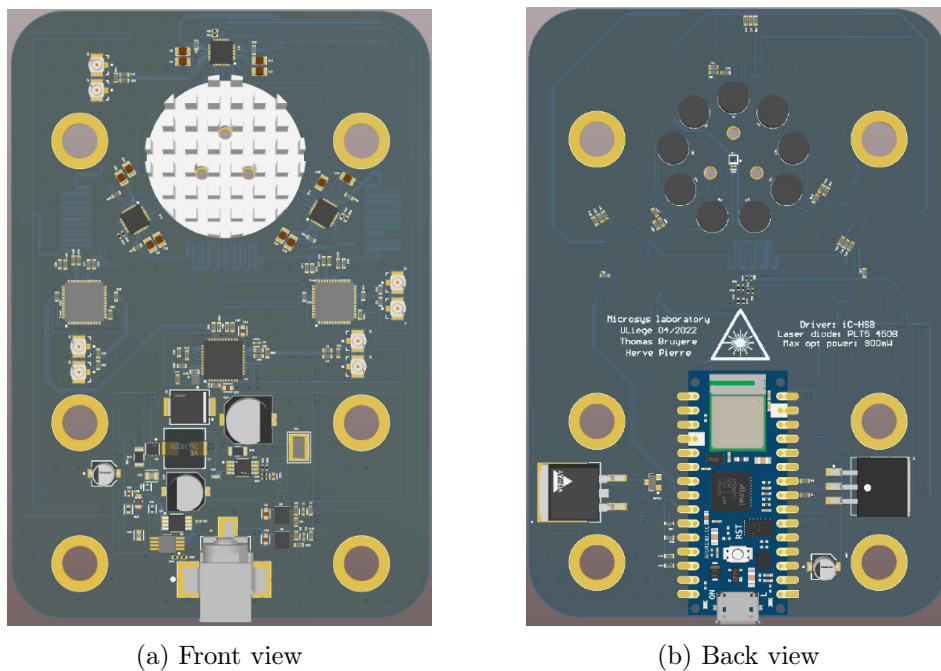


Figure 3.20: 3D PCB model.
Extended view of the PCB in appendix B.

Finally, once all the components are connected and correctly placed on the different layers, the PCB and components can be ordered. This PCB was ordered from JLCPCB [86]. The PCB has dimensions of $75.6 \text{ mm} \times 109.69 \text{ mm}$ ($\approx 8300 \text{ mm}^2$). The appendix B shows the real PCB before and after soldering of the devices and components. The soldering is not done by hand because of the small size of some components. The University of Liege has a soldering oven that allows all components to be soldered at once. The only components that are soldered by hand are those using Through-Hole Technology (THT), *i.e.* where there is an insertion of wires into holes that go through all layers of the PCB. This technology is often used for devices that can be subjected to high temperatures. In this project, the components that use THT and are therefore soldered by hand are the nine **Laser Diodes**.

3.3.3 PCB layout

In this subsection, some elements of layout choices are given. The PCB has four layers, each separated by a dielectric layer. In addition, as shown in section 3.3.2, there is a blue solder mask layer on both sides of the PCB. The different layers are therefore arranged as follows:

- Top solder mask: Thin polymer layer of 0.010 16 mm thickness is required to protect the PCB from any uncertain shortcut and to maintain the integrity of the copper traces.
- Top layer (red): Standard copper thickness of 1oz (0.035 mm). On this layer there are 154 components (Front view in figure 3.20).
- Dielectric layer 2: Thickness of 0.2 mm. A dielectric layer forms the non-conductive substrate layer between the conductive copper layers of the PCB.
- Plane layer 1 (brown): Copper thickness of 0.0175 mm. This layer is a GND plane, *i.e.* all components that have to be connected to the GND are connected to this layer thanks to vias.
- Dielectric layer 1: Thickness of 1.065 mm which has the same function as the dielectric layer 2.
- Plane layer 2 (light blue): Copper thickness of 0.0175 mm. Connections that are not possible on the top or bottom layer are made on this layer. It is therefore an additional layer to avoid connection conflicts.
- Dielectric layer 3: Thickness of 0.2 mm which has the same function as the dielectric layer 2.
- Bottom layer (dark blue): Standard copper thickness of 1oz (0.035 mm). On this layer there are 50 components (Back view in figure 3.20).
- Bottom solder mask: Thin polymer layer of 0.010 16 mm thickness which has the same function as the top solder mask.

The total thickness of the PCB is therefore 1.59032 mm. These different layers can be seen in figure 3.21 below.



Figure 3.21: Different layers of the PCB.

Given the size constraint of the PCB, the four layers are almost essential in order to be able to place all the devices and components and carry out the routing between them.

It is important to mention that the plane GND (plane layer 1) is very important. It is usually connected to electronic devices that heat up to help dissipate heat. But there are three other main reasons for using a GND plan, which are as follows:

- Firstly, it allows a voltage recovery. Most of the components on the PCB are connected to the power supply network, and then the return voltage will come back via the GND network. So the GND plane provides an error-free connection between the devices and the GND network.
- Then, it enables a recovery of the signal. A GND plane ensures an easy signal return process without interrupting several parts of the PCB. For high-speed designs, it is therefore very important to have a clear return path to the GND. Without it, signals can cause great interference to the rest of the PCB.
- Finally, it helps to reduce noise and interference. A huge amount of energy flows through the GND circuit of a PCB. As a result, it produces a lot of useless noise and interference. A GND plane with a larger conductive area helps to reduce interference and noise because it has a lower impedance than a GND network connected by wires.

3.3.4 Usefulness of differential pairs

As mentioned above, differential pairs connect the **Differential Clock Buffers** to other devices. Differential pairs offer a new way to transfer high-speed data streams. They consist of two tracks, routed side by side, and carry signals of equal amplitude and opposite polarity on each track.

Certain rules must be respected when routing differential pairs [87]:

- Spacing between each differential pair: Differential pairs must always be furthest apart. When several differential pairs are routed close to each other, they always interact negatively with each other. Interactions must therefore be avoided and kept as far apart as possible to reduce electromagnetic interference.

- Parallel routing: Try to keep the tracks of each differential pair parallel as much as possible. This avoids any emitted electromagnetic interference and makes it easier to adapt the length of the tracks.
- No sharp turns: It is best to route differential pairs in straight lines, without any bends. However, some curves are sometimes unavoidable. Tight bends emit more electromagnetic interference than a smooth curve.
- Use of vias: It is not recommended to use a lot of vias because their geometry degrades the signal somewhat. However, it is sometimes unavoidable to use them. It is therefore important to adjust any signal delay caused by a via. This can be done by using the same number of vias on both tracks of the differential pair.
- Adjusting the length of tracks: Track length matching is a top priority when routing differential pairs. If the lengths of the differential pairs are different, the time difference will cause destructive interference and degrade signal integrity. The tracks must therefore be as similar in length as possible.
- Adjusting the width of tracks: Track width matching is also important when routing differential pairs. Indeed, the width of the tracks varies the impedance of the differential pairs. However, all the differential pairs must have the same impedance (impedance matching) and therefore the same width. The impedance remains independent of the length. This point is developed further in section 3.3.5.

Taking all these rules into account, differential pairs are routed. The two main advantages of differential pairs are therefore as follows:

- The ability to suppress common-mode noise without the need for filtering is an unique feature of differential pairs. Common mode noise suppression is due to the fact that the difference between the two signals is measured on a differential pair, which can cancel out almost all noise on differential pairs.
- When the two tracks of the pair are closer together, the magnetic fields they generate when switching are identical and opposite. As long as the two signals are in phase and of the same amplitude, the magnetic fields they generate cancel each other out. However, when the tracks are asymmetrical, not all of them cancel each other out, but the magnetic fields remain quite weak.

3.3.5 Impedance matching

There are two impedance modes for a differential pair. On the one hand, the odd-mode impedance is defined as the impedance of a single transmission line when the two lines of a pair are driven differentially, *i.e.* with signals of the same amplitude and opposite polarity. On the other hand, the even-mode impedance is defined as the impedance of a single transmission line when the two lines of a pair are driven by a common-mode signal, *i.e.* with signals of the same amplitude and polarity. In the case of this project, the odd-mode impedance is used.

The impedance matching of the differential pairs is important because the track behaves like a differential transmission line, which then depends on the transmission delay on a given track. The differential impedance is defined as the impedance between the two tracks when the line pair is driven differentially [88]. It is therefore simply equal to twice the odd-mode impedance of each track.

The proper operation of the PCB depends on impedance matching, *i.e.* the ability of the circuit to efficiently transfer signals from the source to the routing and then from the routing to the load. Impedance has a remarkably negative impact on the performance of the circuit if it is not handled correctly. A different impedance produces a signal reflection which is a process of bouncing off a substrate that does not fully absorb it. This reflection depends on the difference between two mismatched impedances. The more the impedance mismatch, the greater the produced reflection and this affects the integrity of the signal. The signal reflection overlays the real signal, which is therefore misunderstood and therefore misdecoded [89].

The width of all tracks of the differential pairs is 0.154 mm. The space between the tracks of each differential pair is 0.127 mm. This has been calculated using an online calculator (JLCPCB [90]) to give an impedance of $100\ \Omega$ for a 4-layer PCB with a total thickness of 1.6 mm.

3.4 Thermal Dissipation

The PLT5 450B Laser Diodes used in this project must operate under safe temperature conditions. As explained in section 1.1.3, the problem with laser diodes is that the emission of photons is highly temperature-dependent. The diodes are already operating close to their limit and can therefore become very hot in a relatively short time. Therefore, it is essential to dissipate this heat, otherwise, it can influence the amount of light emitted and the current of the laser diodes [91].

The maximum operating temperature of a Laser Diode is 70°C. The junction-to-case thermal resistance of the PLT5 450B is 34°C/W (from datasheet).

For a single Laser Diode, the total power dissipation in the worst condition operates when the forward current is maximum (165 mA) and the forward voltage is also maximum (7 V). In this situation, as detailed in section 3.2.4, the total power dissipated by a single Laser Diode is 1.155 W. This means that for a single Laser Diode, in the worst case, the temperature will rise by 39.27°C, which is an acceptable situation.

However, when the nine Laser Diodes are operated at the same time, the operating temperature may be exceeded due to the total power dissipation. Indeed, the total power dissipated by the nine Laser Diodes is 10.395 W, as also detailed in section 3.2.4. This means that when all nine Laser Diodes are working, in the worst case the temperature will rise by $10.395 \times 34 = 353.43^\circ\text{C}$. This is a totally unacceptable situation, knowing that the proper functioning of the Laser Diodes is highly temperature-dependent.

Therefore, in order to properly dissipate the temperature, an aluminium heat sink is added [92]. The heat sink used in this project is passive, *i.e.* it does not consist of any mechanical components and does not need a power supply, making them totally reliable. It consists of aluminium fins that dissipate heat by convection. For the passive heat sink to work at full capacity, there must be a constant flow of air moving through the fins.

This heat sink is placed on the top layer above the Laser Diodes pins. Due to the special geometric shape of the circle formed by the Laser Diodes ($\varnothing = 28\text{ mm}$), there is no suitable heat sinks on the market for this type of application. For this reason, a heat sink was designed from scratch to meet the exact requirements of this project.

Fusion 360 [93] is a 3D modelling platform for product design and manufacturing. The platform enables products to be designed and created considering form, fit and function criteria. For these reasons, this platform is used to design the heat sink.

The first step is to design the heat sink on the Fusion 360 platform. Several constraints must be respected:

- The heat sink must be able to be attached to the PCB. It, therefore, has a flat surface designed to fit the PCB as well as possible. There must also be fixing holes on the heat sink as well as on the PCB. The three fixing holes are illustrated in figure 3.22a.
- The diameter of the heat sink should be equal to the diameter of the circle formed by the laser diodes. However, the pins of the Laser Diodes are through-holes, as explained in section 3.3.2.

Part of the heat sink must therefore be positioned above these pins without touching them. Therefore, as shown in figure 3.22b, the diameter of the base of the heat sink is smaller ($\varnothing = 18\text{ mm}$) so that it can be placed as well as possible on the PCB. While the upper part of the heat sink has a diameter equal to that of the circle formed by the laser diodes ($\varnothing = 28\text{ mm}$).

- As mentioned earlier, a constant flow of air must pass through the fins of the heat sink. The heat sink must be oriented so that the air can rise parallel through the fins. These fins must also be sparsely arranged because if they are densely grouped they will prevent convection. The heat sink is therefore made up of a substantial amount of fins, spaced far enough apart as seen in figure 3.22c, to ensure that it operates at full capacity.

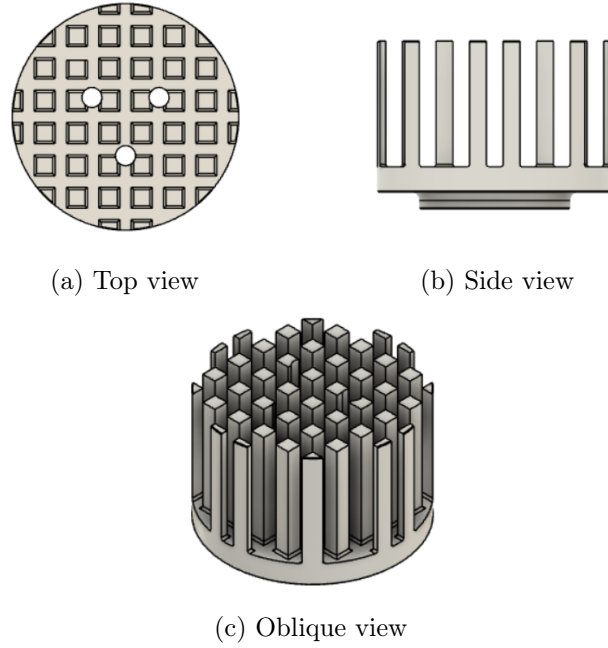


Figure 3.22: Heat sink designed on Fusion 360.

The second step is to design the heat sink in three dimensions. The University of Liege has the equipment to use Computer Numerical Control (CNC) machining, which is a method of metal fabrication where a written code controls the machines in the manufacturing process, which allows the heat sink to be manufactured with great precision. The material used to design the heat sink is aluminium because of its high thermal conductivity ($237\text{ W/m }^{\circ}\text{C}$). It is true that copper has a better thermal conductivity ($380\text{ W/m }^{\circ}\text{C}$). However, aluminium (2.7 g/cm^3) has a much lower density than copper (8.92 g/cm^3). For this reason, aluminium is chosen.

The last step is to attach the heat sink to the PCB. As the fixing holes of the heat sink and the PCB are perfectly aligned, this step is quite simple. However, there may be some manufacturing defects on the PCB or on the heat sink. Therefore, due to possible unevenness and irregularities of the PCB and heat sink surfaces, an air gap can form between the two surfaces. This air gap represents a significant resistance to heat flow and should be avoided. To eliminate this air gap, a Thermal Interface Material (TIM) is inserted between the two surfaces. TIMs are thermally conductive materials that can improve the thermal coupling between the heat sink and the PCB. The TIM used is thermal paste. The advantage of thermal paste is that it is liquid, so it can easily fill large gaps more uniformly. The outcome is shown in appendix B.

3.5 Software Architecture

Once the hardware part, which consists first of the electrical schematics, then the PCB and finally machining of the heat sink, is fully developed, the software part is implemented. This section describes how the devices of the system that have the ability to use the I²C protocol interact with each other. Indeed, as stated in section 3.2.9, the core of this project is the **Arduino Nano 33 IoT**. It is thanks to this device that code execution and I²C communication are feasible. All the functions of the Arduino used to make the project of this Master's Thesis functional are explained in this section.

Further details on the operation of the different files, the operation of the different implemented functions to allow the devices to perform correctly, and the organisation of the main build file for this project described in this section are given in appendix C.

To allow everything to work correctly, *.h*, *.cpp* and *.ino* files are used. Indeed, *.h* files, *i.e.* header files, are used to list instance variables, function declarations and accessible methods. Whereas *.cpp* files, *i.e.* implementation files, are used to use these instance variables and to implement the functions and methods declared. The header files are then included in the implementation files using the *#include* statement. Once this inclusion is done, the implementation files can be compiled. The reason for this separation is that header files cannot be compiled into binary code whereas implementation files can. The language used in the implementation files is the C++ programming language described in section 2.3. A pair of files consisting of a header file and an implementation file is called a library. In computer programming, a library refers to a collection of files, programs, routines, scripts, functions, methods or instance variables that can be referenced in the main programming code.

In the case of this project, two libraries are used. The first one is the *wire* library which allows communication with I²C devices. It is already implemented and can therefore be used directly by using the *#include <Wire.h>* statement in the main *.h* file of the project which is *iC_HSB.h* file described below. This library contains many functions that allow you to read or write to the different registers of the different devices.

The second library is created to meet the needs of the project. Indeed, according to the different actions to be done to make the laser source work, some variables and functions are implemented. This programming library is called *iC_HSB* and is therefore made up of a header file, *iC_HSB.h*, and an implementation file, *iC_HSB.cpp*. It is used with the help of the instruction *#include "iC_HSB.h"* in the main code file. This library is detailed throughout this section.

Once all libraries, *i.e.* headers and implementation files, are implemented, the *.ino* file, which is the main code and which is also written in the C++ programming language, is in turn implemented. This file is compiled into a binary format before being uploaded to the **Arduino Nano 33 IoT** programmable board via a USB cable. The *.ino* file must also include the header files. The **Arduino Nano 33 IoT** programmable board is, therefore, able to read the downloaded information as input and transform it into output for other devices. In the *.ino* files, there are always two functions that do not return any value. These two functions are the following:

- *setup* function: This function is executed only once when the code is compiled.
- *loop* function: This function is a loop, *i.e.* it repeats itself continuously if the code is not stopped.

3.5.1 General scan function

As already mentioned above, the **Arduino Nano 33 IoT** is the master and the other devices are the slaves of the I²C bus. The **Arduino Nano** must therefore communicate in I²C with the slaves, of which there are five. The very first thing to do is to detect if all these devices, including the master, are well connected to the I²C bus. Indeed, for the communication to work perfectly well, the devices must be connected to the same I²C bus aiming to transmit all the information. Therefore, a first function named *scan* is implemented to scan and analyse the devices on the I²C bus. This function returns all the I²C addresses that are connected to the I²C bus.

As explained in section 3.2 section, 0Ω resistors have sometimes been added to the PCB in order to define the I²C address of certain devices. The placement of each of these resistors is chosen intelligently so as to have different addresses for the devices. This avoids having address conflicts, *i.e.* several devices with the same address, which would make communication impossible. The addresses of the devices are as follows:

- The I²C address of the **MCP4562 Single Digital Rheostat** device is *0x2C*.
- The I²C address of the first **iC-HSB Ultrafast Laser Driver** device is *0x70*.
- The I²C address of the second **iC-HSB Ultrafast Laser Driver** device is *0x71*.
- The I²C address of the third **iC-HSB Ultrafast Laser Driver** device is *0x73*.
- The I²C address of the **Si5340 Clock Generator** device is *0x76*.

The addresses of the above devices have the form of hexadecimal numbers. These hexadecimal numbers are converted to binary numbers when used in the several functions that are implemented. The addresses in binary numbers are made up of 7 bits which gives a maximum number of $2^7 = 128$ different addresses, as explained in section 2.3. The conversion is as follows:

- The hexadecimal number *0x2C* becomes the binary number *0b0101100*.
- The hexadecimal number *0x70* becomes the binary number *0b1110000*.
- The hexadecimal number *0x71* becomes the binary number *0b1110001*.
- The hexadecimal number *0x73* becomes the binary number *0b1110011*.
- The hexadecimal number *0x76* becomes the binary number *0b1110110*.

The *0x* prefix corresponds to the hexadecimal number while the *0b* prefix corresponds to the binary number. These five devices are the slaves on the I²C bus.

3.5.2 Functions related to iC-HSB Laser Drivers

Once all the slaves have been detected on the I²C bus using the *scan* function, the I²C communication can begin.

The first thing to do is to implement the three **iC-HSB Drivers** which are indispensable for the operation of the **Laser Diodes**. Indeed, as explained in chapter 4, during the first tests of the laser

source it is thanks to the **Test Point** that the drivers are powered. The other I²C devices, *i.e.* the **Clock Generator** and the **Rheostat**, are not used. The first tests performed are essential to test the operation of the **iC-HSB Drivers** because these devices are still in the preliminary development phase. Indeed, these devices are not yet really available on the market. A direct contact was thus made with the manufacturers in order to have the possibility of using these devices because they had all the characteristics necessary for this Master's Thesis.

One consequence of the fact that this is still a device in the development phase is that there is no documentation on its use apart from its datasheet, which is not complete. Moreover, no library has been created for this device. Therefore, the first thing to do for the implementation of the three **iC-HSB Drivers** is to create a library which makes it possible to use the **iC-HSB Drivers** in all the possible situations, while obviously respecting the rules of use.

Firstly, the header file is created. In this file is the definition of the I²C addresses of the three **iC-HSB Drivers** in binary numbers.

Then, all the registers of the **iC-HSB Drivers** are defined in their turn. They are defined in exactly the same way as a slave address, the only difference being that the register address is written to 8 bits, *i.e.* one byte, whereas a slave address is written to 7 bits, as explained in section 2.4. Furthermore, each register consists of 8 bits which do not represent its address but its data, *i.e.* its information. It is important not to confuse the 8 bits that form its address and the 8 bits that constitute its data. Each data bit has a specific function. Indeed, depending on the state of each of the data bits composing the register, *i.e.* low (0) or high (1), the function of the register is different. There are two categories of registers:

- The first category is reading registers. It is therefore not possible to write to a register of this type. This category groups read-only registers which are sub-divided into status registers and measurement registers. These registers are used to take measurements and then return possible errors to the device by setting the different data bits to 1 or 0 depending on whether there is an error or not. Errors can be an overcurrent, an overvoltage, the impulse length which is longer than limit, etc. The registers of this first category have the addresses *0x00* to *0x05*.
- The second category is the configuration registers or so-called read-write registers. It is, therefore, possible to read or write to these registers. These are the important registers with which it is possible to configure the different parameters of the three **iC-HSB Drivers**. The registers of this second category have the addresses *0x10* to *0x1F*.

Moreover, the third part of the header file is to enumerate the set of data bits. An enumeration is defined using the keyword *enum*. This is used to assign names to constants to ensure the program code is easy to read and maintain.

Finally, all the functions that are implemented in the implementation file for this project are each defined in a class, either private or public, in the header file. Thus, it is possible to call these functions in the main build file.

Once the addresses of the three **iC-HSB Drivers**, the addresses of the registers for these slaves and the data bits constituting these registers are defined and enumerated, the header file, *i.e.* *.h* file, is

ready to be used. The variables and constants defined in this file can then be invoked in the implementation of the functions necessary to operate the **iC-HSB Drivers**. These functions, described in the following sections, are implemented in the implementation file, *i.e.* `.cpp` file.

3.5.2.1 Function to write a single bit to a register

The first function relating to the **iC-HSB Drivers** is the `write_one_bit_in_register` function which, as its name indicates, allows a single data bit to be written into a register which comprises 8 data bits. This function, therefore, allows the state of one data bit in a register to be changed at a time.

3.5.2.2 Function to write two bits to a register

The second function relating to the **iC-HSB Drivers** is the `write_two_bit_in_register` function which, as its name indicates, allows two data bits to be written into a register which comprises 8 data bits. This function, therefore, allows the state of two data bits in a register to be changed at a time.

3.5.2.3 Function to write one byte to a register

The third function relating to the **iC-HSB Laser Drivers** is the `write_full_bits_in_register` function which, as its name indicates, writes a byte, *i.e.* 8 data bits, in a register which comprises 8 data bits. This function, therefore, allows the state of all data bits in a register to be changed at once.

3.5.2.4 Function to read one byte from a register

The fourth and last function relating to the **iC-HSB Drivers** is the `read` function which allows to read one byte, *i.e.* 8 data bits, in a register which comprises 8 data bits. This function, therefore, allows the state of all data bits in a register to be determined.

This function is used to read status and measurement registers, *i.e.* read-only registers. It is also used to read the configuration registers once they have been modified by the write functions. In fact, it allows to verify that the writing has proceeded as desired.

3.5.2.5 Function to reset registers

When the `.ino` file is uploaded to the **Arduino Nano 33 IoT** programmable board, each of the data bits of the different registers are in their initial state. Then, the state of some data bits is modified thanks to the implemented write functions. One way to reset the data bits of the registers is to disconnect the USB cable from the programmable board and then reconnect it. However, this is not always efficient and the connection may take some time to re-establish.

Therefore, a function which allows all the data bits of all the registers to be reset is implemented. This function writes the data bits to their initial state of all registers in which it is possible to do so, thanks to the function `write_full_bits_in_register`. This `reset` function is not run at the beginning of each compilation of the `.ino` file but can be run at any time when it is called. This is explained in section [3.5.4](#).

3.5.3 Functions related to MCP4562 Single Digital Rheostat

Once the verification tests on the **iC-HSB Drivers** have been achieved thanks to the different functions described in section 3.5.2, another I²C device which is the **Rheostat** is made operational. Indeed, after the verification tests, the three **iC-HSB Drivers** are no longer powered by the **Test Point** but by the **Power Socket** described in section 3.2.1. The resistor possessed by the **Rheostat** must therefore be adjusted in order to have the right voltage and current value to supply the **iC-HSB Drivers**.

3.5.3.1 Function that configures the rheostat

The function relating to the MCP4562 Single Digital Rheostat is the *configuration_of_rheostat* function which, as its name indicates, allows the rheostat to be configured in order to have the right voltage and current value to power the three **iC-HSB Drivers**. This function is implemented in the *iC_HSB.cpp* file.

3.5.4 Main build file

The main build file which is uploaded to the **Arduino Nano 33 IoT** programmable board is the *.ino* file. It is in this main file that all the functions defined in the header file, *i.e.* the *.h* file, and implemented in the implementation file, *i.e.* the *.cpp* file, are executed. The very first thing to do in this main build file is to include the library containing all the functions defined and implemented to get the project operational. This is achieved by using the *#include "iC_HSB.h"* statement. In doing so, the *#include <Wire.h>* library is included as well. With this statement, the whole set of functions can be executed.

The main construction file is divided into three parts and a finalization part, which are described in detail in the four sections below.

3.5.4.1 First part: initialization and definition

This first part includes the definition of each of the pins that are used in this project of the **Arduino Nano**, *i.e.* the master, as well as the constants corresponding to the addresses of the different devices, *i.e.* the slaves.

Indeed, as shown on the figure 3.18, several pins of **Arduino Nano** are used. It is therefore necessary to define them in the main build file in order to program them in the *setup* function.

There is also the formation of several pointers which allow to point to the constants which correspond to the addresses of the five slaves. These pointers are *hsb1*, *hsb2*, *hsb3*, *rheostat* and *pll* which point respectively to the constants *iC_HSB_ADDRESS1*, *iC_HSB_ADDRESS2*, *iC_HSB_ADDRESS3*, *RHEOSTAT_ADDRESS* and *PLL_ADDRESS* which correspond to the addresses *0x70*, *0x71*, *0x73*, *0x2C* and *0x76* respectively.

3.5.4.2 Second part: *setup* function

Firstly, this second part initializes the serial monitor, *i.e.* it sets the communication rate in number of characters per second for the serial communication. The unit of the number of characters per second is the baud. To do this, the following instruction tells the serial object to perform the initialization steps to send and receive data:

Serial.begin(9600);

This corresponds to a communication of 9600 characters per second, *i.e.* a baud rate of 9600, which is the default value in serial communication.

Then, some pins of the **Arduino Nano** are configured to meet the needs of the project. The **NST-BYx**¹⁶ pins are all configured to the low state which does not put any **iC-HSB Driver** in stand-by mode. Indeed, for the tests carried out, all nine **Laser Diodes** are required so the **iC-HSB Driver** are as well.

As for the **Clk_In_Sel0** and **Clk_In_Sel1** pins, they are configured to the low state. This means that the signal comes from outside through the **Coaxial Connectors** connected to the **Differential Clock Buffer**. In a second step, when the optical laser source will be integrated onto the interface board containing the FPGA module, the **Clk_In_Sel0** pin will be configured high and the **Clk_In_Sel1** pin will remain low. This will allow the **Si5340 Clock Generator** to be used which is the internal generator.

Finally, this part also includes the first four steps of the laser source execution process that are performed only once during the compilation of the main file. Therefore, each time the main build file is compiled, these four steps are systematically executed. These four steps below are described for only one **iC-HSB Driver**. It is an identical process for the other two by simply pointing to the correct address.

Note that initially, the **iC-HSB Drivers** start in operation mode with the default configuration. The data bit 7 of the register with address *0x10* of each of the three **iC-HSB Drivers**, *i.e.* the data bit *DISLSR*, is set to 1. This means that the laser is disabled.

First step

The first step is to switch to configuration mode in order to configure all registers. To perform this switch, the two data bits *MODE* of the register with the *0x1C* address have their state changed.

Second step

The second step resets all registers to their initial value of the **iC-HSB Driver**, except the register with the *0x1C* address which must remain in configuration mode. This reset is a safety feature to ensure that no registers are misconfigured.

Third step

The third step is very important because it configures the system parameters. It is during this step that all configuration registers are adjusted for the operation of the laser source. All registers with *0x10* to *0x1F* address are configured in this third step.

¹⁶NSTBY1, NSTBY2 and NSTBY3.

Fourth step

The fourth step verifies that the third step has taken place as expected. Indeed, this step allows to read back the registers that have been configured to verify the correct data transfer. If what is read corresponds to the byte that was written in the register in the previous step, then the compilation can continue and the third part of the laser source execution process can begin. If this is not the case, then there is an error in the compilation of the main build file and it cannot continue.

3.5.4.3 Third part: *loop* function

This third part includes the different functions that can be executed several times depending on what the user wants. In the framework of this project, the loop function is not a loop that repeats itself over and over again. Indeed, thanks to the serial monitor which is initialised, it is possible to send commands to it in order to choose which function is executed. If no command is sent, no function is executed. A command corresponds to a single character. The different commands available are as follows:

- If the “p” command is sent: This command executes the *scan* function explained in section 3.5.1. It is, therefore, possible to check at any time whether the devices, *i.e.* the slaves, are still connected to the I²C bus.
- If the “r” command is sent: This command re-executes the second part without the fourth step, *i.e.* the first three steps of the *setup function*. It is therefore possible to return to the previous steps without systematically disconnecting the **Arduino Nano 33 IoT**.
- If the “d” command is sent: This command re-executes the fourth step of the *setup* function explained in section 3.5.4.2. It is therefore possible to read back the registers that have been configured to verify the correct data transfer as many times as necessary.
- If the “e” command is sent: This command executes the fifth step of the laser source execution process. The fifth step enables the laser. The laser is enabled but not yet turned on. Indeed, the **iC-HSB Driver** is still in configuration mode and not yet in operation mode.
- If the “s” command is sent: This command executes the sixth step of the laser source execution process. The sixth step verifies that there are no errors with the **iC-HSB Drivers** such as an overcurrent, an overvoltage, the impulse length which is longer than limit, etc. Indeed, this step allows the status and measurement registers to be read. If some data bits indicate that there is an error, it is not recommended to proceed to the next step as this could damage the devices.
- If the “o” command is sent: This command executes the seventh step of the laser source execution process. The seventh and final step is to switch to the operation mode. This activates the entire configuration registers that were set in the third step. When the operation mode is established, the laser source turns on.

This part, therefore, includes the last three steps, *i.e.* the fifth, sixth and seventh steps, of the laser source execution process. Before executing anything in this third part of the main build file, the **iC-HSB Laser Drivers** are in configuration mode. In addition, the configuration registers are properly configured and checked. The last three steps described above are identical for all three **iC-HSB Drivers**.

3.5.4.4 Fourth part: finalization

At the end of the first three parts of the main build file, *i.e.* at the end of the seven steps, the laser source is turned on. The necessary measurements for the tests can be taken. These are explained in chapter 4.

At this point, the commands “p”, “d” and “s” are sent regularly to the serial monitor to ensure that everything is working correctly. To turn off the laser source, the command “r” is sent which restarts the laser source execution process at step one and steps two and three are also re-executed. With the different commands, it is, therefore, possible to turn the laser source off and on as many times as necessary without having to disconnect anything.

3.6 Main Problems Encountered and Solutions

Designing the PCB with Altium software was a long step in this project. Because of the number of components and devices on the PCB, a small mistake could have had a big impact on the whole PCB. Errors such as shortcuts, too narrow tracks, poorly implemented differential tracks, overvoltage, overcurrent and overtemperature had to be avoided. Therefore, the entire PCB was checked frequently in order to avoid all these errors. Once the PCB had been fully checked, the latter was ordered. Once the PCB was received, the devices and components were assembled at the University of Liege using the soldering oven at its disposal. The first tests could therefore be carried out.

A first problem occurred while measuring the voltage at each power supply pin. Unfortunately, the right voltages, *i.e.* 5 V, 3.3 V and 1.8 V, were not correct. The entire PCB was then analysed under the microscope and a number of shortcuts induced by different bad soldering were noticed. Some components had to be desoldered and then resoldered by hand without creating a shortcut.

New tests were therefore carried out in order to measure the voltages at the supply pins. Thus, by carrying out these new tests, the 5 V and 1.8 V voltages were correct. However, a shortcut for the 3.3 V voltage was still present. But no error was visible under the microscope. Therefore, an infrared temperature sensor, available at the Microsys laboratory of the University of Liege, was used. Thanks to this sensor, it was possible to see a very high-temperature rise ($\approx 45^{\circ}\text{C}$) at the level of the **Si5340 Clock Generator**. After a detailed study of the components around this device, the error could be noticed. Indeed, the **Crystal Clock Oscillator** was soldered backwards, which created a shortcut. This device was therefore also desoldered and then resoldered. After that, all the power supply voltages were correct.

Another problem occurred during the implementation of the Arduino code and libraries for the **iC-HSB Ultrafast Laser Drivers**. During the first tests to make the laser source work, some registers of the **iC-HSB Ultrafast Laser Drivers** were not responding. However, after a lot of checks, all the Arduino code seemed to be correct in relation to the indications provided in the datasheet. However, after re-reading the datasheet, some inconsistencies, such as two different registers that had the same address were present. Therefore, a lot of emails were exchanged with the manufacturer of this device in order to obtain several clarifications, which took quite some time. After verification on their part, some errors were indeed present in the datasheet. There is an explanation for these errors. Indeed, the **iC-HSB Ultrafast Laser Driver** is a device that is still in the preliminary phase of development. Its datasheet is therefore not yet finalized and it is possible to find some inconsisten-

cies. After correcting the different errors in the datasheet, adapting the libraries that were created for this project and then modifying in the code the elements necessary for the proper functioning of the `Drivers`, everything worked well.

3.7 Conclusion

In this chapter, a complete presentation of the different devices and components to carry out the electrical system was presented. Their role as well as their interaction to operate the optical laser source was also discussed.

Then, a PCB including all these elements was conceived in a first time on the Altium Designer software to be, in a second time, assembled at the University of Liege. It consists of four layers with a total of 174 devices and components. All design rules have been respected in order to avoid as many errors as possible. A few small errors were detected during the assembly, such as shortcuts, but these were quickly corrected.

Afterwards, it was essential to find a method to dissipate the heat from this PCB. A heat sink was therefore machined, using a Computer Numerical Control (CNC), to avoid any overheating on the PCB and more specifically on the laser diodes that could lead to a defect of the devices. Indeed, a drawback of laser diodes is that the emission of photons is highly temperature-dependent.

Finally, the architecture software to implement the optical laser source execution process was developed. It is through the I²C communication protocol that the different devices and components can communicate with each other. Some errors were detected in the datasheet of the drivers used which delayed a little the implementation of the laser source execution process. Once the small problems with the software had been solved, the main built file was uploaded to the `Arduino Nano 33 IoT` to carry out all the tests.

Chapter 4

Laser Source Experimental Phase

The objective of this chapter is to perform different tests of the optical laser source and then analyse them. The first section presents all the equipment constituting the setup that is used to perform the optical tests. The second section explains and analyses the tests that are performed to check the correct functioning of the whole PCB and to avoid any risk of damage to the devices. Moreover, the tests in order to investigate the performances of the optical laser source are performed and analysed in the third section. Finally, a conclusion on the test results is drawn.

4.1 Optical Test Setup

To perform the optical tests of the laser source conceived in this Master's Thesis, a number of electronic measuring instruments is required. In addition, the position and orientation of the PCB is also important in order to perform the optical tests in the optimal conditions. The complete setup is shown in figure 4.1 below.



Figure 4.1: Optical test setup.

The different measuring instruments shown above are the following:

- An **EL302RD Power Supply** directly connected to the **Power Socket** to supply to the whole PCB. This instrument is obviously essential during the whole test process, as it is the main voltage and current generator.
- A **2400 Source Meter** which is connected directly to the **Test Point** to supply the **LD_Voltage** pin of each of the three **iC-HSB Drivers** with the required voltage and current. This source is no longer necessary as soon as the **Rheostat** is correctly configured so that the output of the **Step-Up Converter** is precise enough to supply the **iC-HSB Drivers**. The source meter is only used for the preliminary verification tests described in section [4.2.1](#).
- A **1908 Digital Measurement Multimeter** to measure the voltage and current values in the electrical system to check that there are no anomalies.
- An **AWG-4012 External Signal Generator** with an adjustable frequency up to 150 MHz in square wave. With this instrument, it is possible to send a signal to the two **LMK00301 Differential Clock Buffers** through **Coaxial Connectors**. This external signal generator is required throughout the testing process. Indeed, the **Clock Generator** internal to the PCB is only tested to verify that it is functioning correctly. This device will be of real use when the laser source will be integrated onto the interface board, which is still in the development phase.
- An **RTB2004 Digital Oscilloscope** for viewing and analysing signals at different points in the electrical system. This oscilloscope is essential during the whole test process to verify the signals.

As for the position of the PCB, the latter is fixed in the fixing holes on a mechanics table. In line with the PCB, and more specifically in front of the laser source, are the two very important measuring instruments to analyse the test results of the laser source. These two measuring instruments are used to perform the real tests of the laser source explained in section [4.2.2](#).

- The first one is **S130C** which is a photodiode power sensor with a silicon (Si) detector in the wavelength range of 400 nm to 1000 nm [\[94\]](#). This instrument can detect up to 500 mW optical power and it is therefore thanks to this first measuring instrument that it is possible to really know the optical power of the laser source. The active surface of the sensor is only 9.5 mm in diameter. The tests are therefore performed on a much smaller area than those of the targets that will be pointed at by the laser source during its real use.
- The second one is **PDA015A** which is a high-speed amplified silicon (Si) photodetector designed for the detection of optical signals in the wavelength range of 400 nm to 1000 nm [\[95\]](#). This photodetector is directly connected to the oscilloscope and it is therefore on this photodetector that the laser source is directly emitted. The active surface of the photodetector is only 150 μm in diameter. The signals emitted by the laser source can thus be directly visualized on the oscilloscope thanks to this second measuring instrument.

4.2 Performing Tests

4.2.1 Preliminary verification tests

As already explained in section 3.6, the first tests were performed to verify the correct functioning of the PCB itself. Some problems were encountered after the assembly of the PCB but could be solved.

At this point, the PCB appears fully functional. However, a few tests are performed to check that the optical laser source is functioning correctly, that the different devices are communicating well together and that there are no anomalies. For these tests, some precautionary measures are taken to avoid degrading anything:

- Firstly, the **Test Point** which is connected directly to the **LD_Voltage** pin of the three **iC-HSB Drivers**, *i.e.* the pin that supplies power to the laser diodes, is used to provide an accurate voltage and current to the **Laser Diodes**. Indeed, the source meter is directly connected to this **Test Point**. This **Test Point** is used before testing with the **Rheostat** configuration to ensure that there is no damage risk.
- Secondly, as the **LD_Voltage** pin of each of the **iC-HSB Drivers** is supplied by the **Test Point**, another voltage must not come from the **Step-Up Converter**. This is why the shunt resistors *R19* and *R48* of the figure 3.3 and figure 3.5 respectively are removed from the PCB in order to create an open circuit and disable the **Rheostat**. As a result, the laser diodes are only powered by the **Test Point**.
- Thirdly, the external signal generator provides the necessary signals to both **Differential Clock Buffers** through **Coaxial Connectors**. This external signal generator is used before testing with the internal **Clock Generator** configuration to ensure that there is no risk of damage. However, this internal **Clock Generator** is nevertheless tested at the end of the preliminary verification test but will only be used when the laser source will be integrated onto the interface board.

Consequently, the other I²C devices, *i.e.* the **Si5340 Clock Generator** and the **MCP4562 Single Digital Rheostat**, are not used at first.

For all preliminary verification tests performed with the optical laser source, some parameters are constant. These parameters are as follows:

- The main voltage and current generator is configured to supply the **Power Socket** with 7 V and 1 A.
- The source meter is configured to supply the **Test Point** with 7 V and 1 A. In this way, the laser diodes have a forward voltage of ≈ 7 V.
- The registers with *0x15* address of the three **iC-HSB Drivers** are configured so that the forward current of the **Laser Diodes** is maximum, *i.e.* 165 mA and that the forward voltage is also maximum, *i.e.* 7 V.

4.2.1.1 Laser source composed of a single laser diode

As laser diodes are very expensive, only one is placed on the PCB in the first instance. For this test, the external signal generator provides a 10 MHz frequency signal.

After turning off the laser diode and the main generator and the source meter turning on, they do not consume 1 A each. Indeed, the main generator consumes 160 mA and the output voltage of the LDO is equal to 5 V as desired. As for the source meter, it consumes 225 mA. Therefore, there is a total current consumption of $160 + 225 = 385$ mA. No matter how many laser diodes make up the laser source, if they are all turned off then the total current consumption will always be 385 mA. The voltage at the **Test Point** is 6.90 V. At the LD_Voltage pin of the iC-HSB Driver, the voltage is equal to 6.90 V which is coherent. At the pins of the turned off laser diode, the voltage at the anode is 6.90 V and the voltage at the cathode is 4.25 V.

When the laser diode is turned on, the main generator consumes 170 mA and the source meter consumes 255 mA. Therefore, there is a total current consumption of $170 + 255 = 425$ mA. Therefore, when the laser diode is turned on, there is an additional consumption of 40 mA compared to the total consumption when the laser diode is turned off. At the pins of the activated laser diode, the voltage at the anode is 6.72 V which is the same value as the LD_Voltage pin on the iC-HSB Driver. The voltage at the cathode is 2.78 V.

4.2.1.2 Laser source composed of nine laser diodes

The tests with only one laser diode having been done, the other eight are placed on the PCB. In this section, two tests are performed. For the first one, the frequency is fixed at 10 MHz but for the second one, the frequency is a variable parameter. These two tests are performed to measure the current consumption to check that it is consistent and that the laser diodes are correctly powered.

The figure 4.2 below shows the laser source composed of the nine laser diodes when it is turned off or on. These are the two main operation modes of for this project. However, it is possible to turn on only some of the laser diodes in order to change the configuration of the laser source. This is just done to check the total current consumption of the PCB.

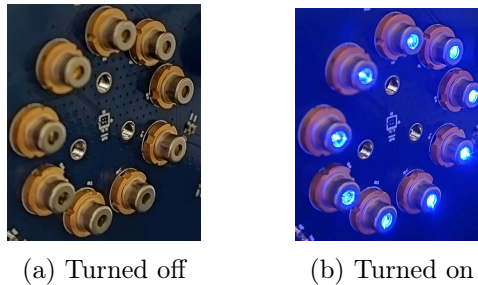


Figure 4.2: Main laser source configurations.

The first preliminary verification test in this section consists of a test of the optical laser source under different configurations. These configurations are listed in table 4.1 below. This test measures the overall current consumption as the laser source configuration varies at a fixed frequency of 10 MHz.

Configuration \ Consumption[mA]	Source Meter	Main Generator	Total Consumption
0 Laser Diode (=0)	225	160	385
1 Driver and 1 Laser Diode (=1)	255	170	425
1 Driver and 2 Laser Diodes (=2)	285	180	465
2 Driver and 1 Laser Diodes each (=2)	290	180	470
1 Driver and 3 Laser Diodes (=3)	315	190	505
3 Drivers and 1 Laser Diodes each (=3)	320	190	510
2 Driver and 2 Laser Diodes each (=4)	345	200	545
2 Drivers and 3 Laser Diodes each (=6)	405	220	625
3 Drivers and 2 Laser Diodes each (=6)	410	225	635
3 Drivers and 3 Laser Diodes each (=9)	495	245	740

Table 4.1: Current consumption [mA] of the source meter, the main generator and the total current consumption of the PCB as a function of the laser source configuration at a frequency of 10 MHz.

The results of these measurements demonstrate that the more laser diodes are activated, *i.e.* turned on, the more current is drawn by the main generator and the source meter. However, it is the consumption of the source meter that increases most significantly. In terms of total current consumption, each activated laser diode consumes additional current which is equal to approximately 40 mA. In fact, the minimum current consumption of 385 mA occurs when the laser source is turned off. As for the maximum current consumption equal to 740 mA, it occurs when all nine laser diodes composing the laser source are turned on. Therefore, the following equation is written:

$$385mA + (9 \times 40mA) = 745mA \approx 740mA \quad (4.1)$$

The evolution of the current consumption of the main generator, the source meter and the total current consumption of the PCB as a function of the laser source configuration is therefore linear. Figure 4.3 below clearly illustrates this linearity.

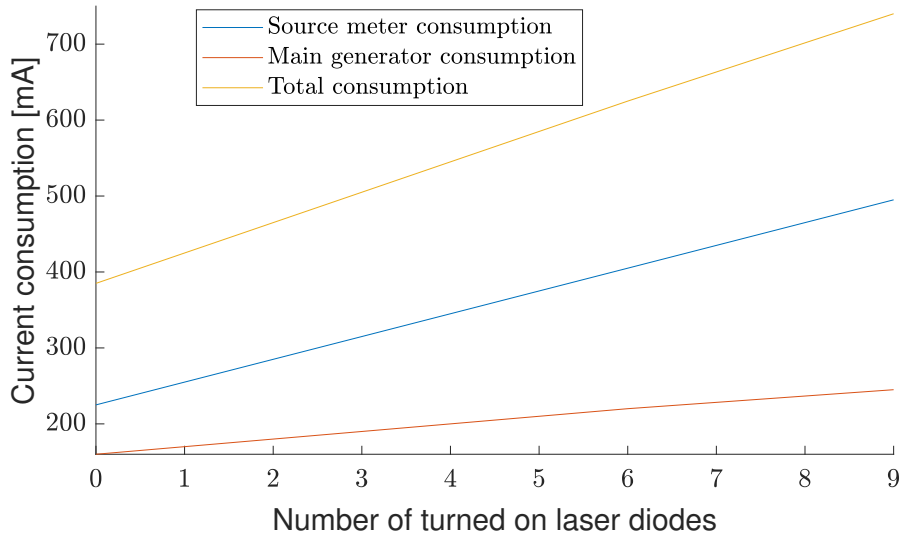


Figure 4.3: Current consumption [mA] of the main generator, the source meter and the total current consumption of the PCB as a function of the laser source configuration at a frequency of 10 MHz.

The second preliminary verification test in this section consists of varying the frequency when the optical laser source consists of the nine activated laser diodes, *i.e.* turned on. The different frequencies are listed in table 4.2 below. This test measures the overall current consumption as the frequency varies.

Frequency [MHz]	Consumption [mA]	Source Meter	Main Generator	Total Consumption
1×10^{-5}		630	295	925
1×10^{-2}		585	290	875
1×10^{-1}		585	290	875
1		570	270	840
5		565	265	830
10		495	245	740
50		490	240	730
100		455	240	695
150		445	240	685

Table 4.2: Current consumption as a function of frequency when all nine laser diodes are turned on.

The results of these measurements demonstrate that as the frequency increases, the current drawn by the main generator and the source meter decreases. However, it is the consumption of the source meter that decreases most significantly. As a result, the total current consumption of the PCB decreases. This is consistent with the frequency getting closer and closer to the bandwidth limit of 150MHz. Therefore, the power consumption does not have time to reach its maximum peak.

For this second preliminary verification test, the voltage at the anode of each laser diode is in the range [5.90: 6.45 V] when the frequency varies from 10 Hz to 150 MHz. This voltage is identical to that of the LD_Voltage pin of each of the **iC-HSB Drivers**. As for the cathode voltage, it is in the range [1.70: 2.70] for the same frequency variation.

4.2.1.3 Test of Si5340 Clock Generator

As said before, this device is not directly used during the operation of the laser source. Indeed, if it is operating correctly, it will be used once the laser source would be integrated onto the interface board using an FPGA module. Therefore, two tests are performed to verify its operation and are as follows:

- The first one consists of obtaining a 10 kHz frequency signal at the output of the **Clock Generator**, *i.e.* low-frequency signal. The signal is then displayed on the oscilloscope using the **Coaxial Connectors** connected to pins OUT0 and OUT0B which are the output clock of the **Clock Generator**.
- The second one is performed in the same way with the only difference that it consists of obtaining a 110 MHz frequency signal at the output of the **Clock Generator**, *i.e.* very high-frequency signal.

Note that the **Clock Generator** is configured directly by a software called ClockBuilder. This software allows to configure the frequency of the output signal of the **Clock Generator** as a function of the frequency that it receives in input by the **Crystal Clock Oscillator**. Note that the equation that relates frequency to time is $f [\text{Hz}] = \frac{1}{t[\text{s}]}$. Therefore, the higher the frequency of the signal, the smaller the time step on the x-axis of the graphs, *i.e.* there is a kind of "zoom" on the signal.

For the first test, *i.e.* when the software is configured to have a 10 kHz frequency output signal, an impulse should occur approximately every 0.1 ms. Figure 4.4 below illustrates that this is the case and the signal is perfectly square.

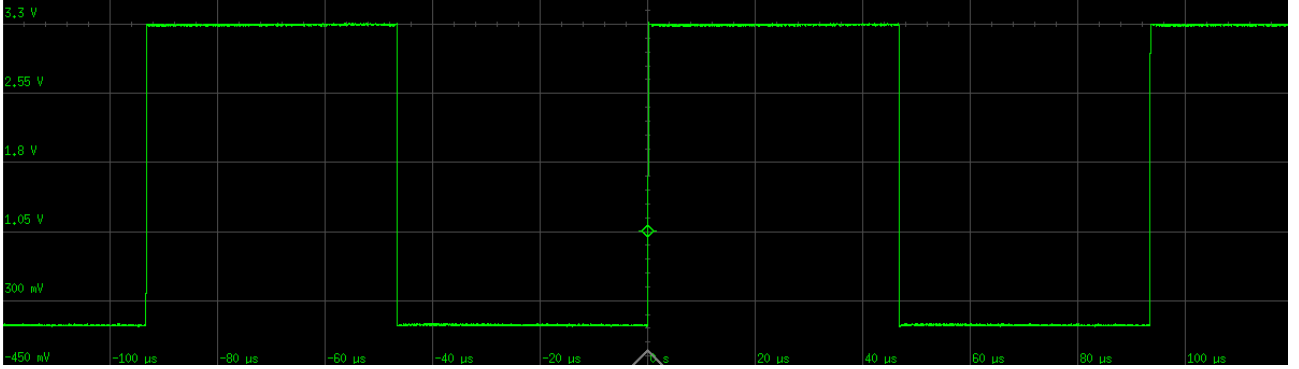


Figure 4.4: Signal at the Clock Generator output when it is configured to have a 10 kHz frequency output signal.

For the second test, *i.e.* when the software is configured to have a 110 MHz frequency output signal, an impulse should occur approximately every 9 ns. Figure 4.5 below illustrates that this is the case. However, for this frequency, the signal is less square because it is at high-frequency and therefore the noise is more accentuated.

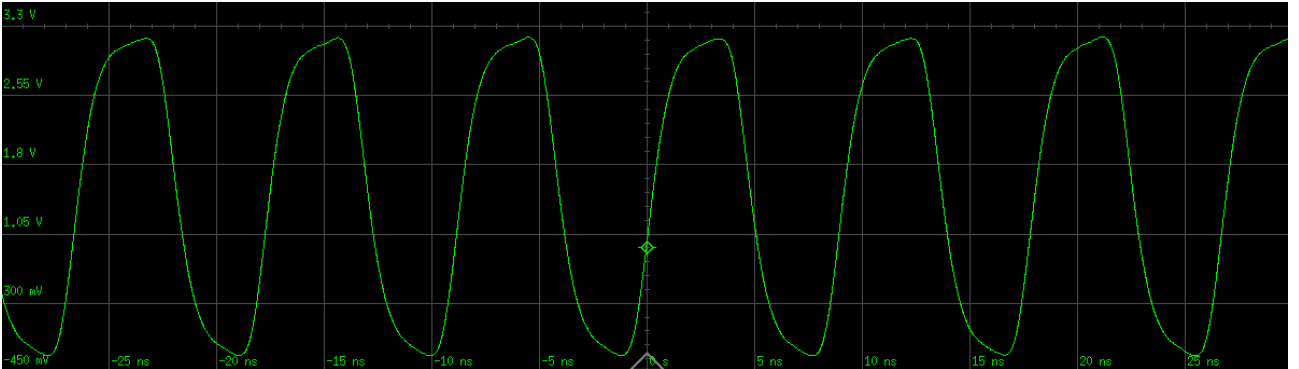


Figure 4.5: Signal at the Clock Generator output when it is configured to have a 110 MHz frequency output signal.

In conclusion, the **Si5340 Clock Generator** reacts well and sends back the right signals. The impulses systematically reach 3.3 V which is consistent with the output voltage of the **Clock Generator**. This device, therefore, operates correctly and could be used.

4.2.2 Performance tests

Once the preliminary verification tests that ensure proper PCB operation and consistent current draw are completed, the main performance tests of the laser source are performed. For these tests, the photodiode power sensor and the photodetector designed for optical signal detection are required.

For these tests, some of the precautionary measures explained in section 4.2.1 no longer need to be applied as the preliminary verification tests went correctly without any damage. Therefore, two modifications of the original setup are made:

- Firstly, the resistors *R19* and *R48* that were removed to create an open circuit and thus disable the **Rheostat** are now soldered onto the PCB. This activates the **Rheostat** which is then programmed in the Arduino build file such that it has a resistance value of 1 k Ω .
- Secondly, as the **Rheostat** is correctly programmed to supply a voltage of 7 V to the laser diodes, there is no longer any need to power the **Test Point** with the source meter. This leaves only the main generator, connected to the **Power Socket**, to provide the desired voltages and currents throughout the PCB's electrical system.

The main voltage and current generator is always configured to supply the socket with 7 V and 1 A and the external signal generator is always used. The total current consumptions are identical to those calculated in table 4.2.

4.2.2.1 Laser source power composed of a single laser diode

Firstly, the performance of the optical laser source when only one laser diode is turned on is measured. This is then compared to the performance of the optical laser source when all the laser diodes are turned on.

For these performance tests, the optical power as well as the irradiance, *i.e.* the power density, of the laser source composed of a single laser diode is measured by means of a photodiode power sensor. Both parameters are determined by varying the distance between the laser diode and the power sensor and the frequency of the signal generated by the external signal generator. For these tests, the power sensor is placed exactly in line with the laser diode in order to obtain its maximum performances.

Table 4.3 below contains the measured optical power values of a single laser diode as a function of the two variable parameters mentioned above.

Distance [cm] Frequency [MHz]	0	2.5	5	10	15	20
1×10^{-5}	106.5	73.9	38	13.9	7	4.1
1×10^{-2}	103.2	70.8	36.9	13.4	6.8	3.9
0.1	94.2	64.7	33.8	12.1	6.1	3.7
1	90.7	61.9	32.4	11.8	6	3.6
5	62.4	48.2	21.6	8.4	4.4	2.6
10	54.2	37.7	19.6	7.5	4	2.4
50	50.9	35.6	18.3	7	3.8	2.1
100	40.5	28.3	14.7	5.8	3.1	1.6
150	39.4	27.5	14.4	5.5	2.9	1.5

Table 4.3: Optical power [mW] of a single laser diode as a function of its distance [cm] from the power sensor and the signal frequency [MHz].

The results of these measurements demonstrate that as the frequency increases, the optical power of the laser diode decreases. Furthermore, as the distance between the laser diode and the power sensor increases, the optical power also decreases. A representation of the evolution of these results is illustrated in figure 4.6 below.

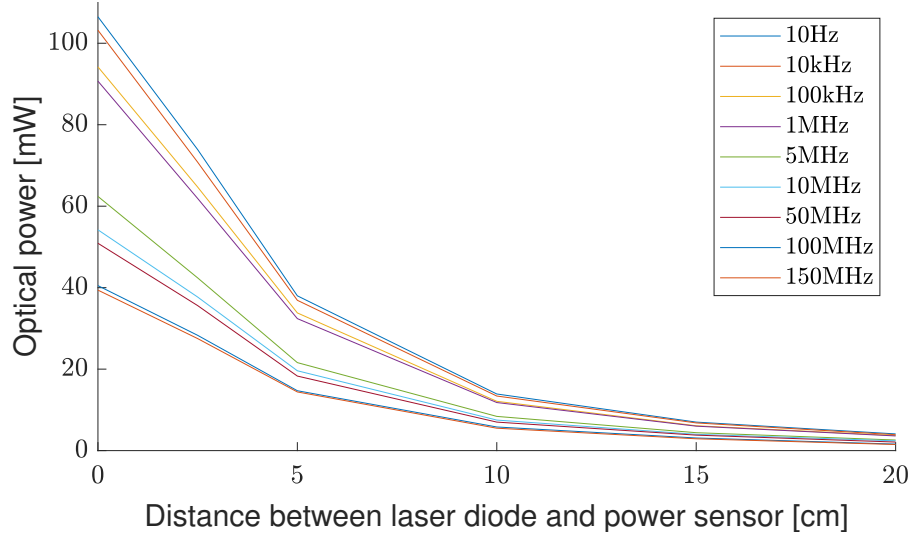


Figure 4.6: Optical power [mW] of a single laser diode as a function of its distance [cm] from the power sensor and the signal frequency [MHz].

Table 4.4 below contains the measured irradiance values of a single laser diode as a function of the two variable parameters mentioned above.

Distance [cm] Frequency [MHz]	0	2.5	5	10	15	20
1×10^{-5}	150.3	104.2	53.5	19.7	9.8	5.9
1×10^{-2}	146.5	99.8	51.7	18.9	9.5	5.6
0.1	133.7	90.6	46.8	16.9	8.6	5.2
1	129.7	89.2	41.4	16	8.4	5
5	77.5	58.1	31.4	12.3	5.7	3.5
10	76.4	53.3	27.5	10.5	5.6	3.4
50	71.6	50.1	25.9	9.9	5.2	2.9
100	57.3	40	20.8	8.1	4.3	2.3
150	55.5	38.8	20.3	7.7	4.1	2.2

Table 4.4: Irradiance [mW/cm²] of a single laser diode as a function of its distance [cm] from the power sensor and the signal frequency [MHz].

The results of these measurements demonstrate that as the frequency increases, the irradiance of the laser diode decreases. Furthermore, as the distance between the laser diode and the power sensor increases, the irradiance also decreases. A representation of the evolution of these results is illustrated in figure 4.7 below.

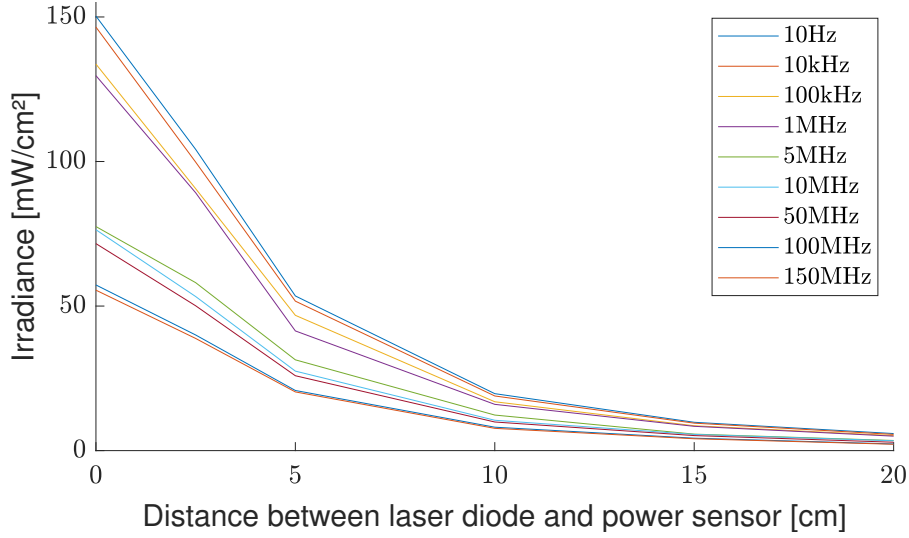


Figure 4.7: Irradiance [mW/cm^2] of a single laser diode as a function of its distance [cm] from the power sensor and the signal frequency [MHz].

In conclusion, obviously, both the optical power and the irradiance parameters show a strong decrease over the first 5 cm between the laser diode and the power sensor. This is the case for all the signal frequencies studied. Beyond the first 5 cm, the decay is weaker and weaker as the distance between the laser diode and the power sensor increases. This is because the laser diodes used in this project emit an orthotropic light source, as explained in section 3.2.4. As a result, the light emitted by the laser diode is very quickly deflected from the target even when the target is very close. Thus, beyond a distance of about 10 cm, the optical power and irradiation of the laser diode are already relatively low and beyond 15 cm, these two parameters become too low. As for the frequency, as it increases the optical power and irradiance decreases. As well as the decrease in total current consumption, this is consistent with the frequency getting closer and closer to the bandwidth limit of 150MHz. Another observation is that the two graphs above clearly have the same shape. This is consistent with the fact that the higher the irradiation, the higher the optical power, and vice versa.

4.2.2.2 Laser source power composed of nine laser diodes

The tests with a single laser diode turned on are measured, those with all the laser diodes turned on to form the laser source are then performed.

For these performance tests, with the full laser source, *i.e.* composed of nine laser diodes, the power sensor is still used to measure the optical power as well as the irradiance. Both parameters are determined by varying, as for the laser source composed of a single laser diode tests, the distance between the laser source and the power sensor and the frequency of the signal generated by the external signal generator. For these tests, the power sensor is placed exactly in line with the centre of the circle formed by the laser diodes. Note that the diameter of the circle formed by the laser diodes is 28 mm while the diameter of the active part of the detector is only 9.5 mm (surface $\approx 70 \text{ mm}^2$). Therefore, the power sensor is not placed exactly in front of a particular laser diode. The results will then be compared to the results obtained for the laser source composed of a single laser diode described in the previous section 4.2.2.1.

The table 4.5 below contains the measured optical power values of the full laser source as a function of the two variable parameters mentioned above.

Distance [cm] \ Frequency [MHz]	2.5	5	10	15	20	25	30	55
1×10^{-5}	26.6	60	36.6	20.8	13	8.7	6	1.8
1×10^{-2}	24.1	56.2	35.7	20.4	12.8	8.5	5.9	1.7
0.1	23.5	53.3	34.9	19.1	12.5	8.3	5.9	1.7
1	22.6	52.8	34.3	19.7	12.3	8.1	5.7	1.6
5	21.9	51.2	33.6	19.1	11.8	7.8	5.6	1.6
10	19.3	45.7	30.1	17.3	10.6	7.1	5.1	1.5
50	17.6	41.6	27.5	15.7	9.9	6.4	4.7	1.3
100	14	32.9	21.9	12.6	7.7	5.1	3.7	1.1
150	12.9	30.4	20.1	11.6	7.2	4.7	3.4	1

Table 4.5: Optical power [mW] of the full laser source as a function of its distance [cm] from the power sensor and the signal frequency [MHz].

The results of these measurements demonstrate that there is a maximum optical power when the power sensor is placed exactly 5 cm from the laser source. Therefore, beyond and below 5 cm, *i.e.* when the distance between the laser diode and the power sensor increases and decreases respectively, the optical power decreases. As for the frequency, when it increases, the optical power decreases. A representation of the evolution of these results is illustrated in figure 4.8 below.

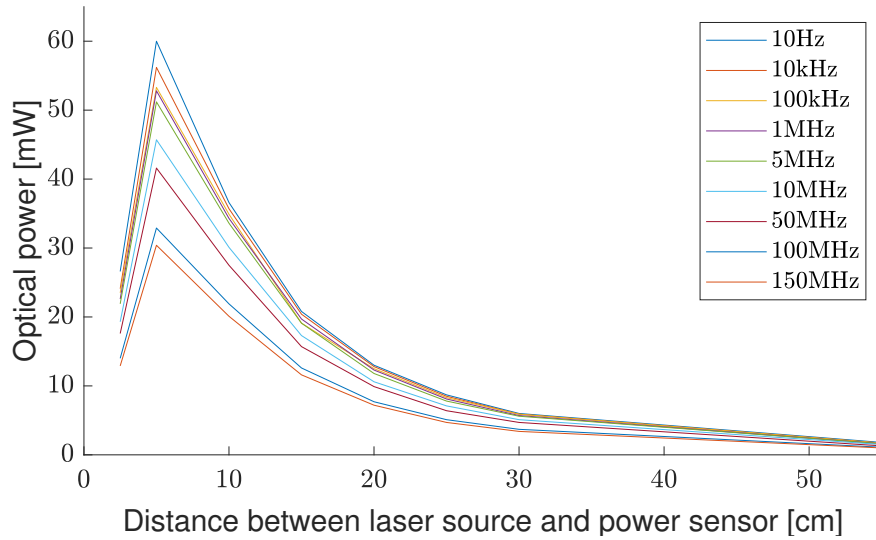


Figure 4.8: Optical power [mW] of the full laser source as a function of its distance [cm] from the power sensor and the signal frequency [MHz].

The table 4.6 below contains the measured irradiance values of the full laser source as a function of the two variable parameters mentioned above.

Distance [cm] Frequency [MHz]	2.5	5	10	15	20	25	30	55
1×10^{-5}	37.4	84.5	51.6	29.2	18.3	12.3	8.4	2.5
1×10^{-2}	33.9	81.4	50.3	28.6	17.9	11.9	8.3	2.4
0.1	32.4	75.1	49	28.2	17.6	11.5	8.2	2.4
1	31.9	74.5	48.3	27.7	17.4	11.4	8.1	2.3
5	30.8	72.2	47.3	27	16.7	11	7.9	2.2
10	27.2	64.5	42.6	24.3	15.1	10	7.2	2
50	24.9	58.9	38.9	22.3	14	9	6.6	1.9
100	19.8	46.4	30.9	17.7	10.9	7.2	5.2	1.5
150	18.2	43.1	28.5	16.5	10.1	6.6	4.8	1.4

Table 4.6: Irradiance [mW/cm^2] of the full laser source as a function of its distance [cm] from the power sensor and the signal frequency [MHz].

The results of these measurements demonstrate that there is a maximum of irradiation when the power sensor is placed exactly 5 cm from the laser source. Therefore, beyond and below 5 cm, *i.e.* when the distance between the laser diode and the power sensor increases and decreases respectively, the irradiation decreases. As for the frequency, when it increases, the irradiation decreases. A representation of the evolution of these results is illustrated in figure 4.9 below.

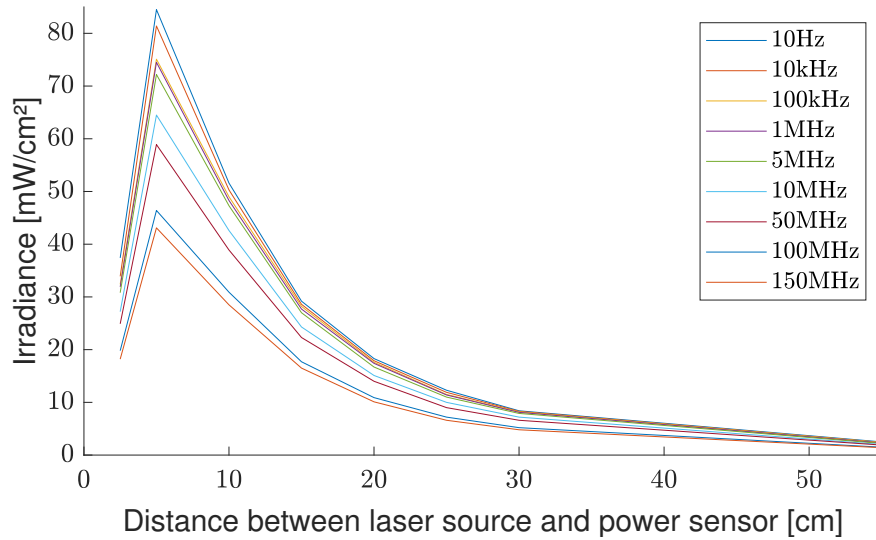


Figure 4.9: Irradiance [mW/cm^2] of the full laser source as a function of its distance [cm] from the power sensor and the signal frequency [MHz].

In conclusion, obviously, the optical power and irradiance parameters show a maximum peak when the power sensor is placed 5 cm from the laser source. That is the case for all the signal frequencies studied. This is due, firstly, to the fact that the power sensor is not placed exactly in front of a particular laser diode and, secondly, to the fact that the diameter of the circle formed by the diodes is about three times larger than that of the active surface of the detector. Therefore, as the power sensor gets closer and closer to the laser source, lesser light is emitted on the power sensor until none is emitted at all. When the distance varies from 5 to 15 cm, the decay is very strong. Beyond 15 cm, the decay is weaker and weaker as the distance between the laser diode and the power sensor increases and beyond 30 cm, the optical power and irradiance become too low. As for the frequency, as it increases, the optical power and irradiance decrease for the same reasons explained in the previous section 4.2.2.1. Another observation is that the two graphs above clearly have the same shape. This is consistent with the fact that the higher the irradiation, the higher the optical power, and vice versa.

4.2.2.3 Laser source efficiency

To calculate the efficiency of the optical laser source, the following equation is used:

$$Efficiency = \frac{Optical\ Power\ [W]}{Total\ Current\ Consumption\ [A] \times V_{in}[V]} \quad (4.2)$$

where the optical power values are shown in table 4.5 and those for total consumption in table 4.2 and where $V_{in} = 7\text{ V}$.

The efficiency of the laser source composed of a single laser diode is compared to the full laser source. Table 4.7 below contains the efficiency values as a function of distance between the laser source and the power sensor for a frequency of 10 MHz generated by the external signal generator. At this frequency, the total current consumption for a single laser diode is 425 mA and for the full laser source is 740 mA.

Configuration \ Distance [cm]	2.5	5	10	15	20
Single laser diode	1.26	0.65	0.25	0.13	0.08
Nine laser diodes	0.37	0.88	0.58	0.33	0.21

Table 4.7: Efficiency [%] of a single laser diode and the full laser source as a function of distance between the laser source and the power sensor at a frequency of 10 MHz.

For the same distances but at a different frequency, the efficiency values are similar. Indeed, as said before, when the frequency increases, the total current consumed as well as the optical power decreases. When the frequency decreases, the opposite effect occurs. The efficiency of the laser source is therefore mainly influenced by the distance between the laser source and the power sensor.

The different efficiency values are consistent with the optical power measured in the previous tests. Indeed, before 5 cm, the single laser diode has a better efficiency. However, from 5 cm and beyond, the full laser source has a better efficiency. The greater the distance between the laser source and the power sensor, the greater the ratio between the efficiency of the full laser source and the efficiency of the single laser diode. Obviously, when the distance is too great, the efficiency tends towards 0. A representation of the evolution of these results is shown in the figure 4.10 below.

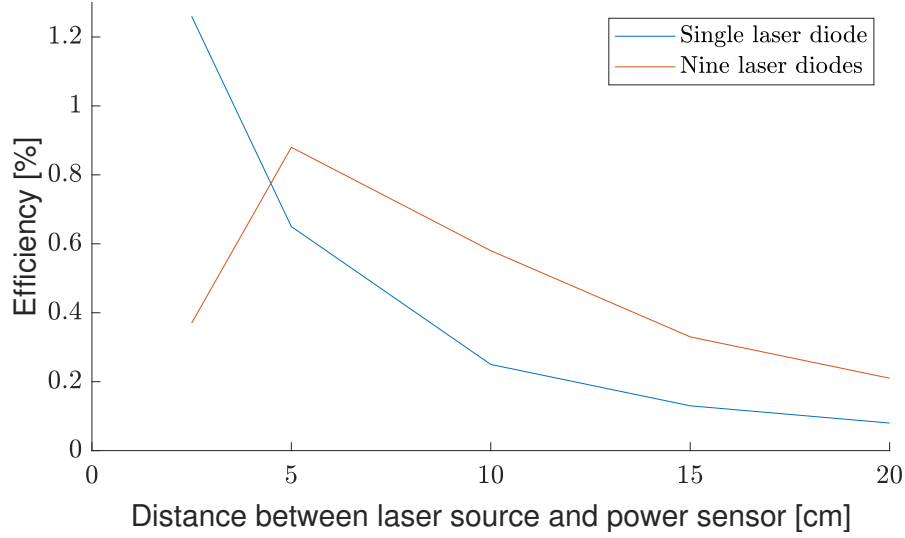


Figure 4.10: Efficiency [%] of a single laser diode and the full laser source as a function of distance between the laser source and the power sensor at a frequency of 10 MHz.

The calculated efficiency values are not very high. Indeed, for the full laser source, the efficiency does not exceed one percent. The only way to increase the efficiency is to increase the optical power of the laser source. In order to do this, all nine laser diodes would have to be focused on a single point. However, this would exclude one of the objectives of this laser source, which is to emit the light over a wide area. Therefore, this percentage of efficiency is sufficient for the application of the optical laser source conceived in the framework of this project.

4.2.2.4 Comparison between the full laser source and that of a single laser diode

The main difference is the variation of the optical power as a function of the distance between the laser source and the power sensor.

For distances less than 2.5 cm at all frequencies, the single laser diode has a much higher optical power than the full laser source. However, from a distance of 5 cm and beyond, the optical power of the full laser source becomes greater than that of the single laser diode.

For a more mathematical comparison, the measurements obtained when the power sensor is placed at 5 cm, 10 cm, 15 cm and 20 cm are compared:

- Distance of 5 cm: the optical power of the full laser source is 1.6 to 2.1 times higher than that of the single laser diode, depending on the signal frequency.
- Distance of 10 cm: the optical power of the full laser source is 2.6 to 3.6 times higher than that of the single laser diode, depending on the signal frequency.
- Distance of 15 cm: the optical power of the full laser source is 2.9 to 4 times higher than that of the single laser diode, depending on the signal frequency.
- Distance of 20 cm: the optical power of the full laser source is 3.2 to 4.8 times higher than that of the single laser diode, depending on the signal frequency.

The higher the distance of the power sensor from the optical laser source, without exceeding a certain limit, the higher the ratio between the optical power of the complete laser source and that of the laser source composed of a single laser diode. The optical powers are relatively similar when the power sensor is placed 30 cm from the full laser source and 15 cm from the single laser diode. At these distances, however, the optical powers are too low.

Regarding the efficiency of the optical laser source, if the results are compared mathematically at a distance of 5 cm, 10 cm, 15 cm and 20 cm:

- Distance of 5 cm: the efficiency of the full laser source is 1.35 times higher than that of the single laser diode.
- Distance of 10 cm: the efficiency of the full laser source is 2.32 times higher than that of the single laser diode.
- Distance of 15 cm: the efficiency of the full laser source is 2.53 times higher than that of the single laser diode.
- Distance of 20 cm: the efficiency of the full laser source is 2.62 times higher than that of the single laser diode.

In conclusion, the full laser source is more suitable for this project as one of the functions of the optical laser source will be to emit the light over a wide area at a relatively long distance, *i.e.* more than 15 cm, rather than to converge it to a very close point.

4.2.2.5 Optical signal of the full laser source

For the final performance tests with the full laser source, the photodetector designed for optical signal detection, directly connected to the oscilloscope, is used to analyse the signals emitted by the laser source. As the diameter of the active part of the photodetector is only 150 μm (surface $\approx 0.018\text{ mm}^2$), it cannot be placed too far away from the laser source to perform the tests. The photodetector is therefore positioned at 15 cm from the laser source. Beyond 15 cm, the photodetector starts to perceive the signal less well.

Three tests are therefore performed to analyse the signals emitted by the laser source. The three tests are as follows:

- The first one consists in analysing the signals that are emitted directly on the photodetector by the laser source when the external signal generator generates a signal with a frequency of 1 MHz. It is therefore a medium frequency signal. The signal is displayed on the oscilloscope using a coaxial cable connected directly to the photodetector.
- The second one is realized in the same way with the only difference that the external signal generator generates a signal with a frequency of 10 MHz. It is therefore a high-frequency signal.
- The third one is also realized in the same way but with a signal with a frequency of 100 MHz generated by the external signal generator. It is therefore a very high-frequency signal.

As said before, the higher the frequency of the signal, the greater the "zoom" on the signal.

Figure 4.11 below illustrates the signal received by the photodetector in the first test. The signal is overall quite square and quite noisy but it is possible to observe that an impulse occurs every $1\text{ }\mu\text{s}$ which is consistent with the 1 MHz frequency.

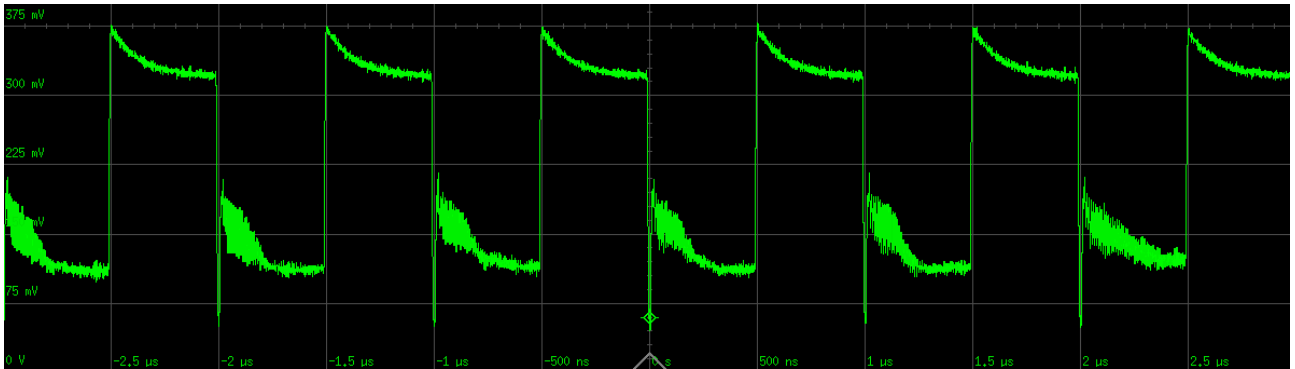


Figure 4.11: Signal received by the photodetector when a 1 MHz frequency signal is generated.

Figure 4.12 below illustrates the signal received by the photodetector in the second test. The signal tends to be less and less square but is slightly less noisy than in the first test. As a result, it is possible to observe that an impulse occurs every 100 ns which is consistent with the 10 MHz frequency.

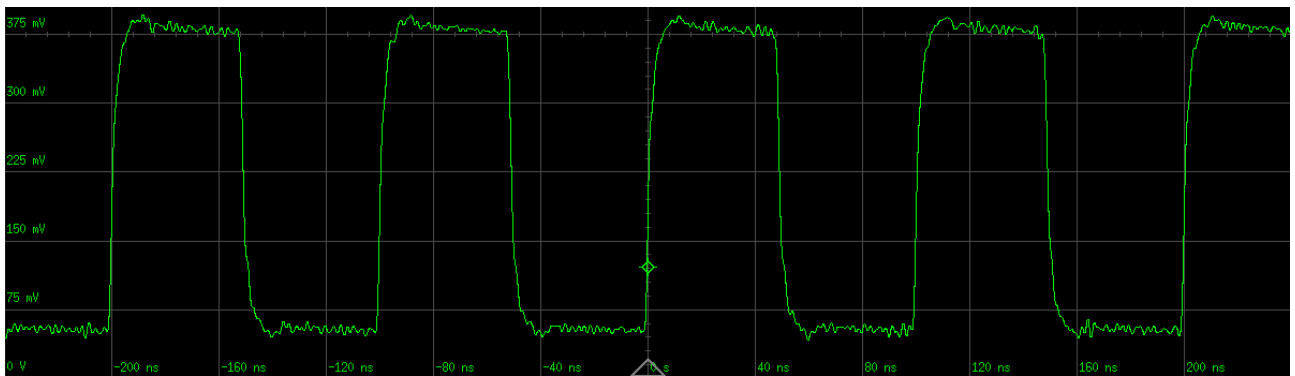


Figure 4.12: Signal received by the photodetector when a 10 MHz frequency signal is generated.

Figure 4.13 below illustrates the signal received by the photodetector in the third test. The signal is not really square anymore but is not very noisy. It is possible to observe that an impulse occurs every 10 ns which is consistent with the 100 MHz frequency.

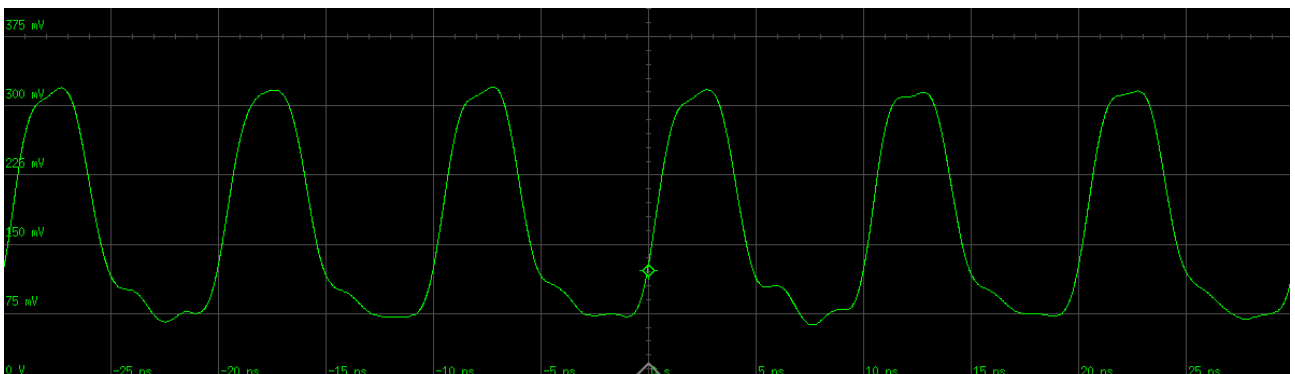


Figure 4.13: Signal received by the photodetector when a 100 MHz frequency signal is generated.

In conclusion, the signals received by the photodetector are very consistent with the frequency generated by the external signal generator. As the material used is not the most optimal, the signals are noisy. However, this does not prevent the laser source from operating correctly and the latter functions and reacts correctly according to the frequency.

4.3 Conclusion

Preliminary verification tests as well as performance tests of the optical laser source were therefore carried out in order to verify whether the objectives set at the beginning of this thesis had been achieved. For the preliminary verification tests, some precautionary measures were adopted to avoid any risk of damage. For the performance tests, these precautionary measures were no longer necessary.

First of all, preliminary verification tests have demonstrated that the PCB operates as desired. Indeed, the current consumption are coherent and no device or component overheats even during long term use of the optical laser source.

Then, the different devices correctly interact and the drivers are correctly controlled by the **Arduino Nano**. Indeed, it is possible to configure the laser source with a variable number of diodes between zero and nine. It is therefore possible to adjust the power of the laser source.

Finally, the **Si5340 Clock Generator** was tested and works correctly. Therefore, this device will be used as soon as the laser source will be integrated onto the interface board using an FPGA module.

As the performance tests are concerned, the performances of the optical laser source composed of nine laser diodes were compared with those of a laser source composed of only one diode. As the two main objectives of this project are to conceive an optical laser source that, on the one hand, has a high power and, on the other hand, emits light over a wide area, the full laser source is the most appropriate to achieve them. Indeed, the full laser source has a higher optical power and irradiance from a distance of 5 cm and beyond and will therefore be able to consider more easily the possibility of integrating the two functions described in section 1.2.2 subsequently.

Furthermore, from a distance of 5 cm and beyond, the efficiency of the full laser source is higher than that of the laser source composed of only one diode. As one of the functions of this project will be to emit the light over a wide area at a relatively long distance, *i.e.* greater than 15 cm, the full laser source is more suitable. However, in general, the efficiency of the laser diodes is very low, *i.e.* less than 1%, but this is one of the main characteristics of lasers.

Finally, the signals emitted by the optical laser source are analysed. Impedance matching, which is the ability of the circuit to efficiently transfer signals from the source to the routing and then from the routing to the load, has a remarkably negative impact on the performance of the circuit if it is not handled correctly. This is therefore a crucial point in this project. The results of the signals emitted by the laser source illustrate the fact that impedance matching is well handled. Therefore, the whole PCB is properly routed.

Chapter 5

Possible Improvements

The objective of this chapter is to present the possible improvements of the optical laser source conceived in the framework of this project. As far as the choice of devices and components is concerned, very good ones were chosen and found perfect for this type of application, *i.e.* the conception of a laser source. However, there are some possible improvements that could enhance the performances of the laser source and that could make it easier to use and configure.

5.1 Enhance Laser Source Performances

As explained in the section 1.2.2, the two main objectives of this work were to conceive an optical laser source that, on the one hand, has a higher power and, on the other hand, emits light over a wider area than that developed by the two PhD students of the Microsys laboratory. The last objective was to make the laser source configurable. As all these objectives are achieved, the laser source will be used to meet the two specific functions required, namely, on the one hand, to measure the distance between a sensor and a target according to the ToF principle and, on the other hand, to realize a three-dimensional camera capable of observing a whole area of this same target.

As also explained in section 1.2.2, as the PhD student's interface board is not yet achieved, the integration of the optical laser source and consequently the testing of the above two functions cannot yet be performed. However, I wondered if it would already be possible to improve the laser source to meet the two specific functions required even by further increasing the distance between the sensor and the target. The answer is yes, but this would require the following two additional features:

- In order to measure a greater distance between the sensor and the target, the first feature would be to have the power of the optical laser source increased.
- In order to realize a three-dimensional camera capable of observing a whole area of a target at a longer distance, the second feature would be to have the moment when the optical laser source is deflected from the target as delayed as possible.

One solution to obtain these two additional features would be to place a convex optical lens in alignment with the laser source and close enough to it as the laser diodes emit an orthotropic light. A convex optical lens is a lens that merges the light rays passing through it at a particular point. The intended purpose would be as theoretically illustrated in the following figure:

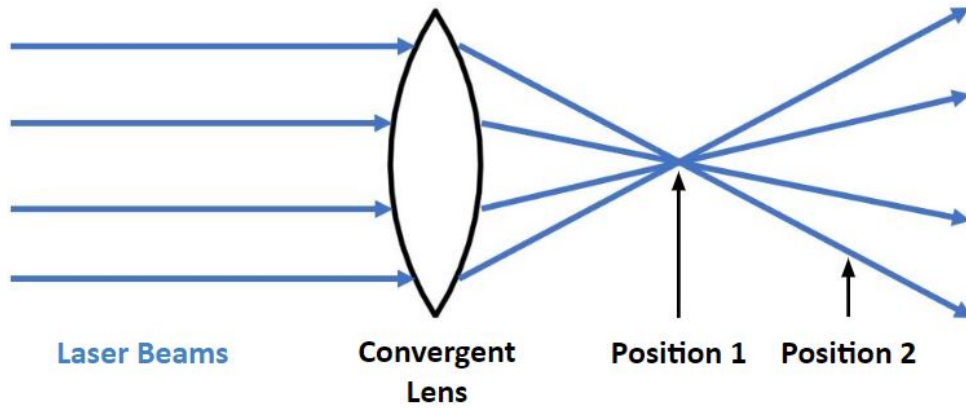


Figure 5.1: Laser source emitted on a convergent lens.

A solution to obtain the first feature would therefore be to use the convergent optical lens as shown in the figure above. This would allow all nine laser diodes to be focused at a single point which is POSITION 1. Therefore, the target should be placed at this POSITION 1 as this is where the optical power would be maximum.

A solution to obtain the second feature would also be to use the same convergent optical lens. Indeed, depending on the area of the target to be observed, this target should be placed at about POSITION 2.

One solution to improve the performance of the optical laser source conceived in this project would therefore be to use a convergent optical lens. However, a first disadvantage of using a convergent optical lens would be that it would be necessary to choose between either to measure the distance between the sensor and the target or to observe the whole area of the target. These two uses of the laser source could no longer be performed simultaneously. A second disadvantage would be the different reflections of the laser beams on the target.

5.2 Facilitate Laser Source Use

5.2.1 Graphical User Interface

The first improvement to facilitate the use of the optical laser source would be to use a Graphical User Interface to control this laser source. This interface would have several features:

- The first one would be to regulate the current that supplies the nine laser diodes. This would make it possible to put some diodes on stand-by and to power others as needed.
- The second one would be to be able to give the temperature of the heat generated by the laser source in real-time and thus be able to monitor that there is no overheating. For this purpose, a temperature sensor would be used, which is the second possible improvement to this project described in the following section 5.2.2.
- The third one would be to be able to give the voltage across the laser diodes directly in order to monitor that there is no overvoltage. This explains why there is the LD_Voltage pin on Arduino Nano.

- The fourth one would be to be able to give the current consumed by the laser diodes directly to monitor that there is no overcurrent. This explains the presence of the LD_Current pin on **Arduino Nano**.
- The fifth one would be to return all the errors of the **iC-HSB Drivers**, *i.e.* the errors that the status registers of the **iC-HSB Drivers** return. This is why there is the NCHK pin on **Arduino Nano**.

These functions are already possible thanks to the serial monitor which allows communication with the **Arduino Nano**. However, a GUI is much more instinctive and would make the laser source easier to use.

This improvement has already been started but due to lack of time, could not be finalised. Indeed, thanks to the PyQt tool described in the section 2.2, the GUI is already created and its extended view is to be found in appendix D. The pins to connect the GUI with **Arduino Nano** are also already present. What remains to be done is to make the necessary connections between the GUI and the **Arduino Nano** by implementing all the functions so that the **Arduino Nano** will respond to the different information sent by the GUI and so that the **Arduino Nano** will send the information that the GUI requests.

5.2.2 Temperature sensor

The second improvement to facilitate the use of the optical laser source would be to add a temperature sensor in the centre of the laser source, *i.e.* in the middle of the circle formed by the nine laser diodes. This should have been the case. However, because of Covid-19, some components have been out of stock. Therefore, the temperature sensor could not be ordered.

This temperature sensor was included in the design of the PCB. Indeed, on sheet 1 of 8 of appendix A, the temperature sensor is part of the electrical circuit. It had to use the I²C communication protocol to communicate with the **Arduino Nano** and give the temperature to the GUI in real-time. Therefore, to monitor the temperature, an infrared temperature sensor was used but was not convenient.

Chapter 6

Final Conclusion

This Master's Thesis presented the conception of a high-power, high-frequency optical laser source able to emit light over a wide area and also to be configurable.

The first part of this thesis presented the different aspects of the Time-of-Flight (ToF) principle and the concept of the Single Photon Avalanche Diode (SPAD). The ToF principle consists in measuring the time needed for light to travel between a sensor and a target in order to provide an accurate distance measurement. A SPAD is a photodetector device consisting of a P-N junction. When a single photon impacts this junction, it triggers an avalanche which generates a current flow. For applications such as 3D imaging, SPADs are excellent photodetectors.

The theories of operation of a Light-Emitting Diode (LED) and a laser diode were then explained in order to compare the advantages and drawbacks of each of them in order to conceive the optical laser source. After analysis, it was found that laser diodes were more suitable for this type of application because of their advantages, namely:

- A laser diode emits convergent light, whereas the light emitted by a LED is highly divergent. The light from a laser diode is therefore described as coherent, whereas that from a LED is described as incoherent.
- A laser diode has a single wavelength and is therefore monochromatic, whereas a LED is polychromatic.
- The response time of a laser diode is much shorter than that of a LED.
- A laser diode has a higher optical efficiency than a LED.

Consequently, laser diodes are used in optics and electronics, while LEDs are used for lighting.

The second part of this thesis detailed the complete carrying out of the electrical system of the optical laser source composed of nine diodes.

First of all, the different electrical devices and components needed and their connections were developed.

Then, the Printed Circuit Board (PCB) was conceived considering the assembly details of the different devices and components. The PCB has the following dimensions: 75.6 mm × 109.69 mm ($\approx 8300 \text{ mm}^2$). It consists of four layers with a total of 174 devices and components. Some assembly problems were present, like shortcuts while soldering. These problems were quickly solved and the PCB could be made operational.

The next step was to develop a method to dissipate the heat from the PCB and more specifically from the laser diodes. Indeed, a drawback of laser diodes is that the emission of photons is highly temperature-dependent. It was, therefore, essential to dissipate this heat so that it did not affect the amount of light emitted and the current of the laser diodes. For this reason, a heat sink was machined using a Computer Numerical Control (CNC) system and placed above the nine laser diodes.

Finally, the software architecture was implemented in order to establish the I²C communication protocol between the devices forming the laser source. The core of this project is an **Arduino Nano 33 IoT** thanks to which the communication could be established. As regards this subject, one of the problems encountered during the implementation of the software concerned the datasheet of the **iC-HSB Ultrafast Laser Drivers**. Indeed, this latter contained a certain number of errors which delayed the achievement of this part. The origin of this problem can be explained by the fact that the **iC-HSB Ultrafast Laser Drivers** are devices which are still in the preliminary development phase.

The third part concerned the practical experimentation of the optical laser source conceived entirely previously.

Firstly, preliminary verification tests were performed. They demonstrated that, on the one hand, the current consumption of the PCB is consistent and does not lead to overheating and, on the other hand, that the different devices operate correctly.

Secondly, more extensive performance tests were performed. The performances of the laser source composed of nine diodes were compared to those of a laser source with only one diode. These tests revealed several elements:

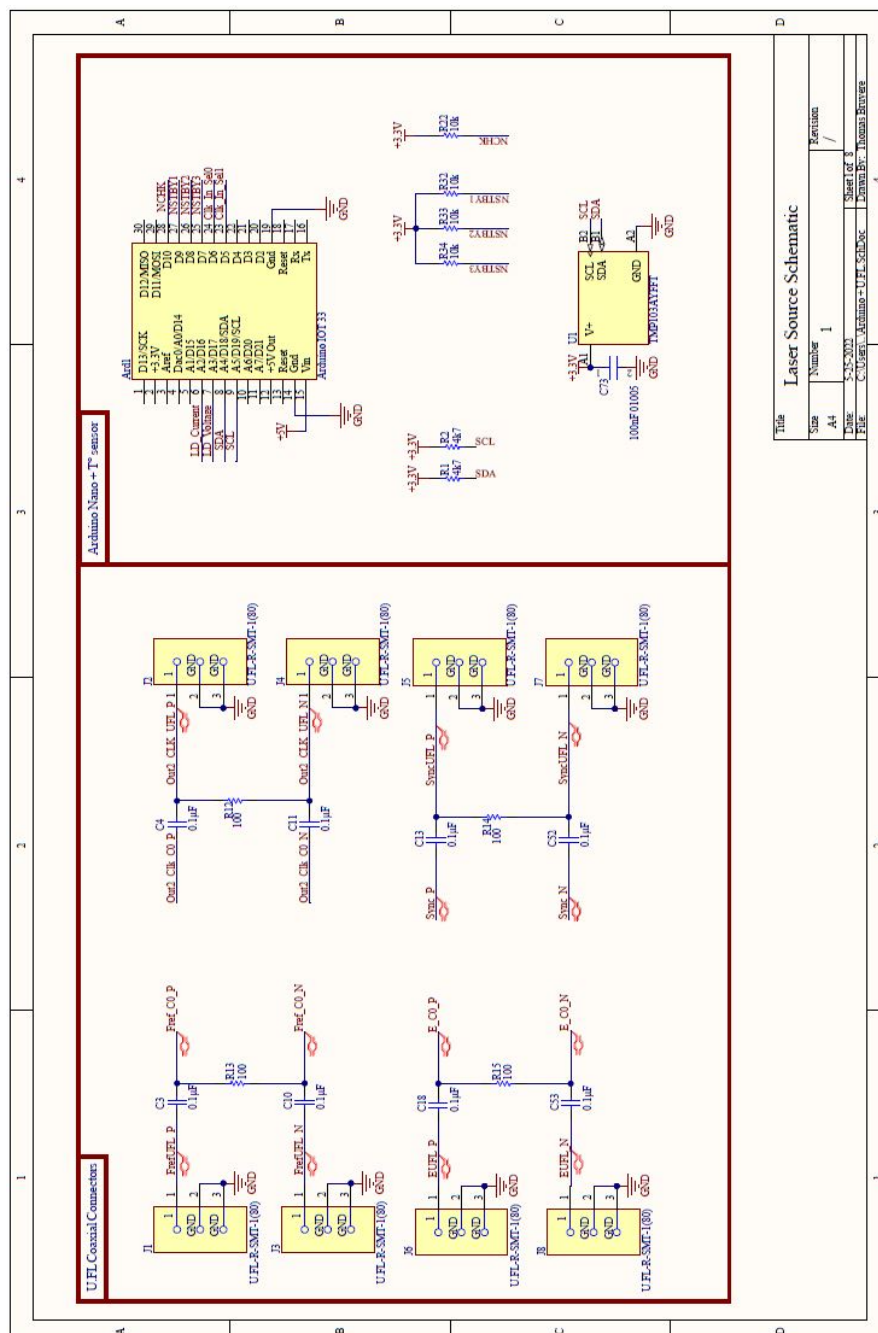
- From a distance of 5 cm from the laser source and beyond, the optical power, irradiance and efficiency are higher for the full laser source than for the one composed of a single diode.
- From a distance of 15 cm, the performances of the full laser source remain relatively good and are much better than those of the laser source with a single diode which, for it, become very weak at this same distance.
- The emitted signals from the full laser source at a distance of 15 cm were analysed and were very consistent.

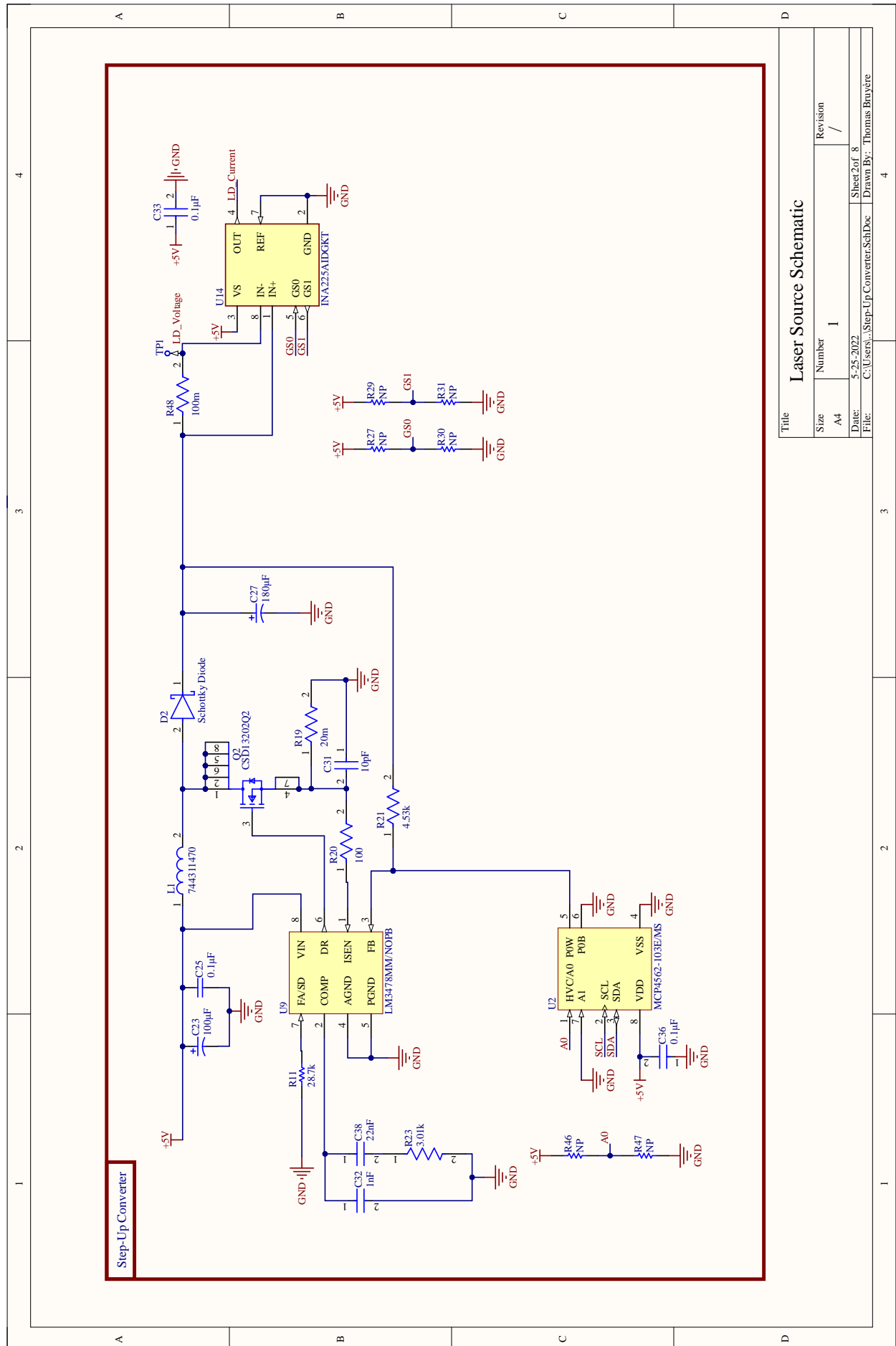
All these results validate the correct operation of the optical laser source and consequently, the different objectives that had been set out.

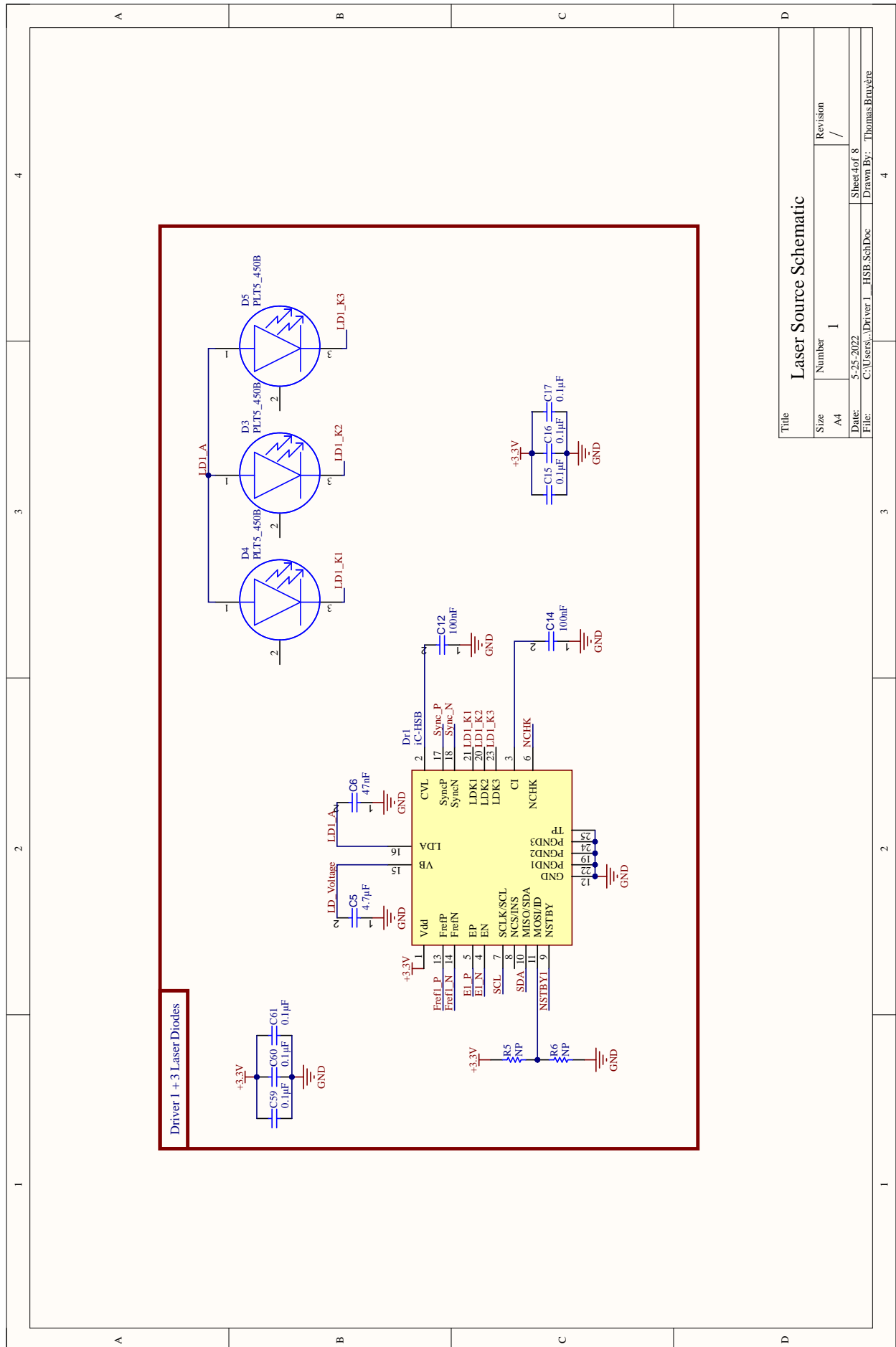
Some possible improvements have been discussed in order to, on the one hand, enhance the performances of the optical laser source and, on the other hand, facilitate its use. These improvements are respectively the use of a convergent optical lens and the implementation of a Graphical User Interface (GUI) with the integration of a temperature sensor. The first one would improve the two specific functions mentioned below.

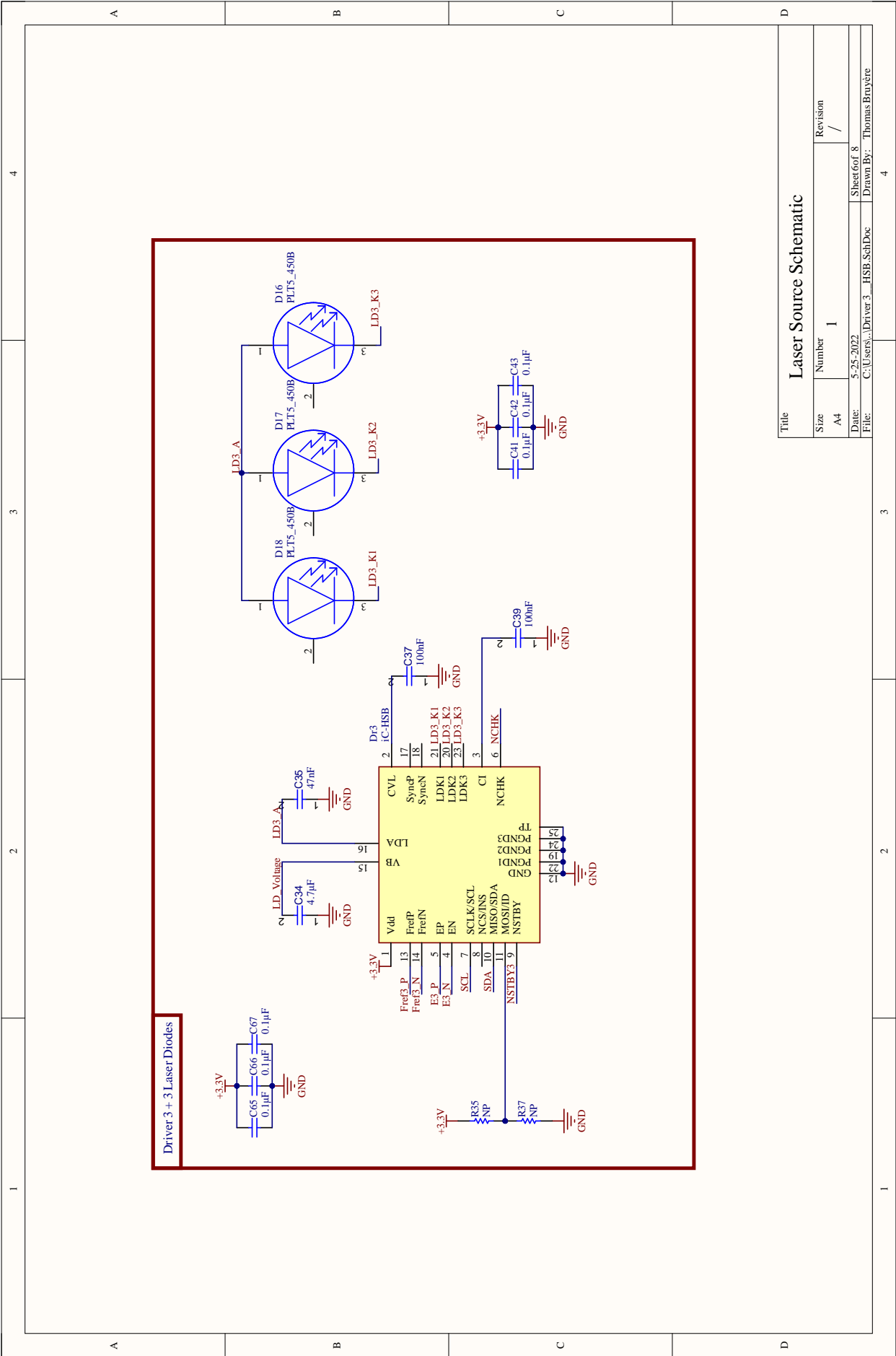
The next step, which is outside the scope of this thesis, will be to integrate the optical laser source onto an interface board containing an integrated sensor, peripheral circuits and an FPGA module in order to test the two specific functions which are, on the one hand, the measurement of the distance between a sensor and a target according to the ToF principle and, on the other hand, the realization of a three-dimensional camera capable of observing a whole area of this same target. This interface board is under development in the Microsys laboratory.

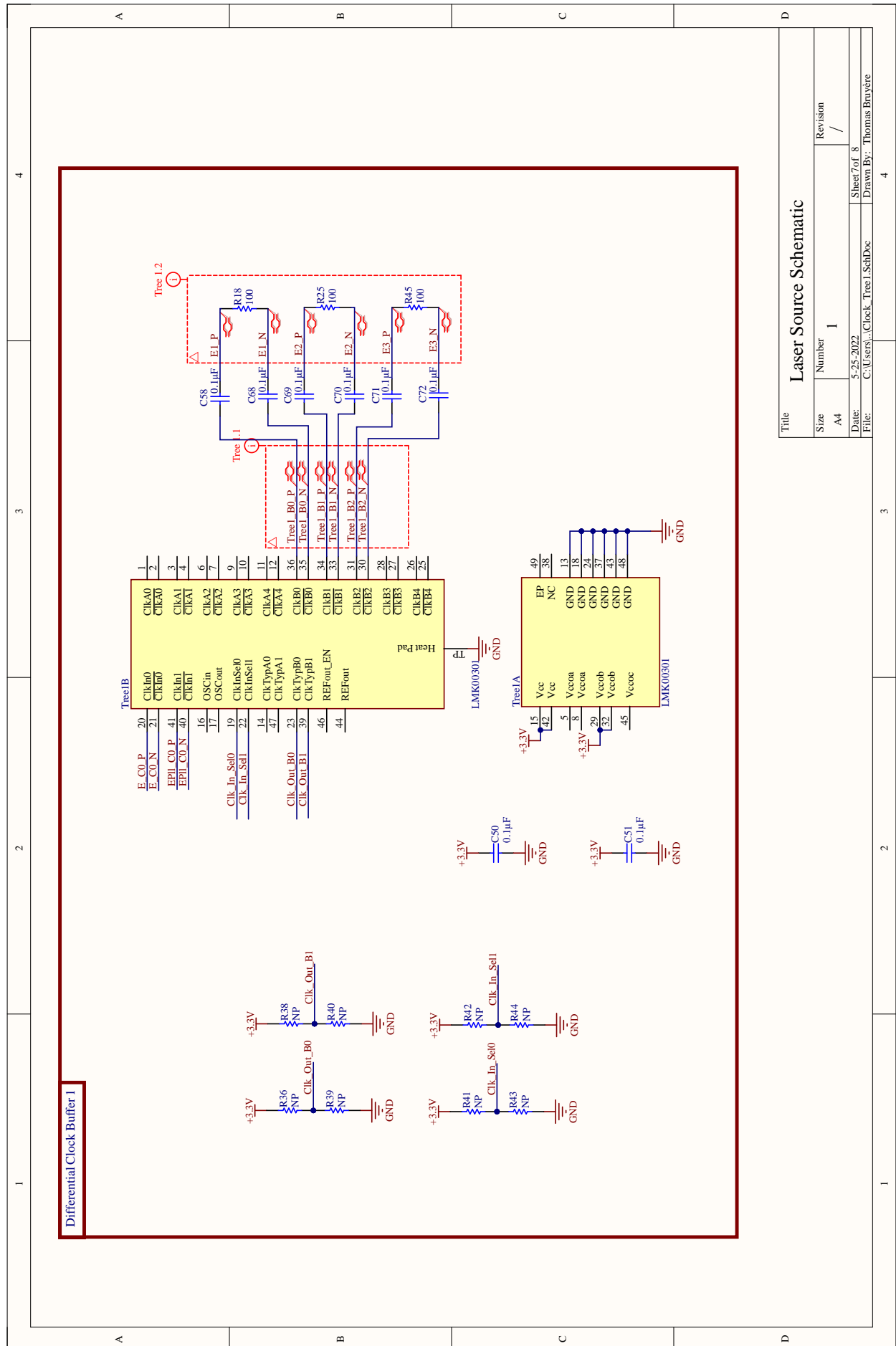
Altium Complete Schematics







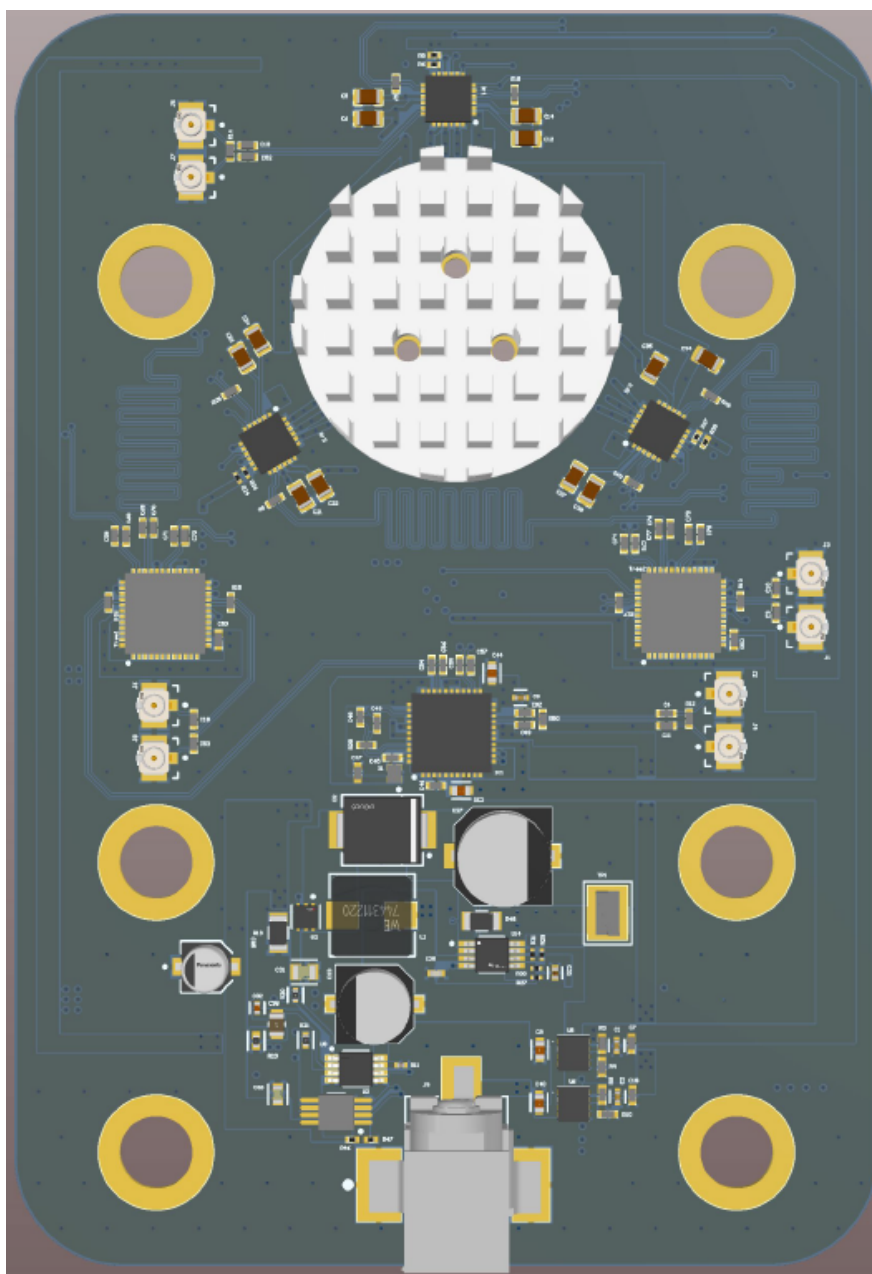




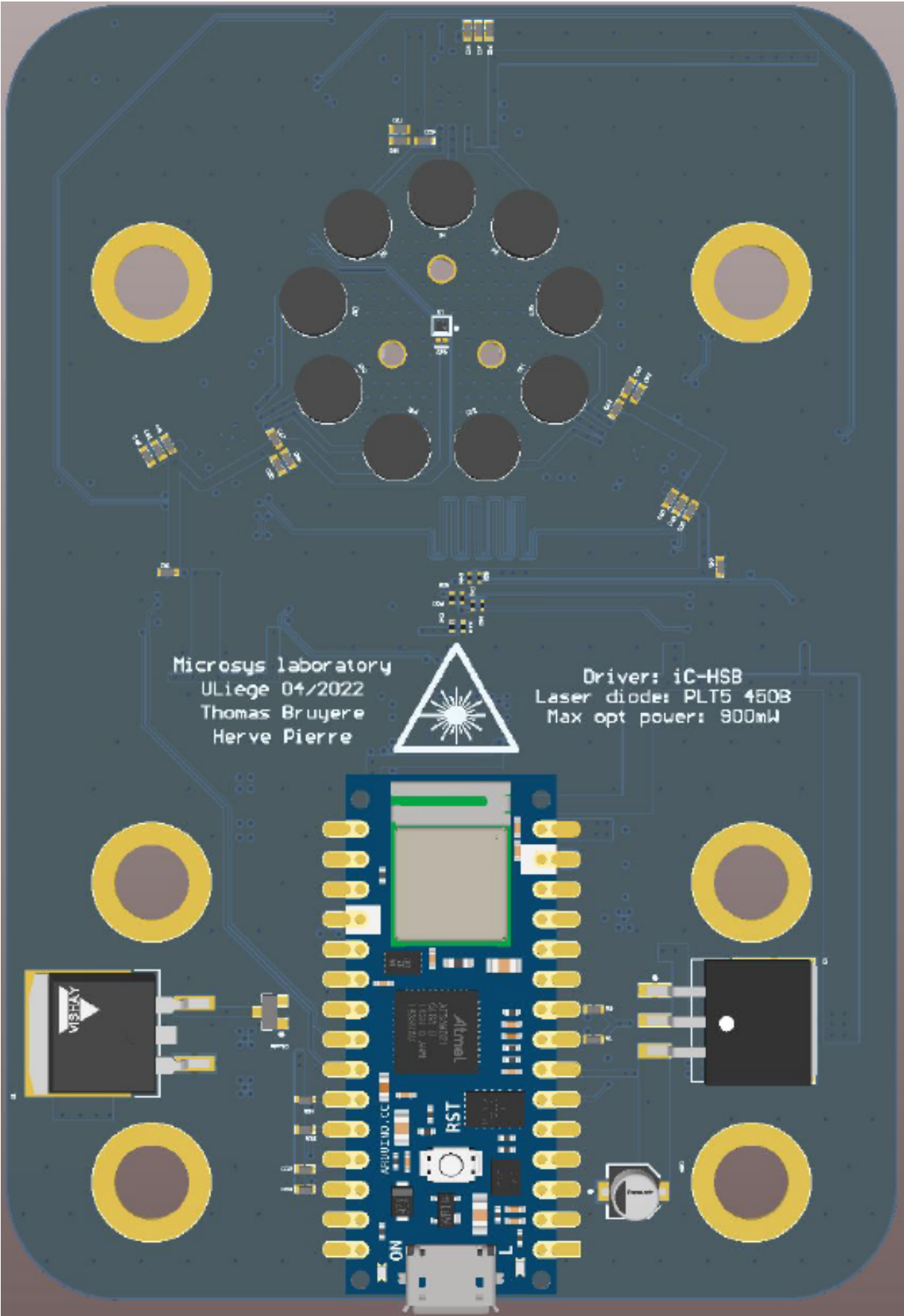
Appendix B

Complete PCB

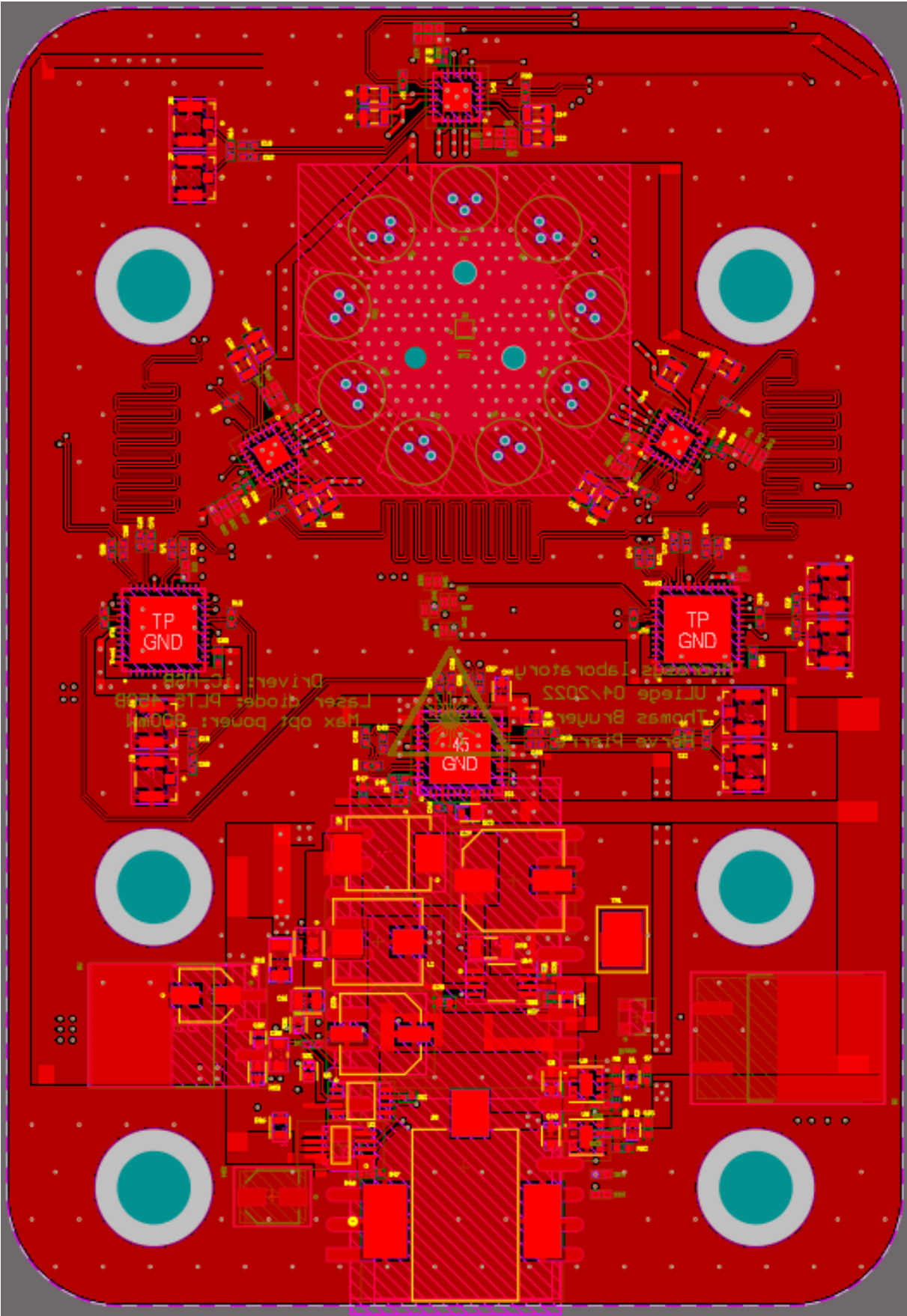
B.1 3D PCB - Front view



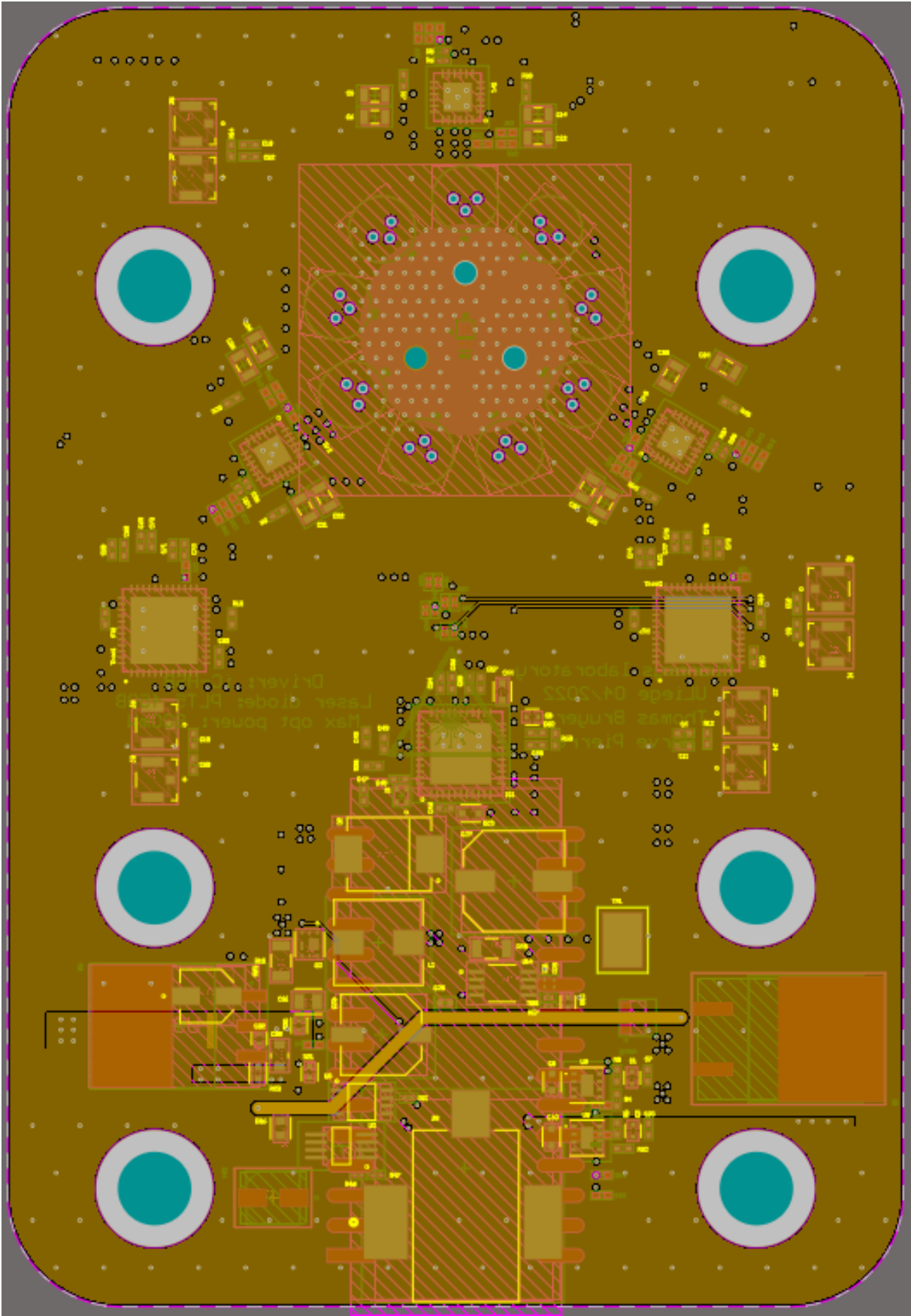
B.2 3D PCB - Back view



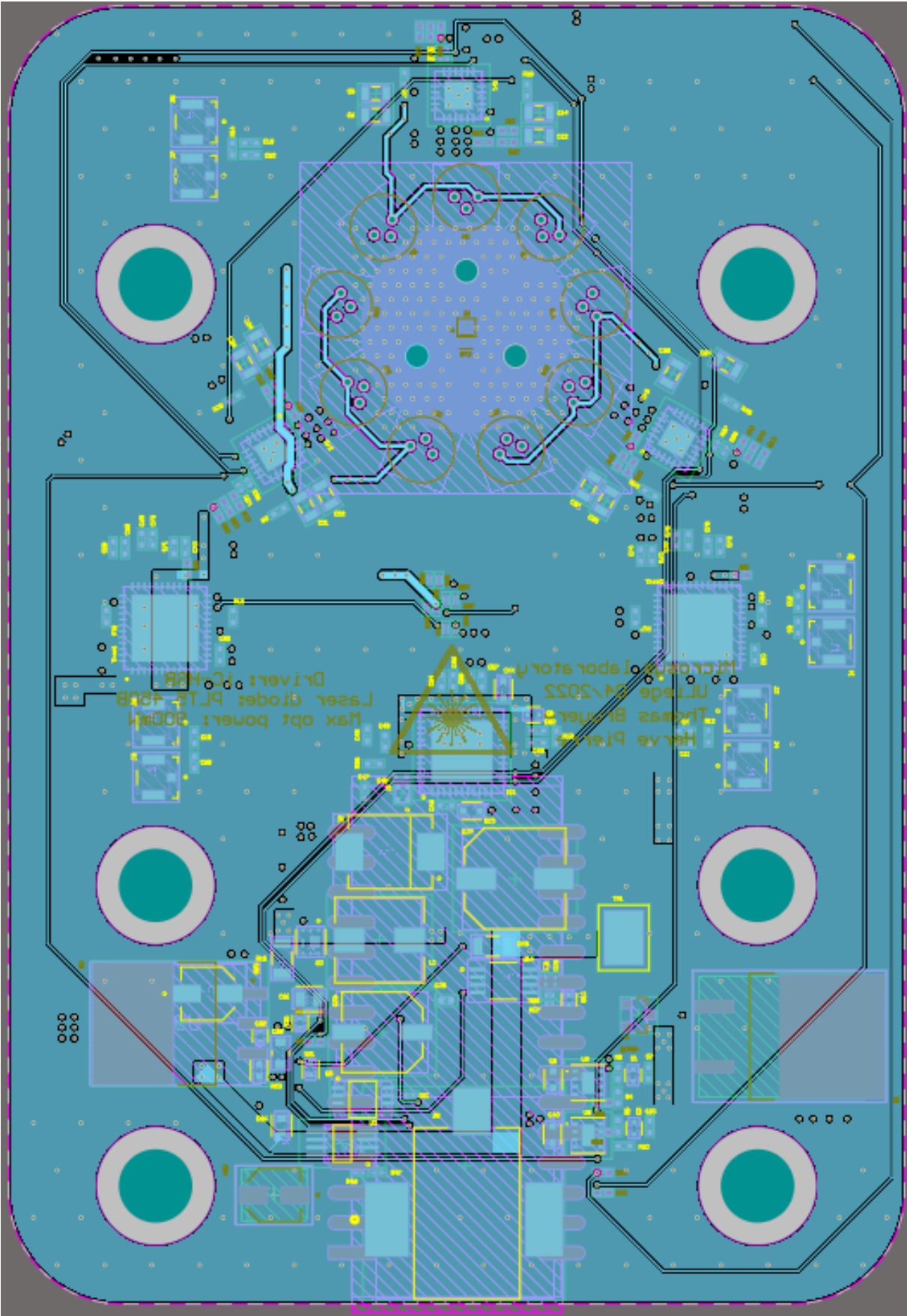
B.3 2D PCB - Top Layer



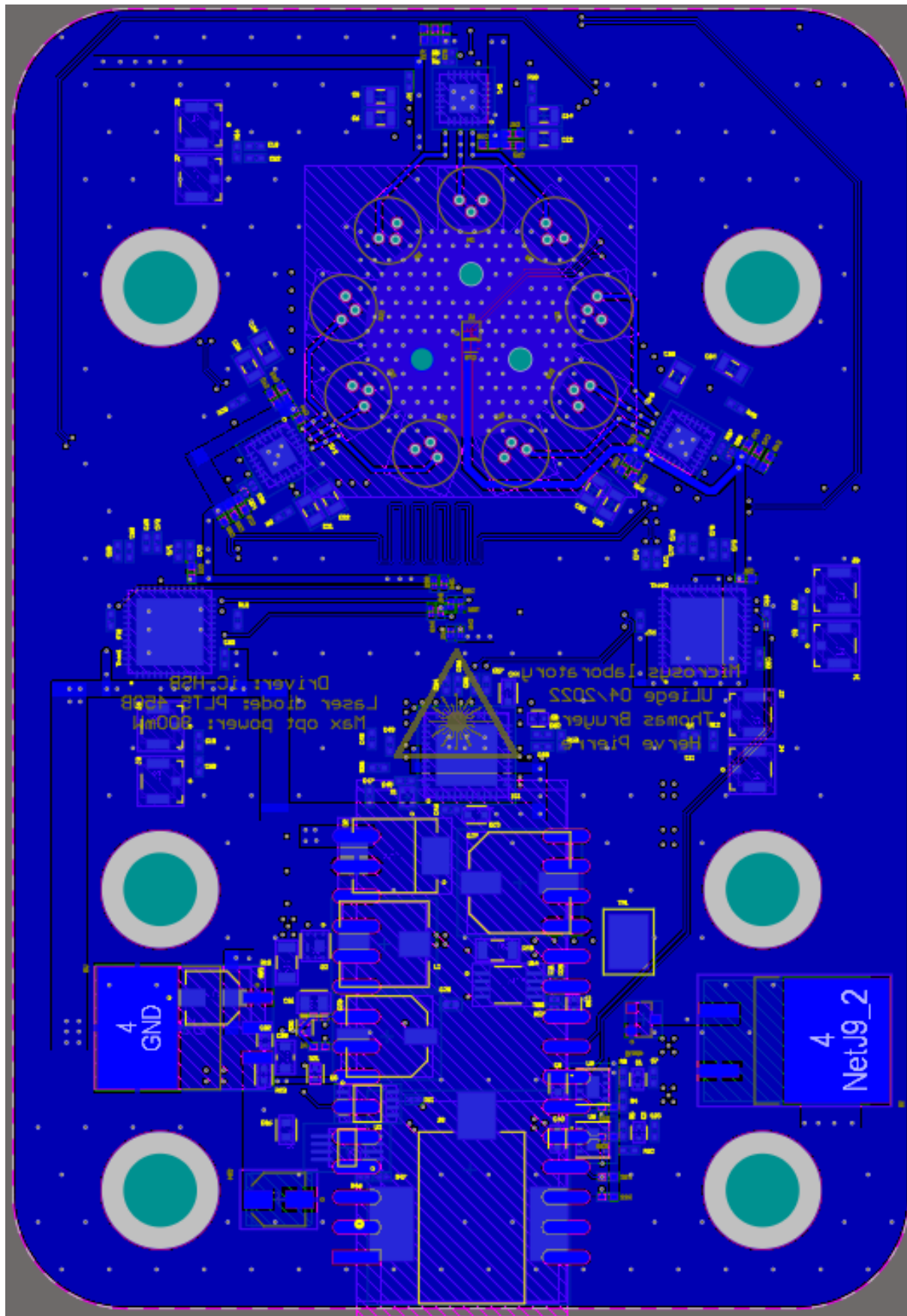
B.4 2D PCB - Plane Layer 1



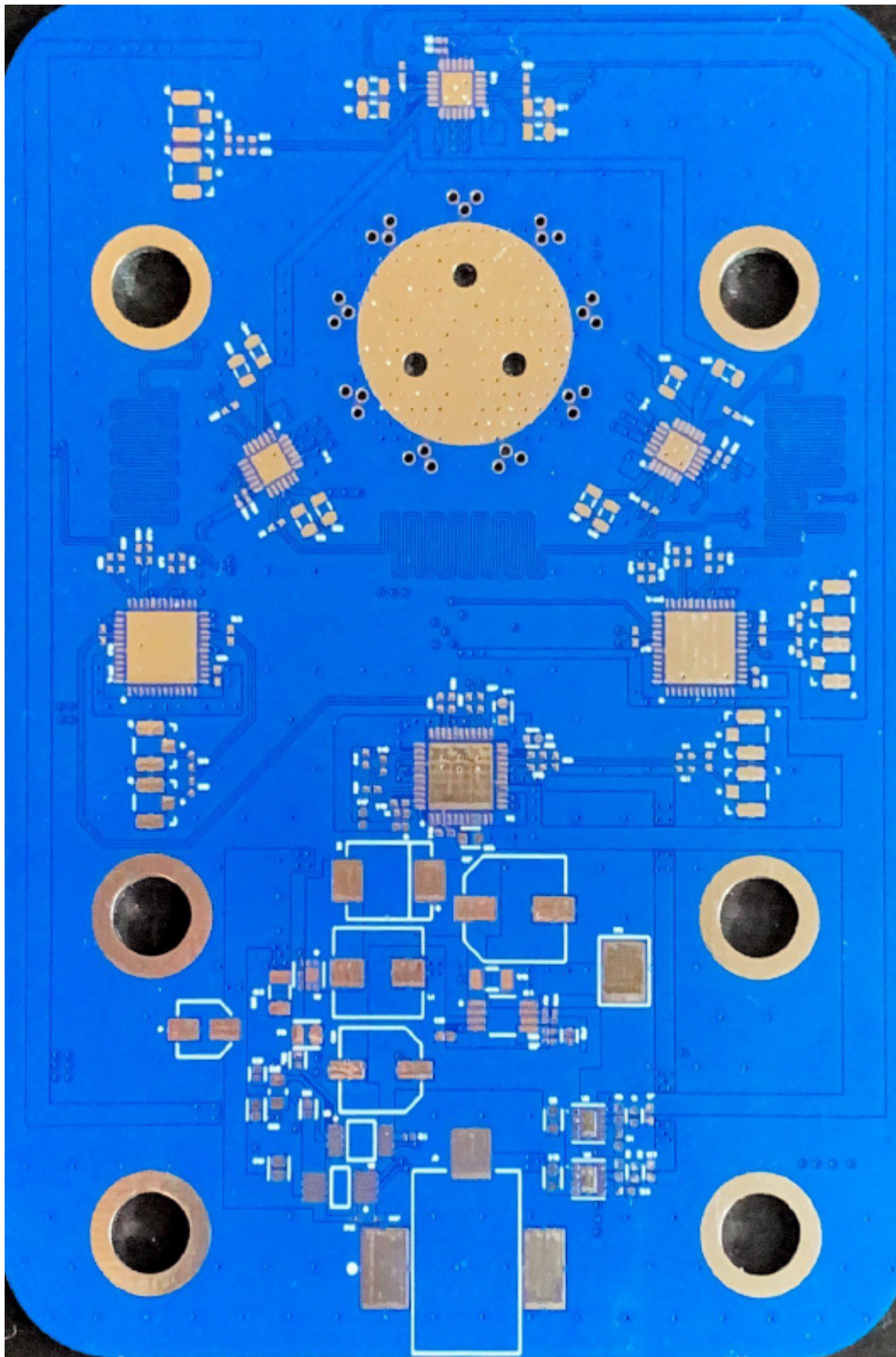
B.5 2D PCB - Plane Layer 2



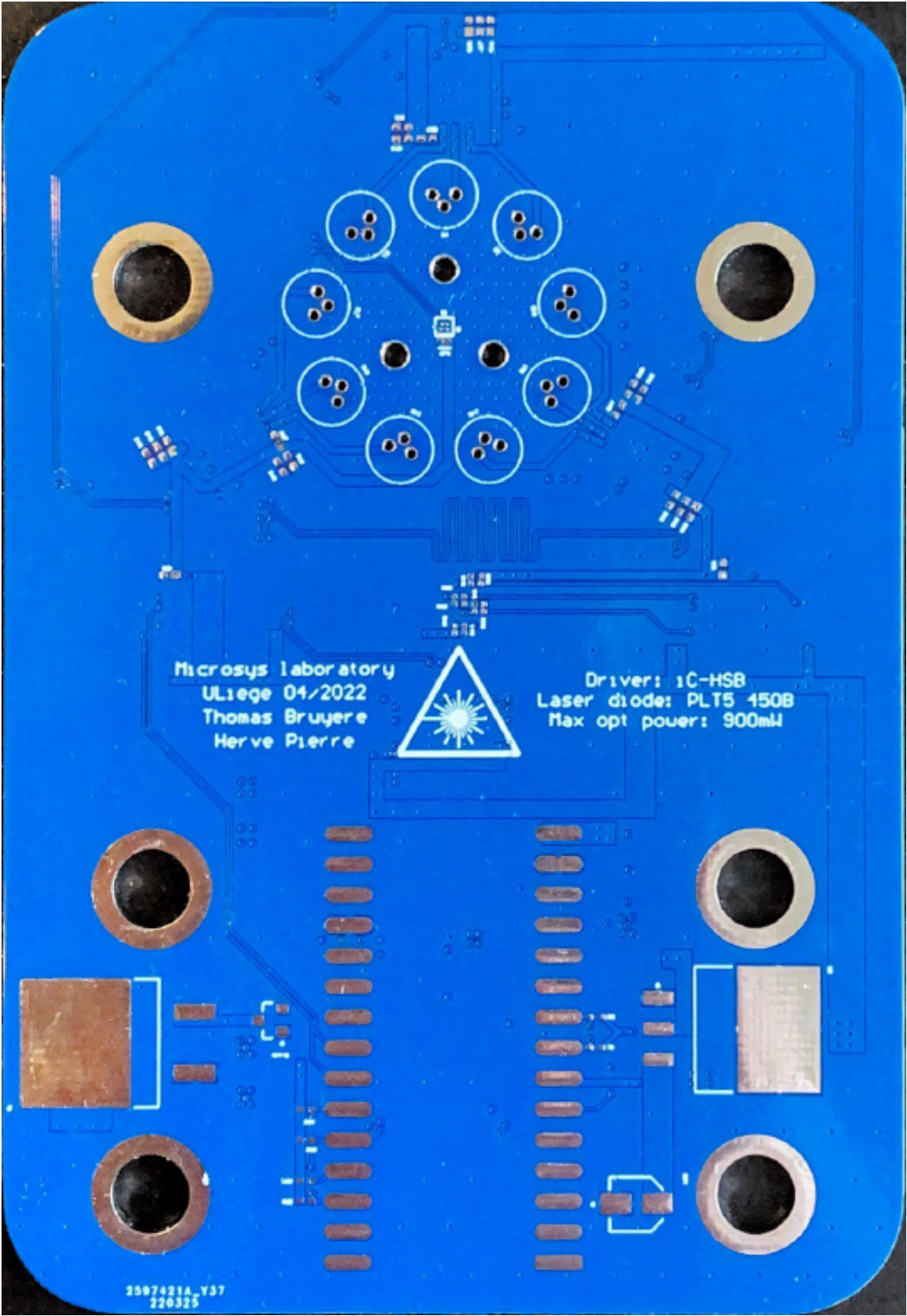
B.6 2D PCB - Bottom Layer



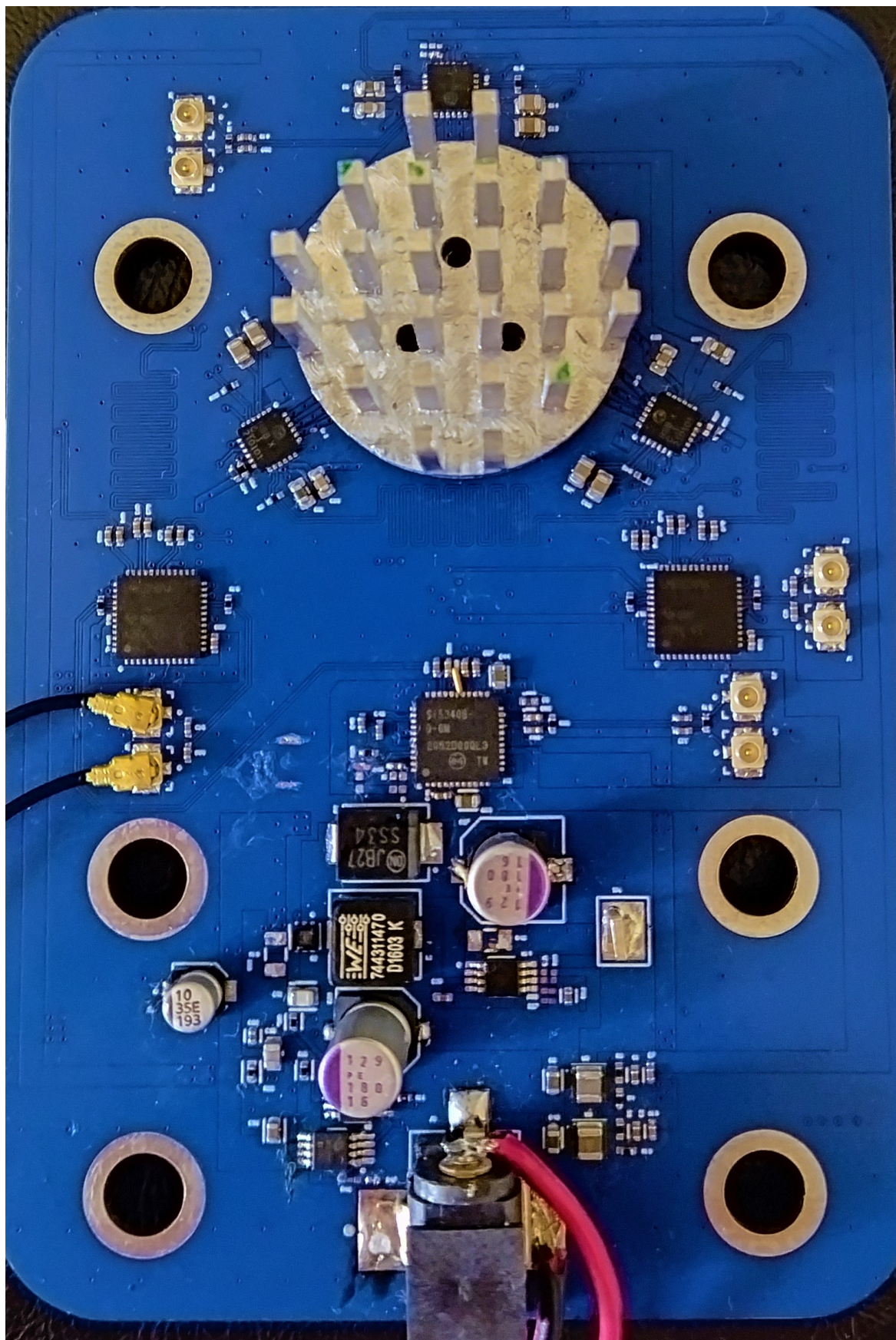
B.7 Real PCB - Front view before soldering



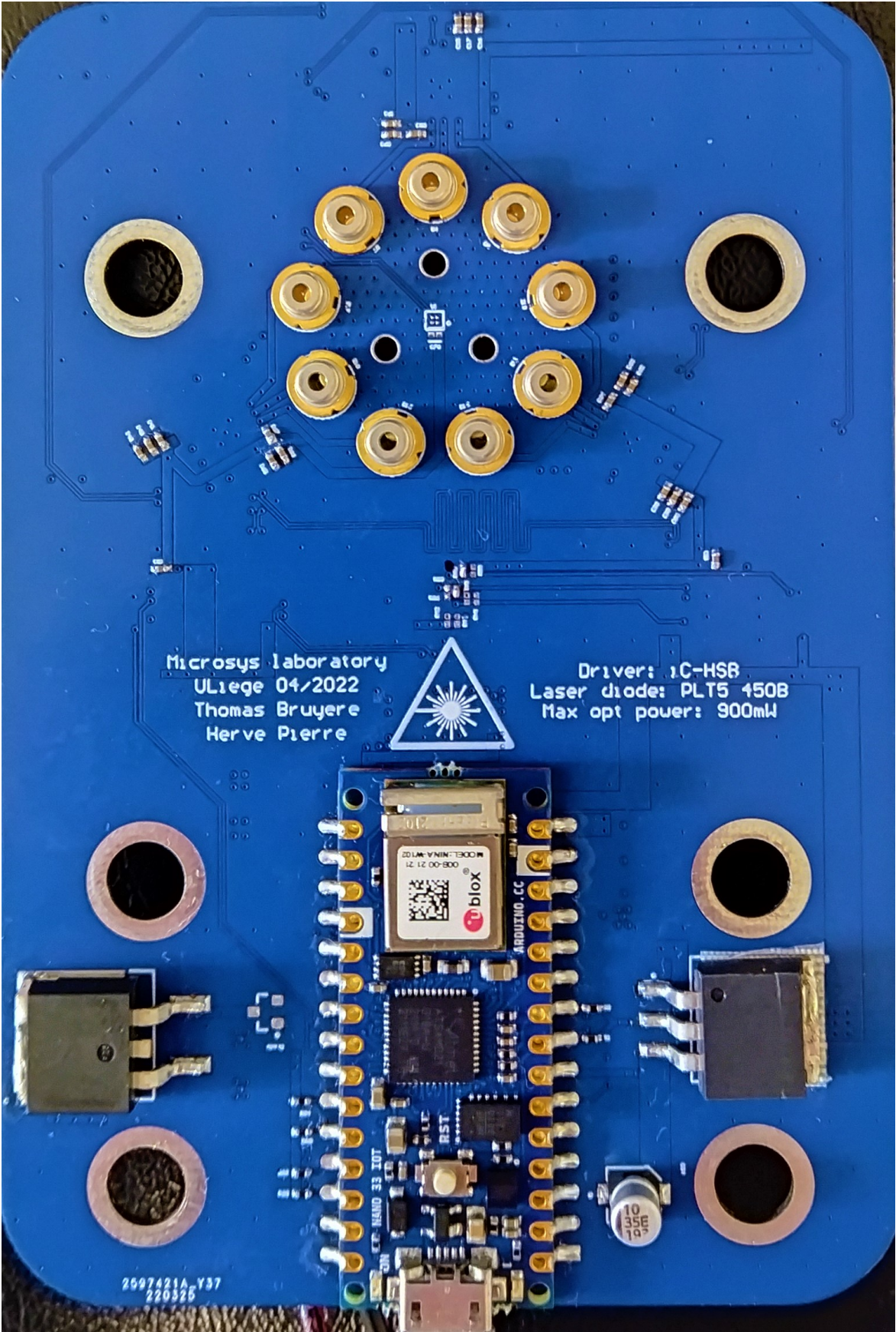
B.8 Real PCB - Back view before soldering



B.9 Real PCB - Front view after soldering



B.10 Real PCB - Back view after soldering



Appendix C

Further Explanations on the Software Part

Definition of I²C addresses in binary

For example, for the first iC-HSB Driver whose hexadecimal address is 0x70, the definition of this address is noted:

```
#define iC_HSB_ADDRESS1 0b1110000;
```

where *#define* is the statement and *iC_HSB_ADDRESS1* is the name of the constant which is used in the different files and corresponds to the binary number 0b1110000. The other two iC-HSB Drivers are defined in the same way with their respective binary address.

Enumeration of the set of data bits

For example, what is implemented to enumerate bit 7 of register 0x10 is:

```
enum iC_HSB_laser_enabled_disabled {iC_HSB_DISLSR_0 = 0b00000000,  
iC_HSB_DISLSR_1 = 0b10000000};
```

where *iC_HSB_laser_enabled_disabled* is the name of the enumeration, *iC_HSB_DISLSR_0* is the first constant whose associated binary number is 0b00000000 and *iC_HSB_DISLSR_1* is the second constant whose associated binary number is 0b10000000. These two constants are used if bit 7 of register 0x10 is to be set high to enable the laser or low to disable it. Obviously, some operations on the iC-HSB Drivers require the configuration of several bits. For example, setting the current at the LDA pin requires 4 data bits of the 0x15 register. There are then $2^4 = 16$ different bit combinations to choose the desired current value. Therefore, 16 different enumerations are required in the header file.

Operation of the write_one_bit_in_register function

The operation of this function is as follows:

- First, the transmission begins with a condition *start* and then by pointing to the address of the slave to be communicated with. The master, therefore, attracts the attention of the right slave, *i.e.* the right iC-HSB Driver.

- Then the address of the register in which the set of data bit states is to be changed is pointed to.
- Afterwards, there is a *restart* condition, *i.e.* the transmission is not finished. The master thus continues its transmission.
- After that, the master tells the slave that it wants to read one or more bytes from the register it pointed to before. The slave then returns the number of available bytes to the master, which is always 1 in the case of the **iC-HSB Drivers** because the registers are composed of only one byte. The master then reads this byte that the slave has sent back in order to know the states of the different data bits.
- The master, therefore, knows the state of the various bits and their position in the register being pointed to. Therefore, it can point to a single data bit in order to change its state using the *bitWrite* statement.
- Finally, the transmission is definitely ended with a condition *stop*.

Operation of the `write_two_bit_in_register` function

The operation of this function is almost identical to the *write_one_bit_in_register* function which allows a single bit to be changed. The only difference is when the master points to a single data bit to change its state. To change the state of two data bits, it first points to the first bit whose state it wants to change using the *bitWrite* statement. Then it points to the second bit whose state it wants to change again using the same statement. It, therefore, performs the same statement twice, one after the other. Then it also ends the transmission with a condition *stop*.

Operation of the `write_full_bits_in_register` function

The operation of this function is as follows:

- First, the transmission begins with a condition *start* and then by pointing to the address of the device to be communicated with. The master, therefore, attracts the attention of the right slave.
- Then the address of the register in which the set of data bit states is to be changed is pointed to.
- Afterwards, the data bits are written to the register that was pointed to.
- Finally, the transmission is ended with a condition *stop*.

For this function, the entire data bits are changed in the register. Therefore, it is not necessary to first read the data bits in order to know their position and then modify the bit to the desired position. In fact, since the number of possible bit positions in the register is equal to the number of bits written to the register, the MSB and LSB data bits are written to the far-left (bit 7) and far-right (bit 0) in the register, respectively. The other data bits are written to their default position.

Operation of the read function

The operation of this function is as follows:

- First, the transmission begins with a condition *start* and then by pointing to the address of the slave to be communicated with. The master, therefore, attracts the attention of the right slave, *i.e.* the right **iC-HSB Driver**.
- Then the address of the register from which the set of data bit states is to be read is pointed to.
- Afterwards, there is a *restart* condition, *i.e.* the transmission is not finished. The master thus continues its transmission.
- After that, the master tells the slave that it wants to read one or more bytes from the register it pointed to before. The slave then returns the number of available bytes to the master, which is always one in the case of the **iC-HSB Drivers** because the registers are composed of only one byte. The master then reads this byte that the slave has sent back in order to know the states of the different data bits.
- The master has therefore completed its reading. It finally sends the stop condition to end the transmission.

First part of the main build file

To define the used pins of **Arduino Nano**, there is a specific statement to write. For example, the `LD_Current` and `NCHK` pins are defined as follows:

```
#define LD_CURRENT 16
#define CHECK_NCHK 10
```

where `#define` is the statement and where `LD_CURRENT` and `CHECK_NCHK` are the names of each of the constants associated with pins 16 and 10 respectively.

Second part of the main build file

Once the pins of **Arduino Nano** are defined, their state must be configured to meet the needs of the project. For example, to set pin `NSTBY1` to the low state, the following statements are written:

```
pinMode(STANDBY_NSTBY1, OUTPUT);
digitalWrite(STANDBY_NSTBY1, LOW);
```

where the first statement defines pin `STANDBY_NSTBY1`¹ as being an output of **Arduino Nano 33 IoT**. The second statement sets the `STANDBY_NSTBY1` pin to the low state.

¹Name given to the constant in the code but corresponds to the `NSTBY1` pin of the Arduino.

First step

For this step, the following statement is written:

```
hsb1.write_two_bits_in_register(iCHSB_REG_CONTROL_STANDBY_CONFIG_MODE,  
0, 0, 1, 1);
```

where *hsb1* points to the address of the first **iC-HSB Laser Driver** and *iCHSB_REG_CONTROL_STANDBY_CONFIG_MODE* is the constant corresponding to the register with the address *0x1C*. The function *write_two_bits_in_register* writes to the data bits *MODE*, *i.e.* positions 0 and 1, of the register *0x1C* the states 0 and 1 respectively. This corresponds to the configuration mode.

Second step

For this step, the following statement is written:

```
hsb1.reset();
```

where *hsb1* points to the address of the first **iC-HSB Laser Driver** and *reset* is the function that resets all registers.

Third step

For this step, to give a typical example, to set the register with *0x10* address, the following statement is written:

```
hsb1.write_full_bits_in_register(iCHSB_REG_CONTROL_LVDS_ENABLE,  
iC_HSB_0x10_0);
```

where *hsb1* points to the address of the first **iC-HSB Laser Driver** and *iCHSB_REG_CONTROL_LVDS_ENABLE* is the constant corresponding to the register with the *0x10* address. The function *write_full_bits_in_register* writes a byte in the *0x10* register. This byte corresponds to the 8 data bits provided by the constant *iC_HSB_0x10_0* which is enumerated in the header file. All registers with *0x10* to *0x1F* address are configured in the same way.

Fourth step

For this step, to give a typical example, to read the register with the *0x10* address that was configured, the following statement is written:

```
hsb1.read(iCHSB_REG_CONTROL_LVDS_ENABLE);
```

where *hsb1* points to the address of the first **iC-HSB Laser Driver** and *iCHSB_REG_CONTROL_LVDS_ENABLE* is the constant corresponding to the register with the *0x10* address. The function *read* reads a byte in the *0x10* register.

Third part of the main build file

“e” command: Fifth step

This step enables the laser. Data bit 7 of the register with the *0x10* address of the **iC-HSB Laser Driver**, *i.e.* data bit *DISLSR* is set to 0. This means that the laser is enabled. For this, the following statement is written:

```
hsb1.write_one_bit_in_register(iCHSB_REG_CONTROL_LVDS_ENABLE, 7, 0);
```

where *hsb1* points to the address of the first **iC-HSB Laser Driver** and *iCHSB_REG_CONTROL_LVDS_ENABLE* is the constant corresponding to the register with the *0x10* address. The function *write_one_bit_in_register* therefore sets data bit 7, *i.e.* data bit *DISLSR*, to 0.

“s” command: Sixth step

The sixth step verifies that there are no errors with the **iC-HSB Drivers**. To give a typical example, to read the status register with the *0x00* address, the following instruction is written:

```
hsb1.read(iCHSB_REG_STATUS_ONE);
```

where *hsb1* points to the address of the first **iC-HSB Laser Driver** and *iCHSB_REG_STATUS_ONE* is the constant corresponding to the status register with the *0x00* address. The function *read* reads a byte in the *0x00* register.

“o” command: Seventh step

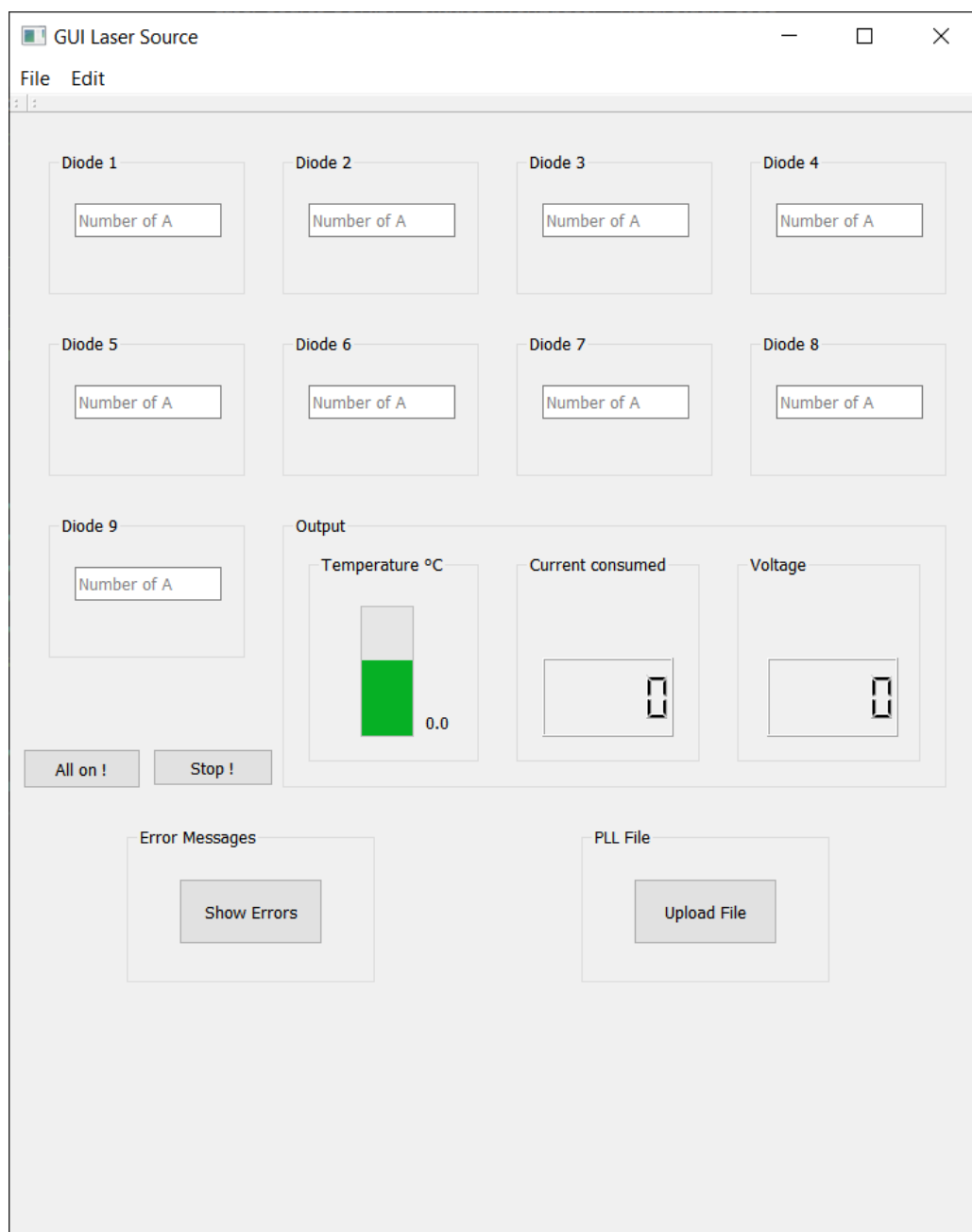
For this step, the following statement is written:

```
hsb1.write_two_bits_in_register(iCHSB_REG_CONTROL_STANDBY_CONFIG_MODE,  
                                0, 1, 1, 0);
```

where *hsb1* points to the address of the first **iC-HSB Laser Driver** and *iCHSB_REG_CONTROL_STANDBY_CONFIG_MODE* is the constant corresponding to the register with the *0x1C* address. The function *write_two_bits_in_register* writes to the data bits *MODE*, *i.e.* positions 0 and 1, of the register *0x1C* the states 1 and 0 respectively.

Appendix D

Graphical User Interface



Bibliography

- [1] Jesse Levinson, Jake Askeland, Jan Becker, Jennifer Dolson, David Held, Soeren Kammel, J. Zico Kolter, Dirk Langer, Oliver Pink, Vaughan Pratt, Michael Sokolsky, Ganymed Stanek, David Stavens, Alex Teichman, Moritz Werling, and Sebastian Thrun. “Towards Fully Autonomous Driving: Systems and Algorithms”. In: *IEEE Sensors Journal* vol. 20.no. 9, May 2020, pp. 4901–4913. Accessed: 2022-02-16.
- [2] Cibby Pulikkaseril and Stanley Lam. “Laser eyes for driverless cars: the road to automotive LIDAR”. In: *Optical Fiber Communication Conference (OFC) 2019*. OSA, 2019. Accessed: 2022-02-17.
- [3] François Piron, Daniel Morrison, Mehmet Rasit Yuce, and Jean-Michel Redouté. “A Review of Single-Photon Avalanche Diode Time-of-Flight Imaging Sensor Arrays”. In: *IEEE Sensors Journal* vol. 21.no. 11, June 2021, pp. 12654–12666. Accessed: 2022-05-09.
- [4] François Blais. “A Review of 20 Years of Range Sensor Development”. In: *Electronic Imaging Journal* vol. 13.no. 1, 2004, pp. 231–243. Accessed: 2022-05-07.
- [5] Federica Villa, Danilo Bronzi, Bojan Markovic, and Alberto Tosi. “SPAD Smart Pixel for Time-of-Flight and Time-Correlated Single-Photon Counting Measurements”. In: *IEEE Photonics Journal* vol. 4.no. 3, June 2012, pp. 795–804. Accessed: 2022-05-08.
- [6] S. Bellisaia, F. Villaa, S. Tisab, D. Bronzia, and F. Zappaa. “Indirect time-of-flight 3D ranging based on SPADs”. In: *Proc. of SPIE* vol. 8268.no. 3, Jan. 2012, pp. 282–289. Accessed: 2022-05-09.
- [7] Darek P. Palubiak and M. Jamal Deen. “CMOS SPADs: Design Issues and Research Challenges for Detectors, Circuits, and Arrays”. In: *IEEE Journal Of Selected Topics In Quantum Electronics* vol. 20.no. 6, Nov. 2014, pp. 409–426. Accessed: 2022-05-09.
- [8] Jesse Levinson, Jake Askeland, Jan Becker, Jennifer Dolson, David Held, Soeren Kammel, J. Zico Kolter, Dirk Langer, Oliver Pink, Vaughan Pratt, Michael Sokolsky, Ganymed Stanek, David Stavens, Alex Teichman, Moritz Werling, and Sebastian Thrun. “Towards Fully Autonomous Driving: Systems and Algorithms”. In: *2011 IEEE Intelligent Vehicles Symposium (IV)*, June 2011. Accessed: 2022-02-15.
- [9] Kiyosumi Kidono, Takeo Miyasaka, Akihiro Watanabe, Takashi Naito, and Jun Miura. “Pedetrian Recognition Using High-definition LIDAR”. In: *in 2011 IEEE Intelligent Vehicles Symposium (IV)*, June 2011. Accessed: 2022-02-16.
- [10] Lars Lindner, Oleg Sergiyenko, Moisés Rivas-Lopez, Mykhailo Ivanov, Julio C. Rodriguez-Quinonez, Daniel Hernandez-Balbuena, Wendy Flores-Fuentes, Vera Tyrsa, Fabian N. Muerrieta-Rico, and Paolo Mercorelli. “Machine Vision System Errors for Unmanned Aerial Vehicle Navigation”. In: *2017 IEEE 26th International Symposium on Industrial Electronics (ISIE)*, June 2017. Accessed: 2022-02-18.

- [11] Cristiano L. Niclass, Alexis Rochas, Pierre-André Besse, and Edoardo Charbon. “A CMOS Single Photon Avalanche Diode Array for 3D Imaging”. In: *2004 IEEE International Solid-State Circuits Conference*, Feb. 2004. Accessed: 2022-02-18.
- [12] Daniel Morrison, Simon Kennedy, Dennis Delic, Mehmet Rasit Yuce, and Jean-Michel Redouté. “A 64×64 SPAD Flash LIDAR Sensor using a Triple Integration Timing Technique with 1.95 mm Depth Resolution”. In: *IEEE Sensors Journal*, 2020. Accessed: 2022-02-15.
- [13] Chao Zhang, Scott Lindner, Ivan Michel Antolovic, Juan Mata Pavia, Martin Wolf, and Edoardo Charbon. “A 30-frames/s, 252×144 SPAD Flash LiDAR With 1728 Dual-Clock 48.8-ps TDCs, and Pixel-Wise Integrated Histogramming”. In: *IEEE Journal of Solid-State Circuits*, vol. 54.no. 4, Apr. 2019, pp. 1137–1151. Accessed: 2022-02-19.
- [14] A. Rochas, M. Gani, B. Furrer, P.A. Besse, Radivoje Popovic, Grégoire Ribordy, and Nicolas Gisin. “Single photon detector fabricated in a complementary metal–oxide–semiconductor high-voltage technology”. In: *The Review of scientific instruments* vol. 74.no. 7, July 2003, pp. 3263–3270. Accessed: 2022-05-08.
- [15] Sam W. Hutchings, Nick Johnston, Istvan Gyongy, Tarek Al Abbas, Neale A. W. Dutton, Max Tyler, Susan Chan, Jonathan Leach, and Robert K. Henderson. “A Reconfigurable 3-D-Stacked SPAD Imager with In-Pixel Histogramming for Flash LIDAR or High-Speed Time-of-Flight Imaging”. In: *IEEE Journal of Solid-State Circuits* vol. 54.no. 11, Nov. 2019, pp. 2947–2956. Accessed: 2022-02-19.
- [16] Federica Villa, Rudi Lussana, Danilo Bronzi, Simone Tisa, Alberto Tosi, Franco Zappa, Alberto Dalla Mora, Davide Contini, Daniel Durini, Sasha Weyers, and Werner Brockherde. “CMOS Imager With 1024 SPADs and TDCs for Single-Photon Timing and 3-D Time-of-Flight”. In: *IEEE Journal of Selected Topics in Quantum Electronics* vol. 20.no. 6, Nov. 2014, pp. 364–373. Accessed: 2022-02-15.
- [17] D. Resnati, I. Rech, A. Gallivanoni, and M. Ghioni. “Monolithic time to amplitude converter for time correlated single photon counting”. In: *Photon Counting Applications, Quantum Optics, and Quantum Information Transfer and Processing II*, May 2009. Accessed: 2022-02-20.
- [18] Yibing M. Wang, Lilong Shi, Chunji Wang, Kwang Oh Kim, Ilia Ovsianikov, and Sungwoo Hwang. “A Direct TOF Sensor with In-Pixel Differential Time-to-Charge Converters for Automotive Flash LiDAR and Other 3D Applications”. In: *Proc. International Image Sensor Workshop*, June 2019, R24. Accessed: 2022-05-10.
- [19] Fabio Remondino and David Stoppa. “TOF Range-Imaging Cameras”. In: *Springer-Verlag Berlin Heidelberg*, July 2013. Accessed: 2022-05-07.
- [20] Daniel Morrison, Simon Kennedy, Dennis Delicy, Mehmet Yuce, and Jean-Michel Redouté. “A Triple Integration Timing Scheme for SPAD Time of Flight Imaging Sensors in 130 nm CMOS”. In: *2018 25th IEEE International Conference on Electronics, Circuits and Systems (ICECS)*, Dec. 2018. Accessed: 2022-02-17.
- [21] Yuji Uchida and Tsunemasa Taguchi. “Lighting theory and luminous characteristics of white light-emitting diodes”. In: *Proc. of SPIE* vol. 44.no. 12, Dec. 2005. Accessed: 2022-02-20.
- [22] S. Y. R. Hui, Huanting Chen, and Xuehui Tao. “An Extended Photoelectrothermal Theory for LED Systems: A Tutorial From Device Characteristic to System Design for General Lighting”. In: *IEEE Transactions On Power Electronics* vol. 27.no. 11, Nov. 2012, R24. Accessed: 2022-02-20.

- [23] Physics and Radio-Electronics. *Light Emitting Diode (LED)*. URL: <http://www.physics-and-radio-electronics.com/electronic-devices-and-circuits/semiconductor-diodes/lightemittingdiodeledconstructionworking.html>. Accessed: 2022-02-22.
- [24] Circuit Globe. *Light Emitting Diode (LED)*. URL: <https://circuitglobe.com/light-emitting-diode-led.html>. Accessed: 2022-02-21.
- [25] Energieplus. *Effets photoélectrique et électroluminescent*. URL: <https://energieplus-lesite.be/theories/photovoltaique6/effets-photoelectrique-et-electroluminescent/>. Accessed: 2022-02-23.
- [26] Henry Mathieu. *Physique des semiconducteurs et composants électroniques*. 5e édition. Chapitre 9: Composants optoélectroniques. Dunod, 2001. ISBN: 2-100-05654-9. Accessed: 2022-03-30.
- [27] Avantage LED des lux d'avance. *Composition d'une LED*. URL: <https://www.avantage-led.com/composition-dune-led-pxl-18.html>. Accessed: 2022-02-22.
- [28] Ben G. Streetman and Sankay Kumar Banerjee. *Solid State Electronic Devices*. Sixth Edition. Asoke K. Ghosh, PHI Learning Private Limited, M-97, Connaught Circus, New Delhi-110001, 2006. ISBN: 978-81-203-3020-7. Accessed: 2022-03-08.
- [29] Benoit Vanderheyden. *Electronique Analogiques*. Université de Liège, 2020. Accessed: 2022-04-19.
- [30] G Morthier and P Vankwikelberge. *Handbook of Distributed Feedback Laser Diodes*. Second Edition. Artech, 2013. ISBN: 978-1-60807-701-4. Accessed: 2022-02-25.
- [31] S.O. Kasap. *Optoelectronics and Photonics: Principles and Practices*. Tom Robbins, 2001. ISBN: 0-201-61087-6. Accessed: 2022-03-27.
- [32] Physics and Radio-Electronics. *Laser Diode*. URL: <https://physics-and-radio-electronics.com/electronic-devices-and-circuits/semiconductor-diodes/laserdiode.html>. Accessed: 2022-02-22.
- [33] Inst Tools. *Laser Diode Working Principle*. URL: <https://instrumentationtools.com/laser-diode-working-principle/>. Accessed: 2022-02-23.
- [34] Eclairage o Led. *Quelle est la différence entre une diode LED et une diode laser?* URL: <https://eclairage-o-led.com/conseils/quelle-est-la-difference-entre-une-diode-led-et-une-diode-laser/>. Accessed: 2022-02-24.
- [35] Circuit Globe. *Laser Diode*. URL: <https://circuitglobe.com/laser-diode.html>. Accessed: 2022-02-21.
- [36] David O'Brien. *Sensitivity of Quantum Dot Lasers to External Optical Feedback Supervisors*. PhD thesis, University College, Cork, Ireland. 2006-03. Accessed: 2022-02-28.
- [37] Rens Limpens. *Spectroscopical Investigations of the Space-Separated Quantum Cutting Mechanism*. Master thesis, University of Amsterdam. 2011-10. Accessed: 2022-02-28.
- [38] Tommy Ive and Asa Haglund. "The Nobel Prize in Physics". In: *Science Faculty Magazine* Faculty of Science at University of Gothenburg, Dec. 2014. Accessed: 2022-02-23.
- [39] LED Light house. *Difference Between LED And Laser Diode*. URL: <https://ledlightshouse.com/difference-between-led-and-laser-diode/>. Accessed: 2022-02-21.
- [40] Philippe Vanderbemden. *Sensors, microsensors and instrumentation*. University of Liège, 2021. Accessed: 2022-03-22.
- [41] Learnabout Electronics - Semiconductors. *Laser Diodes*. URL: https://learnabout-electronics.org/Semiconductors/diodes_26.php. Accessed: 2022-02-21.

- [42] INRS. *Rayonnement Laser*. URL: <https://www.inrs.fr/risques/rayonnements-optiques/rayonnement-laser.html>. Accessed: 2022-02-24.
- [43] *Datasheet PLT5 450B*. OSRAM Opto Semiconductors. URL: <https://www.oe-company.com/products/osram-laser-diodes/osram-blue/plt5-450b.pdf>. Accessed: 2022-02-17.
- [44] *Datasheet 11.3 Gbps Low-Power Laser Diode Driver*. Texas Instruments. URL: <https://www.ti.com/lit/ds/sllsei7/sllsei7.pdf>. Accessed: 2022-02-17.
- [45] *Datasheet LMR62421 SIMPLE SWITCHER® 24Vout, 2.1A Step-Up Voltage Regulator in SOT-23*. Texas Instruments. URL: <https://www.ti.com/lit/ds/symlink/lmr62421.pdf>. Accessed: 2022-02-17.
- [46] *Datasheet iC-HS02/05/B ULTRAFast LASER DRIVER*. Rev A0.2. iC-Haus. URL: <https://www.ichaus.de/product/iC-HS20Series>. Accessed: 2022-02-17.
- [47] *Altium Designer*. URL: <https://www.altium.com/fr/altium-designer>. Accessed: 2022-02-18.
- [48] *Python PyQt*. URL: <https://pythonpyqt.com/>. Accessed: 2022-02-18.
- [49] *Python*. URL: <https://www.python.org/>. Accessed: 2022-02-18.
- [50] *Qt*. URL: <https://www.qt.io/>. Accessed: 2022-02-18.
- [51] *Arduino*. URL: <https://www.arduino.cc/>. Accessed: 2022-02-18.
- [52] *Datasheet Arduino Nano 33 IoT*. Arduino. URL: <https://docs.arduino.cc/hardware/nano-33-iot>. Accessed: 2022-02-17.
- [53] Karthik Hemmanur. “Inter-Integrated Circuit (I2C)”. In: *Electrical Computer Engineering*, 2009. Accessed: 2022-03-11.
- [54] Mayank Prasad. *Inter-Integrated Circuits – I2C Basics*. URL: <https://maxembedded.com/2014/02/inter-integrated-circuits-i2c-basics/>. Accessed: 2022-02-25.
- [55] David Kalinsky and Roe Kalinsky. “Introduction to I2C”. In: July 2009. Accessed: 2022-03-10.
- [56] Jayant Mankar, Chaitali Darode, Komal Trivedi, and Prachi Shahare Madhura Kanoje. “Review of I2C Protocol”. In: *International Journal of Research in Advent Technology* vol. 2.no. 1, Jan. 2014. Accessed: 2022-03-10.
- [57] OpenCores. *openMSP430*. URL: <https://opencores.org/projects/openmsp430/serial%20debug%20interface>. Accessed: 2022-02-25.
- [58] Frédéric Leens. “An Introduction to I2C and SPI Protocols”. In: *IEEE Instrumentation Measurement Magazine*, Feb. 2009. Accessed: 2022-03-10.
- [59] Machina Speculatrix. *AVR basics: using the I2C bus 3 – sending data*. URL: <https://mansfield-devine.com/speculatrix/2018/02/avr-basics-using-the-i2c-bus-3-sending-data/>. Accessed: 2022-02-26.
- [60] Aurélien Jarno. *Le Bus I²C*. URL: <https://www.aurel32.net/elec/i2c.php>. Accessed: 2022-02-25.
- [61] *Mouser Electronics*. URL: <https://www.mouser.be/>. Accessed: 2022-02-30.
- [62] *Farnell*. URL: <https://be.farnell.com/fr-BE>. Accessed: 2022-02-30.
- [63] John W. Jewett Jr. and Raymond A. Serway. *Physics for Scientists and Engineers with Modern Physics*. Eighth edition. Mary Finch, 2021. ISBN: 978-1-4390-4875-7. Accessed: 2022-03-06.
- [64] Tony Chan Carusone, David A. Johns, and Kenneth W. Martin. *Analog Integrated Circuit Design*. Second Edition. John Wiley Sons, 2011. ISBN: 978-0-470-77010-8. Accessed: 2022-04-14.

- [65] *Datasheet RASM712*. Switchcraft. URL: <https://dir.heisener.com/DatasheetDownload/RASM712.pdf>. Accessed: 2022-02-25.
- [66] *Datasheet LM1084 5-A Low Dropout Positive Regulators*. SNVS037G. Texas Instrument. URL: <https://www.ti.com/lit/ds/symlink/lm1084.pdf>. Accessed: 2022-02-25.
- [67] *Datasheet IRF9640, RF1S9640SM*. Fairchild Semiconductor. URL: <https://www.triopak.fi/files/product/Fairchild/IRF9640.pdf>. Accessed: 2022-02-25.
- [68] *Datasheet LM3478 High-Efficiency Low-Side N-Channel Controller for Switching Regulator*. SNVS085X. Texas Instrument. URL: <https://www.ti.com/lit/ds/symlink/lm3478.pdf?ts=1652010088155>. Accessed: 2022-02-25.
- [69] *Datasheet CSD17313Q2Q1 30-V N-Channel NexFET Power MOSFET*. SLPS427D. Texas Instrument. URL: https://www.ti.com/lit/ds/symlink/csd17313q2q1.pdf?ts=1652014053605&ref_url=https%5C%253A%5C%252F%5C%252Fwww.ti.com%5C%252Fproduct%5C%252FCSD17313Q2Q1. Accessed: 2022-02-26.
- [70] *Datasheet 744311470 WE-HCI SMT High Current Inductor*. Texas Würth Elektronik. URL: <https://www.mouser.be/datasheet/2/445/744311470-1721281.pdf>. Accessed: 2022-02-27.
- [71] *Datasheet SS32-S310 Schottky Rectifier*. FairChild. URL: <https://www.farnell.com/datasheets/2303855.pdf>. Accessed: 2022-02-27.
- [72] *Datasheet 7/8-Bit Single/Dual I2C Digital POT with Nonvolatile Memory*. DS22107B. Microchip. URL: <https://www.mouser.be/datasheet/2/268/22107B-1180063.pdf>. Accessed: 2022-02-27.
- [73] Bertrand Cornélusse. *Circuits électriques*. Université de Liège, 2019. Accessed: 2022-03-25.
- [74] *Datasheet INA225 36-V, Programmable-Gain, Voltage-Output, Bidirectional, Zero-Drift Series, Current-Shunt Monitor*. SBOS612A. Texas Instrument. URL: https://www.ti.com/lit/ds/symlink/ina225.pdf?HQS=dis-mous-null-mouser-mode-dsf-pf-null-ww&ts=1652014756303&ref_url=https%5C%253A%5C%252F%5C%252Fwww.mouser.be%5C%252F. Accessed: 2022-02-27.
- [75] Philippe Vanderbemden. *Analyse et conceptions des systèmes de mesures électriques*. Université de Liège, 2019. Accessed: 2022-04-02.
- [76] *Datasheet SMT Test Terminal*. Harwin. URL: <https://cdn.harwin.com/pdfs/S2751R.pdf>. Accessed: 2022-02-28.
- [77] *Datasheet TPS82084 (2-A) / TPS82085 (3-A) High Efficiency Step-Down Converter MicroSiP Modules with Integrated Inductor*. SLVSCN4D. Texas Instrument. URL: <https://www.ti.com/lit/ds/symlink/tps82085.pdf>. Accessed: 2022-02-24.
- [78] Robert W. Erickson and Dragan Maksimovic. *Fundamentals of Power Electronics*. Second Edition. Kluwer Academic, 2001. ISBN: 0-306-48048-4. Accessed: 2022-04-12.
- [79] Jean-Louis Meyzonnette and Thierry Lépine. *Base de Radiométrie optique*. Second Edition. Cépaduès, 2001. Accessed: 2022-02-25.
- [80] David Crecraft and Stephen Gergely. *Analog Electronics: Circuits, Systems and Signal Processing*. Butterworth-Heinemann, 2002. ISBN: 0-7506-5095-8. Accessed: 2022-04-10.
- [81] *Datasheet Si5341/40 Rev D Data Sheet*. Silicon Labs. URL: <https://www.digikey.nl/html/datasheets/production/3205090/0/0/1/si5341a-c-gmr.pdf>. Accessed: 2022-02-22.

- [82] *Datasheet Ultra Miniature SMD Crystal Clock Oscillator*. ABRACON. URL: <https://www.mouser.be/datasheet/2/3/ASCO-245430.pdf>. Accessed: 2022-02-24.
- [83] *Datasheet Ultra Small Surface Mount Coaxial Connectors - 1.9mm or 2.4mm Mated Height*. HRS. URL: https://datasheet.lcsc.com/lcsc/1811091710_HRS-Hirose-U-FL-R-SMT-1-80_C88374.pdf. Accessed: 2022-02-20.
- [84] *Datasheet LMK00301 3-GHz 10-Output Ultra-Low Additive Jitter Differential Clock Buffer/Level Translator*. SNAS512I. Texas Instrument. URL: <https://www.ti.com/lit/ds/symlink/lmk00301.pdf>. Accessed: 2022-02-19.
- [85] *Datasheet Customer Information Sheet*. S2751-46R. Harwin. URL: <https://cdn.harwin.com/pdfs/S2751R.pdf>. Accessed: 2022-03-10.
- [86] *JLCPCB*. URL: <https://jlcpcb.com/>. Accessed: 2022-02-28.
- [87] Zachariah Peterson. *Que sont les paires différentielles et les signaux différentiels ?* URL: <https://resources.altium.com/fr/p/what-are-differential-pairs-and-differential-signals>. Accessed: 2022-03-28.
- [88] Tan Yan, Pei-Ci Wu, Qiang Ma, and Martin D. F. Wong. “On the Escape Routing of Differential Pairs”. In: *IEEE/ACM International Conference on Computer-Aided Design (ICCAD)*, 2010. Accessed: 2022-02-23.
- [89] Mohammad S. Sharawi. “Practical issues in high speed PCB design”. In: *IEEE Potentials* vol. 23.no. 2, Apr. 2004, pp. 24–32. Accessed: 2022-02-23.
- [90] JLCPCB. *Impedance Calculation*. URL: <https://cart.jlcpcb.com/impedanceCalculation>. Accessed: 2022-02-28.
- [91] Hasna Louahlia and Sébastien Yon. “Dissipation Thermique dans les Composants/Systèmes Electroniques”. In: *Normandie AeroEspace*, July 2015. Accessed: 2022-04-17.
- [92] Seunghyun Cho and Joseph Y. Lee. “Heat Dissipation of Printed Circuit Board by the High Thermal Conductivity of Photo-Imageable Solder Resist”. In: *IEEE Journal of Selected Topics in Quantum Electronics* vol. 6.no. 4, Dec. 2010, pp. 167–172. Accessed: 2022-04-17.
- [93] *Fusion 360*. URL: <https://www.autodesk.fr/products/fusion-360/overview?term=1-YEAR&tab=subscription>. Accessed: 2022-03-24.
- [94] *Datasheet Slim Dual Range Power Head with Silicon Detector*. Thorlabs. URL: <https://www.thorlabs.com/thorproduct.cfm?partnumber=S130C>. Accessed: 2022-05-10.
- [95] *Datasheet PDA015A(/M) Si Amplified Detector*. Thorlabs. URL: <https://www.thorlabs.com/thorproduct.cfm?partnumber=PDA015A/M>. Accessed: 2022-05-10.